The Pennsylvania State University

The Graduate School

College of Engineering

AN INVESTIGATION OF WALKING INDUCED ELECTROSTATIC FIELD EFFECTS ON INDOOR PARTICLE RESUSPENSION

A Thesis in

Architectural Engineering

by

Bin Hu

Submitted in Partial Fulfillment
of the Requirements
for the Degree of

Doctor of Philosophy

May 2008

The thesis of Bin Hu was reviewed and approved* by the following:

James D. Freihaut
Associate Professor of Architectural Engineering
Thesis Adviser
Chair of Committee

Stanley A. Mumma
Professor of Architectural Engineering

William P. Bahnfleth
Professor of Architectural Engineering

James L. Rosenberger
Professor of Statistics

Chimay J. Anumba
Professor of Architectural Engineering
Head of the Department of Architectural Engineering

*Signatures are on file in the Graduate School

ABSTRACT

Airborne concentration of particulate matter (PM) is an important index of indoor air quality. Researches have demonstrated the strong correlation between airborne particulate concentration and human health. Micron-sized particulate sources are commonly found in the enclosed indoor environment. Human activity is considered the main reason causing indoor particle resuspension, which leads to human secondary exposure to PM. However, no general rules have been established to empirically relate airborne particle concentration from resuspension with specific types of human activity.

This work studies the effects of electrostatic field, generated by human walking, a common human activity, on indoor particle resuspension. Particle resuspension forces, generated by human walking on indoor surface particles, can mainly be decomposed into three types: mechanical vibration, aerodynamic drag and electrostatic forces. A parametric study is carried out to compare the magnitudes of different particle resuspension force components, as well as the particle-surface adhesion force. The comparison shows that electrostatic force is a significant particle resuspension force, while the theoretically calculated particle adhesion force is much larger than each of the resuspension force components. This work suggests that real particle adhesion force is much smaller than the theoretically calculated values due to imperfect contact and thus the resuspension forces, introduced by human activity, can overcome the adhesion force to resuspend particles into the air. To testify this idea, experiments are designed to measure the real adhesion force between different particles and flooring materials with the electrostatic detachment method.

This work uses particle resuspension chamber as the major facility to systematically study the walking-induced electrostatic effects on particle resuspension. Experiments are designed to measure the floor surface electrostatic field strength that can be generated by human walking in indoor environment. The measured field strength profile is used for the electrostatic field simulation in the resuspension chamber experiments. The validity of the chamber experiments is testified by comparing the resuspension coefficients concluded from the resuspension chamber experiments with the results reported from field experiments. The results of chamber experiments show that the electrostatic fields introduced by human walking can have a significant influence on indoor particle

resuspension. The electrostatic effects are strongly related with such factors as particle type, flooring type, relative humidity and field polarity.

Besides, this work also studies the applicability of multizone airflow and contaminant dispersion model in simulating particle resuspension and dispersion in indoor environment with a heating, ventilation and air-conditioning (HVAC) system.

TABLE OF CONTENTS

List of Figures

List of Tables

Nomenclature

English symbols

Symbol	Description	Dimension*
a	Acceleration	L/t^2
A	Amplitude of vibration	L
A	Room floor area, particle deposition area	L^2
A	Hamaker constant, which depends on the materials involved and ranges from $6\sim150\times10^{-20}$	FL
A_C	Contact area	L^2
C	Capacitance	C/V
C_b	Capacitance of human body	C/V
C_C	Cunningham slip factor	-
C_{Air}	Airborne concentration of particles with certain diameter	M/L^3 ,or $\#/L^3$
C_f	The skin-friction coefficient	-
C_{fx}	Local shear stress coefficient	-
C_S	Surface concentration of particles	M/L^2 ,or $\#/L^2$
D	Particle deposition loss rate	t^{-1}
D	Effective removal rate, [volume of air/time]	L^3/t
d_p	Particle diameter	L
$d_{p,aero}$	Aerodynamic diameter of particles	L
d_S	Number weighted area diameter	L
d_V	Number weighted volume diameter	L
d_e	Equivalent mass diameter	L
e	Charge of an electron = 1.60217646 × 10-19 coulombs	C
E	Electric field strength	V/L
E_L	Surface electric field strength limit	V/L
f	Frequency	t^{-1}
f_{ji}	Internal filter factor from room j to room i .	-
F	Particle deposition flux	$\#/(L^2t)$

F_{adh}	Adhesion force	F
$F_{adh,\exp}$	Adhesion force from experimental measurement	F
F_d	Air drag force	F
F_e	Electrostatic force	F
F_g	Gravitational force	F
F_L	Surface boundary flow lifting force	F
G	Generation rate, [particle #/time]	t^{-1}
H	Room space height	L
h	Ventilation rate	t^{-1}
I	Electric current	C/t
$I_{particle}$	Particle transportation current	C/t
k	Mean height of rough protrusions on the surface	L
K_E	Electrostatic constant of proportionality or Coulomb force constant, which is 9.0×10^9 N·m^2/C^2.	-
L_e^+	Dimensionless turbulent length scale, based on energy, $=2.25\mathrm{Re}_\theta^{3/4}$	-
M	Total mass of particles	M
MMD	Mass median diameter	L
$\overline{n}$	Boltzmann equilibrium charge number per particle	-
n_e	Number of equivalent particles	-
N_i	Ion concentration in the air	L^{-3}
n_w	Walking steps in unit time	t^{-1}
$n(t)$	Transportation particles in unit time	t^{-1}
P	Atmosphere pressure	F/L^2
Q	Electric charge	C
q_d	Electric charge of particles with diameter d	C
q_p	Electric charge per particle	C
q_L	Particle charge limit	C
Δq_{step}	Charge separated between shoe soles and floor surface by each step of human walking	C
r	Particle radius	L
R	Surface particle removal rate	M/ (L^2t), or #/ (L^2t)

R_b	The body resistance to the ground	Vt/C
Re	Reynolds number	-
Re_θ	Reynolds number, based on boundary layer momentum thickness θ	-
r_f	Surface particle removal fraction	-
RF	Resuspension factor	L^{-1}
RH	Relative humidity, %	-
RR	Resuspension rate	t^{-1}
S	Source rate of particulate contaminants, [particle #/time];	t^{-1}
t	Time	t
T_i	Turbulence intensity	-
U	Free-stream air flow velocity	L/t
u_τ	Friction velocity	L/t
v	Velocity	L/t
v_d	Particle deposition velocity for certain diameter	L/t
V	Room space volume	L^3
V_b	The electrostatic body voltage	V
$V_{body-ground}$	Voltage of human body to the ground	V
$V_{body-floor}$	Voltage of human body to floor surface	V
$V_{floor-ground}$	Voltage of floor surface to the ground	V
$\dot{V}_{IA,ji}$	Infiltration from room j to room i	L^3/t
$\dot{V}_{SA}$	Supply air rate from HVAC system	L^3/t
x	Distance	L
y	Displacement	L
Z_i	Mobility of ions, $\approx 1.5\times10^{-4}$ $m^2/V\cdot s$.	$M^2/(Vt)$

* The dimensions are defined as:

C = electrical charge	M = mass	t = time	# = particle number
F = force	N = mols	T = temperature	
L = length	Q = energy	V = voltage	

Greek symbols

Symbol	Description	Dimension*
ε	Permittivity	-
ε_0	Permittivity of free space, ≈8.8542×10^{-12} C^2/(N·m^2)	-
ε_r	Relative permittivity, $= \varepsilon / \varepsilon_r$	-
Λ_C	Contact frequency	t-1
λ	Air mean free path	L
μ	Dynamic viscosity of air, ≈1.84E-5 at 20°C	Ft/L^2, M/(Lt)
ρ	Particle resistivity	RL
ρ	Density of fluid	M/L^3
ρ_p	Density of particle	M/L^3
ρ_w	Density of water, = 1000 kg/m^3	M/L^3
ρ_{air}	Density of air	M/L^3
σ_g	Geometric standard deviation	-
τ_p	Particle relaxation time	t
τ_w	Wall shear stress	F
ν	Kinematical viscosity	L^2/t

* The dimensions are defined as:

C = electrical charge	M = mass	t = time
F = force	N = number	T = temperature
L = length	Q = energy	V = voltage
# = particle number	R = electric resistance	

Acknowledgements

I would like to express my sincere thanks to my advisor, Professor James D. Freihaut for his valuable guidance and help in completion of this thesis. His high standards and deep knowledge in research have provided me the most valuable help in my research work.

Many thanks to my wife, Tieying Xu. Without her consistent support of my work, it would be extremely hard for me to overcome all the difficulties and to fulfill my PhD research work.

I would also express my great gratitude to the other faculty members at the Pennsylvania State, Professor William P. Bahnfleth, Professor Stanley A. Mumma, Professor James L. Rosenberger and Professor Richard A. Behr and Dr. Brandolyn Thran from US Army Center, for their kindness and support.

The funding support of this work by US Army Center for Health Promotion and Preventive Medicine (USA CHPPM) contracts DABJ05-03-P-1210 and W91ZLK-05-P-0838 is gratefully acknowledged.

I thank my colleague Carlos Gomes for his generous help and collaboration throughout my research. I thank Research Associate Paul A. Kremer for his tremendous help in my experiments. I would also like to thank all my other colleagues in the Architectural Engineering Program for their collaboration and friendship.

CHAPTER 1. INTRODUCTION

1.1 Problems with indoor particle resuspension

In economically developed societies, people spend most of their time indoors (Robinson and Nelson 1995). Consequently, indoor air quality becomes an important factor for human health. The airborne concentration of particulate matter (PM) can be an important index of indoor air quality.

Researches have demonstrated strong correlations between airborne specific types of particulate concentrations and human health. PM such as pollen, fungal spores and smoke are considered as major causes of asthma, a life-threatening respiratory disease. In United States, the National Institute of Environmental Health Sciences (NIEHS 1997) reported that 10 million people suffered from allergic asthma. The National Center for Health Statistics (NCHS 2001) estimated more than 4,000 deaths each year due to asthma. The National Heart, Lung, and Blood Institute (NHLBI 2002) estimated an annual cost of 14 billion dollars due to medical care of asthma as well as missed school and work days.

Ambient airborne PM is also considered an important factor related to cardiovascular diseases such as ventricular arrhythmias and congestive heart failure (CHF) (Dockery et al 2005, Rich et al 2005, Rich et al 2006, Sarnat et al 2006, Wellenius et al 2006). Increases in death rates from respiratory and cardiovascular morbidity were observed as the result of increasing exposure to PM (Clancy et al 2002, Dockery 2001, Gold et al 2005).

The Environmental Protection Agency (EPA 1997) defines “inhalable particles” as having an aerodynamic diameter smaller than 10 μm (PM10) and capable of depositing anywhere in the respiratory system. The EPA defines “respirable particles” as having an aerodynamic diameter smaller than 2.5 μm (PM2.5) and capable of penetrating into the lungs. Figure 1 demonstrates the human exposure to PM10 and PM 2.5.

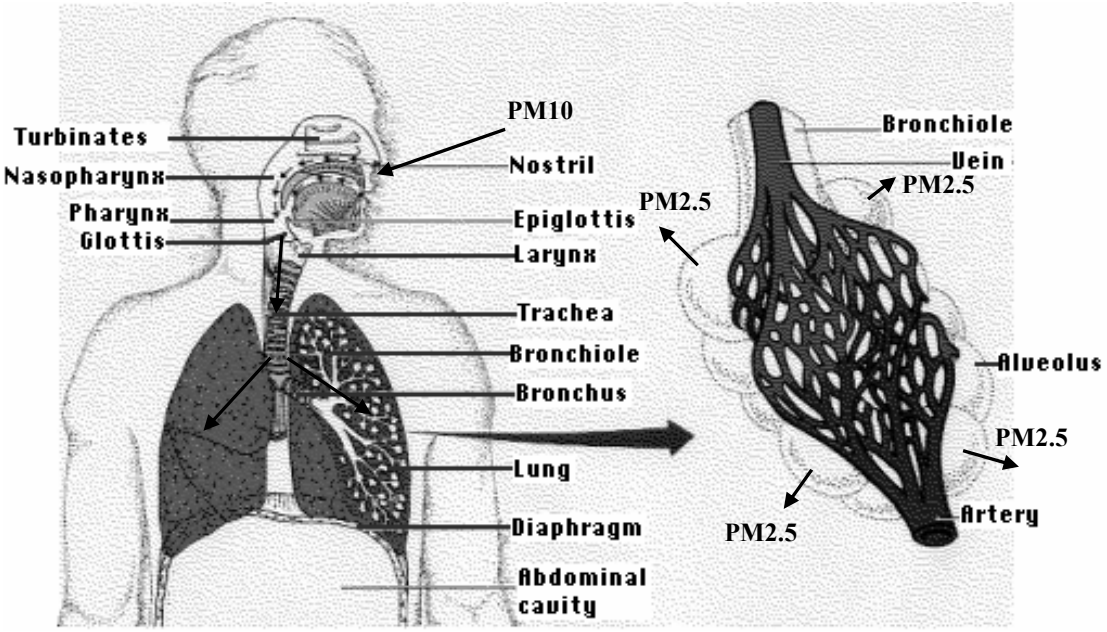

Figure 1 Human exposure to PM
(Background drawing from http://www.rcn.com)

A study (Wallace 1996) has shown that particulate sources found in the indoor environment can influence personal exposure to micron-sized particulate matter (PM). Micron-sized particulate sources are commonly found in the enclosed indoor environment. Smoking and cooking are considered the two major sources of indoor PM10 and PM 2.5 (Wallace 1996). Micron-sized PM can remain suspended in room air for long periods of time before eventually depositing onto surfaces of indoor environment. Human activity, such as walking and vacuuming, resuspend deposited particles into the air to generate secondary human exposure. The particulate concentrations generated by resuspension are usually much lower than those from direct release of particulates into the air, such as smoking and cooking. However, due to persistence of particulate contaminants in indoor floor reservoirs and continuous human activity disturbances, the long term secondary exposure may pose considerable negative risks to human health. Secondary inhalation exposure paths are apparently a significant factor associated with the epidemic increases in economically developed societies for respiratory diseases, such as asthma.

Human activity is responsible for indoor particle resuspension (Clayton et al 1993, Kamens et al 1991, Lefcoe and Inculet 1975, Lioy et al 1990, Raunemaa et al 1989, Thatcher and Layton 1995). Thatcher and Layton (1995) found that walking inside a room increases the airborne concentration of micron-sized particles by 100% and the increases were even greater for vigorous activities such as vacuum cleaning. However, research on human activity related indoor particle resuspension is still very limited (Walsh 2002, Abu-Eid et al 2002). Reported research indicates a significant variation in particle resuspension coefficients by human activity. No study has generalized the relationship between human activity and particle resuspension levels. No general rules have been established to empirically relate airborne particle concentration from resuspension with specific types of human activity. Quantitative extrapolation of results from one set of conditions to another is not possible since mechanisms and models of resuspension are not well defined and the appropriate model variables not identified.

From a phenomenological basis, however, the strong dependence of particulate concentrations in indoor air on human activity is indisputable. The dosage-risk relationships, which have been established for known indoor protein allergens, such as the mite allergen Der p 1, are based on building dust reservoir allergen concentrations instead of corresponding airborne concentrations (Platts-Mills 2000, Chapman 2003). However, allergic responses and diseases caused from such particulate contaminants are known to be inhalation based (Custovic et al 1998, Platts-Mills 2000). Thus, it is necessary to relate allergen airborne concentrations with reservoir concentrations in order to develop an understanding of the secondary exposure processes and subsequently develop risk mitigation strategies. Further work is needed to explore the essential physical principles underlying indoor particle resuspension by human activity.

1.2 Basic definitions of particle resuspension and deposition

(1) Resuspension factor

Resuspension factor (RF) is defined as the pseudo steady-state ratio between airborne particle concentration and surface particle concentration. The definition can be expressed in Equation 1.

$$RF\,(m^{-1}) = \frac{airborne\ \ concentration, C_{Air}\ (\mu g\ m^{-3})}{surface\ \ concentration, C_S\ (\mu g\ m^{-2})} \qquad (1)$$

For outdoor particle resuspension, Sehmel (1984) pointed out that resuspension factor failed to take into account of upwind airborne concentrations and was so specific for the conditions, under which they were determined, that it was difficult to form any generalizations. Similarly, for indoor environments, resuspension factor is not able to describe the room airborne concentrations properly when there are considerable airborne particles introduced by air flow through infiltration or HVAC system.

(2) Resuspension rate

Resuspension rate (RR) is defined as the fraction of a surface species removed in unit time. The definition is described in Equation 2.

$$RR\,(s^{-1}) = \frac{surface\,concentration\,removal\,rate, R\,(\mu g\ m^{-2}\ s^{-1})}{surface\,concentration, C_S\ (\mu g\ m^{-2})} \qquad (2)$$

Contrary to resuspension factor, the value of resuspension rate is not influenced by the particle concentration in ambient air flow. With resuspension rates and airborne particle concentrations from ambient air flows, a proper mass balance equation of airborne particle concentration can be established for an indoor environment.

Given a particular type of particle, different resuspension rates may exist for different size ranges of particles, depending on the type of resuspension disturbances The overall

resuspension rate for particles with a given particle distribution is actually a weighted parameter based on the resuspension rates of different particle size groups within the particle size distribution.

(3) Resuspension fraction

In the definition of resuspension rate as shown in Equations 2, the surface concentration removal rate R is an average value across the contaminated area. However, the actual particle resuspension area disturbed by human activity can often be much smaller than the total contaminated area and depends on the activity type and frequency. Given all the other experimental conditions the same, different total contaminated floor areas give different particle resuspension rates if the conventional resuspension rate definition is used. The larger the total contaminated floor area, the smaller the calculated resuspension rate. Thus, the resuspension rate sometimes may not be a good measure for particle resuspension intensity by different human activity.

To address the shortcoming of resuspension rate, Karlsson et al (1999) introduced the definition of resuspension fraction (r_f), which describes particle resuspension intensity based on actual disturbed area instead of entire contaminated area. A dimensionless resuspension fraction (r_f) can be related to the resuspension rate (RR). Equation 3 shows the definition of resuspension fraction based on human walking.

$$r_f = \frac{A}{A_C \Lambda_C} \cdot RR \qquad (3)$$

Where: A = contaminated room floor area, m^2; A_C = actual contact area between a human foot and floor, m^2; Λ_C = contacting frequency between human feet and floor, s^{-1}.

In Equation 3, the resuspension fraction (r_f) denotes the fraction of particles emitted from the contact area (A_C) during one cycle of disturbance activity (one foot step) on the floor reservoir (A).

(4) Deposition velocity

Particle deposition is driven by gravitational force and is always present when there are suspended particles in the air. Resuspension factor, as mentioned above, is a value achieved under the equilibrium state between the particle resuspension and deposition processes. Deposition velocity is often used to describe the particle deposition phenomena. The deposition velocity ($v_d, m \cdot s^{-1}$) of particles, as shown in Equation 4, is defined as the ratio of the deposition flux ($F, m^{-2}s^{-1}$) divided by the airborne particulate concentration (C_A, m^{-3}) at some height above the surface layer (Chamberlain and Chadwick 1953). It is important to notice that particle deposition velocity is defined as a function of particle diameter.

$$v_d(d) = -\frac{F(d)}{C_A(d)} \tag{4}$$

Equation 5 (Heinsohn and Cimbala 2003) can be used to calculate the particle deposition velocity.

$$v_d = C_A g \frac{\rho_p - \rho_{Air}}{\rho_p} \tau_p \tag{5}$$

Where: g is the acceleration of gravity, = $9.8\, m/s^2$; ρ_p is the density of particles, kg/m^3; ρ_{Air} is the density of air, kg/m^3; τ_p is the particle relaxation time, as defined in Equation 6, s.

$$\tau_p = \frac{\rho_p d_p^2}{18\mu} \tag{6}$$

Where: d_p = diameter of particles, m; μ = dynamic viscosity of air, $\approx 1.84 \times 10^{-5}\ Pa \cdot s$ at 20°C.

Equation 6 is used for spherical particles in Stokes flow and is only an approximation for other flow regimes.

(5) Aerodynamic diameter

Aerodynamic diameter is usually used to describe particle deposition phenomena. Aerodynamic diameter is defined as the diameter assigned to a particle of unknown density and shape that possesses the same terminal deposition velocity as a perfect sphere of density 1000 kg/m^3 (Heinsohn and Cimbala 2003). If a particle settling in air has an observed terminal velocity within the Stokes flow regime and the particle diameter is larger than 1 μm, Equation 7 can be used to estimate the particle aerodynamic diameter ($d_{p,aero}$).

$$d_{p,aero} = d_p \sqrt{\frac{\rho_p - \rho_{air}}{\rho_w - \rho_{air}}} \approx d_p \sqrt{\frac{\rho_p}{\rho_w}} \qquad (7)$$

Where: ρ_w is the density of water, = 1000 kg/m^3.

1.3 Field studies on indoor particle resuspension by human activity

The study of particle resuspension was initially motivated by the requirement of establishing an outdoor air-surface mass transfer model, which is an important boundary condition for atmospheric diffusion and transport models. Tracer particle resuspension data were reported in the literature as early as 1950s (Healy 1955). Since then, field experiments on particle resuspension in outdoor environments have been widely carried out (Sehmel 1984). Outdoor resuspension investigations mainly focus on particles originating from soil or rock erosion and the major resuspension forces are high speed outdoor wind and/or mechanical stresses such as automobile traffic. In Sehmal's

literature review (1984), wide ranges were reported for both particle resuspension factors (10^{-2} to 10^{-10} m^{-1}) and for particle resuspension rates (10^{-6} to 10^{-13} s^{-1}). Many factors may lead to the wide variation of resuspension coefficients, including non-uniform reservoir sources, no-control on particle size and composition, and important environmental conditions, such as relative humidity. Sehmel (1984) concluded that, in order to acquire reliable resuspension coefficients, it was important to control experimental conditions, establish theoretical models and validate the modeling.

The aerosolization phenomena associated with indoor particle resuspension is likely to have quite different characteristics than those with outdoor particle resuspension due to the differences in both particle source and resuspension forces. Smoking and cooking, are major generating sources of indoor aerosols, while the life cycle of pets, insects and fungi can also be the major sources of latent PM_{10} and $PM_{2.5}$ particulates in building reservoirs (Wallace 1996). Human activity, such as walking and cleaning, are considered the main disturbing forces causing indoor particle resuspension from these reservoirs (Clayton et al 1993, Kamens et al 1991, Lefcoe and Inculet 1975, Lioy et al 1990, Raunemaa et al 1989, Thatcher and Layton 1995).

1.3.1 Field experiments in nuclear facilities

The scientific and public concern for indoor particle resuspension originated with the concern about exposure to radioactive dusts. In 1960s, a number of studies (Mitchell and Eutsler 1967, Bronskill 1967, Glauberman 1967, Carter 1970, Fish et al 1967, Jones and Pond 1967) began to focus on resuspension factors, mainly of radioactive dusts, in nuclear facilities due to human activity. The resuspension factors reported from these early researches are listed in Table 1.

Table 1 Indoor resuspension factors from studies in 1960s*

Location	Source material	Resuspension stress	Resuspension factor range, m^{-1}	Reference
Unventilated room	Beryllium	Vigorous sweeping	1×10^{-2}~4×10^{-2}	Mitchell and Eutsler, 1967
Small unventilated room	Alpha floor contamination	People walking	3×10^{-4}~2×10^{-2}	Calculated from Brunskill, 1967
Change room with no ventilation	Alpha on coveralls	Two to four people changing coveralls	$<2\times10^{-4}$~1.7×10^{-2}	Calculated from Brunskill, 1967
Change room, concrete floor, 9 air change/h	10% loose alpha floor contamination	Four to six people moving in room	2×10^{-4}~3×10^{-3}	Brunskill, 1967
Simulated work	Asbestos contaminated coat	Machine operations	1.2×10^{-3}~5.3×10^{-3}	Carter, 1970
		Stacking sheets	2.0×10^{-3}~4.2×10^{-3}	
Room, concrete floor	Plutonium facility	No circulation	1×10^{-5}~2×10^{-4}	Glauberman et al, 1967
		Fan air stress	3×10^{-4}~3×10^{-3}	
		Fan and dolly movement	4×10^{-3}~1.5×10^{-2}	
		No circulation after tests	5×10^{-4}~1×10^{-3}	
Room, concrete floor	Uranium facility	No circulation	7×10^{-5}~4×10^{-4}	
		Fan air stress	3×10^{-5}~2×10^{-4}	
		Dolly movement	1×10^{-4}~2×10^{-4}	
		Fan and dolly movement	2×10^{-4}~1×10^{-3}	

* Adapted from Sehmel 1984

The US Nuclear Regulatory Commission (USNRC) (Beyeler et al 1999) established a resuspension factor parametric value of $1.42\times10^{-5}\,m^{-1}$ for screening analysis and inhalation dose calculation, assuming a 10 percent fraction of loose (removable) dust surface contamination. The USNRC (Abu-Eid et al 2002) subsequently re-evaluated this default RF value and a new RF value of $1.0\times10^{-6}\,m^{-1}$ was recommended for the

screening analysis of the inhalation dose calculation for the building occupancy scenario. The re-evaluation study carried out a literature review and evaluation of measured data for the indoor RF. The RF values from this review are shown in Table 2. The re-evaluation considers the average conditions for a year which represent the building-occupancy scenario with respect to driving forces, ventilation rate, particle size and the removable portions of contamination. The re-evaluation study is mainly based on the experiments of aged contamination, and is considered more applicable to decommissioned nuclear facilities. The previous study in 1999 depended on experiments with freshly deposited contamination, which may have higher portions of removable contamination. Thus, the RF value from re-evaluation study in 2002 is considered more applicable for screening analysis of the inhalation dose calculations.

Table 2 Summary of resuspension factors*

Reference	**Resuspension factor ($\times 10^{-6}\, m^{-1}$)**
Freshly Deposited Contamination	
Fish, 1967	9.4 ~ 710
Ikezawa, 1980	2.3 ~ 180
Jones, 1967	0.3 ~ 177
Cleaned or Aged Contamination	
Breslin, 1966	0.33 ~ 2.08
Eisenbud, 1954	0.1 ~ 0.5
Nardi, 1999	0.067 ~ 0.227
Ruther, 1988	0.055 ~ 0.11
Spangler, 1999	0.425

* adapted from NUREG-1720 Report (Abu-Eid 2002)

1.3.2 Field experiments in residential buildings

Resuspension coefficients in residential buildings may be different from coefficients in nuclear facilities mainly due to variations in activity type and particulate composition. Thatcher and Layton (1995) measured the particle resuspension rates within a two-story residential building and found that human activity had a significant influence on airborne particle concentrations. For four people with light activity in this building, the resuspension rate was found to range from 1.8×10^{-5} to $3.8\times10^{-4}\,h^{-1}$ for different submicron particle sizes, given a particle density of $1.0\,kg\cdot m^{-3}$. The resuspension rates from this study are listed in Table 3. Their findings indicate that particle resuspension rates can vary greatly among different particle sizes and should be a function of particle size.

Table 3 Particle resuspension rates in a residential building*

Particle size rang (μm)	Resuspension rate** (h^{-1})
0.3-0.5	9.9×10^{-7}
0.5-1.0	4.4×10^{-7}
1.0-5.0	1.8×10^{-5}
5.0-10.0	8.3×10^{-5}
10.0-25.0	3.8×10^{-4}
>25.0	3.4×10^{-5}

* This table is adapted from the paper of Thatcher and Layton, 1995
**The human activity is four residents performing light activities in the house

Ferro et al (2004) studied the particle resuspension under the disturbance of different types of indoor human activity, such as dancing, vacuuming and walking in a 75 year-old single family home with one occupant. The family home under study includes three interconnected levels: basement ($36m^2\times2.3m$), first floor ($83m^2\times2.5m$) and attic ($31m^2\times2.1m$). The home under study is professionally cleaned every week and has wood floors partially covered by thin area rugs. The particle resuspension source

strengths are reported for different human activities as shown in Figure 2. However, since the surface particulate contaminant concentrations are not reported, it is not possible to derive resuspension factors or resuspension rates from this work. In Figure 2, particle release flux from smoking is used as a reference. This study concluded that the particle resuspension source strength was a function of the number of persons performing the activity, the vigor of the activity, the type of activity and the type of flooring.

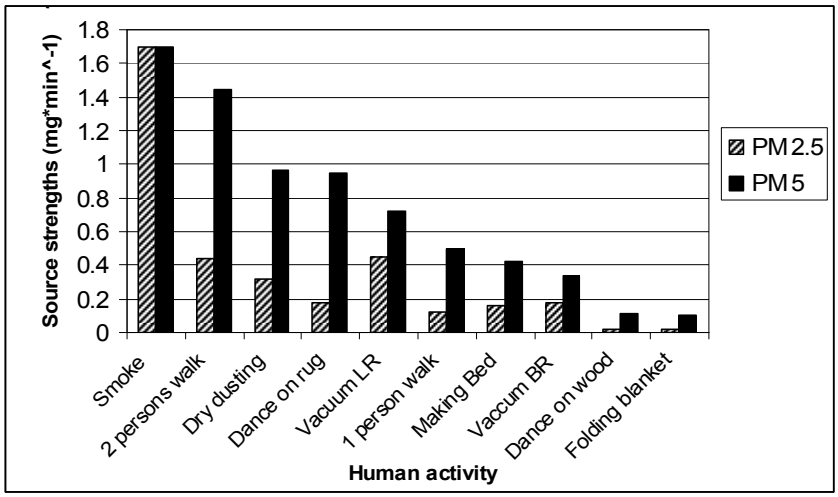

Figure 2 Source strength of particle resuspension by human activity (Ferro 2002)

1.3.3 Field experiments in controlled test rooms

The field experiments mentioned in Section 1.3.1 and 1.3.2 are mainly carried out in working places or residential environments. These experiments help researchers to estimate possible ranges of particle resuspension coefficients, such as resuspension rate and resuspension factor, in real situations. However, such experiments are not well controlled with respect to experimental parameters: particulate contaminants load and size distribution, human activity pattern and intensity, flooring type and relative humidity. Thus, it is difficult to extrapolate such experimental results to different circumstances. A limited number of field experiments on particle resuspension in controlled test rooms are identified in the literature. These controlled experiments reveal research efforts to quantify particle resuspension coefficients which can be generalized.

(1) Experiments by Fish et al (1967)

In this study, zinc sulfide (ZnS) particles and cupric oxide (CuO) particles were freshly dispersed into a test room. The particle size distribution was reported. The test room had painted walls and asphalt tile floor covering. There was no ventilation in the test room. Resuspension factors were measured for different human activities in the test room as shown in Table 4.

Table 4 Resuspension factors from the experiments of Fish et al (1967)

Source material	Resuspension stress	Resuspension factor range, m^{-1}
ZnS MMD* = 3.1 μm $\sigma_{g**} = 1.9$	Vigorous work, sweeping	1.9×10^{-4}
	Vigorous walking	3.9×10^{-5}
	Light work	9.4×10^{-6}
CuO MMD = 2.0 μm $\sigma_g = 2.3$	Light sweeping	7.1×10^{-4}

* Mass median diameter

** Geometric standard deviation of particle diameter

(2) Experiments by Jones and Pond (1967)

Jones and Pond studied the resuspension of plutonium oxide particles and plutonium nitrate from a laboratory floor with an area of 15×7 m^2 and a height of 3.15 m. The particulate contaminants were spread on the floor as a water suspension and left to dry. Four types of floor materials were used in the experiment: wax paper, PVC sheet, waxed linoleum and un-waxed linoleum. Air concentration samples were taken at two heights as 15 cm and 175cm above the floor surface. The studied human activities include walking on the surface at 14 steps/minute, 36 steps/minute and 100 steps/minute. For the experiments with two operators walking at 100 steps/minute, the operators were blowing air with a hair dryer directed at the floor in order to simulate extreme resuspension conditions. It was concluded that, in this study, higher rates of movement beyond 36

steps/minutes did not significantly increase the resuspension factors. The experimental results are listed in Table 5.

Table 5 Resuspension factors from Jones and Pond's experiments (1967)

Source material	Resuspension stress	Min RF (10^{-6} m^{-1})	Max RF (10^{-6} m^{-1})	Median RF (10^{-6} m^{-1})	Recommended RF (10^{-6} m^{-1})
Plutonium oxide	No movement	-	-	-	0.02
	14 steps/min	0.6	20	1.27	10
	36 steps/min	1	177	16.2	50
Plutonium nitrate	No movement	-	-	-	0.02
	14 steps/min	0.3	1.33	0.64	1
	36 steps/min	1	16.2	3.02	5

(3) Experiments by Hambraeus et al (1978)

An operating room with a vinyl floor covering of 35 m^2 was studied by Hambraeus et al (1978). During the resuspension experiment, the ventilation was turned off and all air leaks were sealed to reduce air leakage. The experimental room floor, which was cleaned with 70% ethyl alcohol before each experiment, was contaminated with *Staphylococcus aureus,* with a high proportion of small contaminated particles 3~6 μm. After deposition for 4–12 hours, different human activities were introduced. The experimental results are shown in Table 6. From the results, four people walking in a room resuspended three times more particles than one person blowing the floor using an electric hair-dryer and seventeen times more particles than one person mopping the floor. An interesting phenomenon about this experiment is that human walking generated a higher resuspension factor than the cold air jet from an electronic hair dryer, although a hair dryer provided a much stronger air flow near floor than that introduced by human walking. As explained by the author, the reason for this phenomena is that there are more people present in the walking experiment than in the air blowing experiment and a larger amount of external contaminants are introduced into the laboratory room by the larger amount of people.

Table 6 Resuspension factors of *Staphylococcus aureus* (Hambraeus et al 1978)

Human activity	Mean floor concentration (c.f.u.*/m^2)	Mean airborne concentration (c.f.u./m^2)	Mean RF (m^{-1})	Mean RR (s^{-1})
Blowing for 10 min	1.5×10^{3}	1.46	1.2×10^{-3}	2.0×10^{-6}
Mopping for 10 min	1.6×10^{3}	0.25	2.0×10^{-4}	3.4×10^{-7}
4-person walking for 30 min	3.4×10^{4}	89.2	3.5×10^{-3}	5.9×10^{-6}

* Colony forming units

(4) Experiments by Karlsson et al (1996, 1999)

Karlsson et al (1996) studied the resuspension of 6×4 μm ellipsoidal grass pollen particles. The volume media diameter of the pollen is 6.3±0.2 μm with a geometric standard deviation (σ_g) of 1.2. The pollen was aerosolized into a room with a floor area of 8.75 m^2. One person was actively working at a 0.7 m^2 table for one hour. Based on the actual disturbed table area instead of the total room floor area, a resuspension factor of 8.0×10^{-2} m^{-1} and a resuspension rate of 1.3×10^{-3} s^{-1} were measured.

Another investigation by Karlsson et al (1999) determined the resuspension rates caused by human walking. Spores of *Bacillus Subtilus* (BS) were dispersed into an experimental room with a floor area of 15 m^2. The settled spores formed 10~20 μm clusters from spool-shaped single spore with approximate length of 1.8 μm and diameter of 0.9 μm. The clusters were determined to have a diameter of 12 μm by assuming spherical shape (density=1.3 g/cm^3) and a measured mean deposition velocity of 0.005 m/s. The floor material was PVC while rubber boots were worn during the human walking activity. Two walking frequencies were studied: 75 steps per minute (1 person) or 300 steps per minute (4 persons). The experimental results showed that the resuspension rate was proportional to the number of persons walking on the floor. For one person walking, based on the contact area of one foot (0.028 m^2), the measured resuspension rate for spores was 6.25×10^{-4} s^{-1}. If the whole floor area was considered

instead of the foot area, the resuspension rate for one person walking would be $8.75\times10^{-7}\,s^{-1}$.

In the study of Karlsson et al (1999), the resuspension fraction was introduced as a derivation from resuspension rate to describe particle resuspension intensity. As described in Section 1.2, for human walking, the particle resuspension fraction equals the fraction of particles emitted from the contact area during one cycle of disturbance activity (one foot step) on the floor reservoir. A resuspension fraction of 5×10^{-4} was derived from the resuspension rates in the walking experiments carried out by Karlsson et al. The authors concluded that the resuspension rate must be carefully specified as a function of aerosol size, personal activity and floor material.

(5) Experiments by Buttner et al (2002)

This study was conducted in an experimental room with a HVAC system to measure the resuspension effect of human activity on fungal spores. The studied activity is human walking for 1 minute under a prescribed pattern. The studied spores ranged between 2 and 3 μm in diameter and were evenly spread into the experimental room. Three different flooring types were used in the experiment, including vinyl tile, loop pile (commercial) carpet and cut pile (residential) carpet, under two surface contamination levels (10^6 and 10^7 colony forming units per square meter [c.f.u./m^2] of floor surface). The floor surface concentration was sampled before the walking disturbance and the airborne concentration was measured both before and after the walking disturbance. Buttner et al concluded that the type of flooring material and the settled biocontaminant level affect the airborne concentration of fungal spores resuspended. In Buttner et al's work, both the initial surface concentration and the airborne concentration after 1 minute walking are reported as shown in Table 7. However, the corresponding resuspension coefficients are not reported. These values can be estimated based on the concentration measurement as shown in Section 1.3.4.

Table 7 Spores concentration in Buttner et al's experiments*

Flooring type	Contamination level	Initial concentrations of spore on the floor (c.f.u./m^2)	Airborne spore concentration after 1 minute walking (c.f.u./m^3)
Vinyl tile	10^6	1.36×10^6	2.47×10^1
Commercial carpet		2.04×10^6	2.00×10^1
Residential carpet		2.15×10^6	3.81×10^3
Vinyl tile	10^7	8.22×10^7	1.61×10^3
Commercial carpet		8.04×10^7	1.57×10^3
Residential carpet		5.89×10^7	9.91×10^4

* Three walking trials were reported by Buttner et al 2002. Since the three measurements are quite similar, only the results of the first trial are cited in the table.

In Table 7, the airborne concentrations by resuspension for vinyl tile and loop pile carpet are quite close and proportional to the surface load. The airborne concentration by resuspension for cut pile carpet are much larger than those for the other two flooring types, but also proportional to surface contamination load. It can be concluded that the flooring type has a significant influence on particle resuspension coefficients, given similar activity and type of particulate contaminants.

1.3.4 Comparison of particle resuspension coefficients of human walking

From above review, it can be concluded that human walking, a common activity, is the most widely studied particle resuspension activity. A few well-controlled experiments (Fish et al 1967, Jones and Pond 1967, Hambraeus et al 1978, Karlsson et al 1999, Buttner et al 2002) were carried out to measure the resuspension coefficients associated with human walking. The researches help to define and quantify the human walking effects in indoor particle resuspension.

Most of these controlled resuspension experiments reported either resuspension factors or resuspension rates or both for particle resuspension caused by human walking. Actually, there exists a relationship between resuspension factor and resuspension rate. Given the value of one coefficient, the value for the other coefficient can be calculated or approximated as demonstrated below.

Resuspension factor (RF) and resuspension rate (RR) are most obviously correlated when the particle resuspension and deposition processes reach a dynamic equilibrium state (Hambraeus et al 1978). The relationship is shown by Equation 8, which is derived from the mass balance equation at the floor-air interface.

$$RR = RF \times \frac{V}{A} \times (h + D) \qquad (8)$$

Where: V is the volume of the room, m^3; h is the ventilation rate, s^{-1}; D is the particle deposition loss rate, s^{-1},which can be defined by Equation 9.

$$D = v_d / H \qquad (9)$$

Where: H is the room space height, m.

With Equation 8, either resuspension rate or resuspension factors can be derived given the value of the other parametric value. As shown by Equation 3, resuspension fraction is also a useful resuspension coefficient and can be derived from resuspension rate.

It needs to be noticed that Equation 8 is not applicable to the experiments of Buttner et al (2002) because the equilibrium state between resuspension and deposition was not achieved during the experiments. Using the experimental results, the particle resuspension factors right after the one minute of human walking can be calculated by Equation 1. Assuming the spores were resuspended evenly and the deposition is neglected as compared to the resuspension during the one minute of walking, the resuspension rates can also be calculated.

After above discussion on resuspension coefficients calculation, the three resuspension coefficients from different particle resuspension chamber experiments with walking reservoir disturbances are concluded in Table 8.

Table 8 Comparisons between human walking related experiments

Experiments	Ventilation rate, h (h^{-1})	Airborne particle die-away rate, D (h^{-1})	Floor material	Particulate contaminants[1]	Human walking pattern	Resuspenstion factor (10^{-6} m^{-1})	Resuspension rate (10^{-6} s^{-1})	Resuspension fraction (10^{-6})
Fish et al 1967	0.0	1.67	Asphalt tile floor	ZnS MMD=3.1 μm σ_g=1.9	Vigorous walking[2]	*39.0[8]	0.04	8.5
Jones and Pond 1967[3,4]	10.9	9.2	PVC, lino waxed and polished	Plutonium oxide, NMD=5 μm, 10500 kg m^{-3}	14 steps/min, for 60 min	*4.5	0.08	121.3
					36 steps/min, for 60 min	*29.8	0.52	312.3
				Plutonium nitrate	14 steps/min, for 60 min	*0.7	0.01	19.9
					36 steps/min, for 60 min	*6.3	0.11	66.0
Hambraeus et al 1978	0.0	1.9	vinyl tile floor	Staphylococcus contaminated particles, 3~6 μm	4-person walking for 30 min	*3500.0	5.91	1477.8

Table 8 comparisons between human walking related experiments (continued)

Experiments	Ventilation rate, h (h^{-1})	Airborne particle die-away rate, D (h^{-1})	Floor material	Particulate contaminants[1]	Human walking pattern	Resuspenstion factor (10^{-6} m^{-1})	Resuspension rate (10^{-6} s^{-1})	Resuspension fraction (10^{-6})
Karlsson et al 1999[5]	0.0	6.9	N/A	Spores of Bacillus Subtilus, 12 μm by assuming spherical shape (density=1.3 g/cm^3)	4-person walking at 75 steps/min for 60 min	811.7	4.67	*500.0
Buttner et al 2002[6, 7]	0.0	0.3	Vinyl tile	fungal spores, 2 ~ 3 μm	walking for 1 minute in a prescribed pattern[2]	19.0	6.92	3161.9
			Loop pile carpet			14.9	6.92	3161.9
			Cut pile carpet			1780.0	633.33	289523.8

1. When the particle density is not reported by the research or not easy to identify, the particle density is assumed as 1000 kg/m^3.
2. No detailed information about the walking speed is provided; it is assumed to be 100 steps/minute in the calculation.
3. There are different floor types in this experiment; the results from PVC and waxed lino are very close and cited together to give average RF results.
4. Size distribution and density information are not available for plutonium nitrate in this experiment; the calculation is based on the info from plutonium oxide.
5. The height of the experimental room is not reported and is assumed to be 3.0 m.
6. No detailed information about the walking speed is provided; it is assumed to be 75 steps/min in the calculation.
7. Because Buttner et al concluded that the resuspension coefficients are independent of surface load, the reported values in the table are the average values of different loads for the same carpet type.
8. * means this value is directly reported in the literature; otherwise, the value is estimated in this work from the field measurements in the literature.

In Table 8, the resuspension factors and resuspension rates for walking in various controlled experiments still varies greatly. The resuspension factors vary from 7.0×10^{-7} to $3.5\times10^{-3}\,m^{-1}$ and the resuspension rates vary from 1.0×10^{-8} to $6.3\times10^{-4}\,s^{-1}$.

If the experimental results are divided into two groups according to particle components as mineral particles and organic particles (mainly spores in literature), a more uniform trend of resuspension coefficients can be observed. For example, when the floor covering is made of vinyl tile or similar materials, for mineral particles between 1~10 μm, the resuspension factors ranges from 7.0×10^{-7} to $3.9\times10^{-5}\,m^{-1}$ and the resuspension rates vary from 1.0×10^{-8} to $5.2\times10^{-7}\,s^{-1}$,both within two orders of magnitude; for organic particles between 1~10 μm, the resuspension factors ranges from 8.1×10^{-4} to $3.5\times10^{-3}\,m^{-1}$ and the resuspension rates vary from 4.67×10^{-6} to $6.92\times10^{-6}\,s^{-1}$,both within one order of magnitude. These observations show that particle property has great influence on particle resuspension phenomena, and organic particles generally have larger resuspension coefficients than mineral particles with similar particle size distribution.

The only extremely large resuspension coefficients, derived from Buttner et al (2002), are for the resuspension of spore particles from cut pile carpet. This outlier seems to indicate that floor covering type, just like the particle properties, can influence the particle resuspension phenomena greatly.

The analysis shows that particle resuspension coefficients of walking from controlled experiments have a better repeatability and a uniform trend. However, a few problems still remain to be solved.

1) The underlying physical mechanisms of particle resuspension from walking need to be elucidated for a better understanding of particle resuspension phenomena.
2) Systematic resuspension experiments should be carried out, with controlled variation of such parameters as floor covering type, particle properties, relative humidity and walking pattern.
3) It is still too expensive and time consuming to carry out particle resuspension experiments in large chambers with real human activities. A smaller and well-controlled chamber that can simulate particle resuspension by human activity can be helpful for carrying out systematic particle resuspension studies.

1.4 Objectives of the Research

Indoor particle resuspension is a complicated phenomena, generated under the combined influence of many disturb force components. The proposed research studies the effects of electrostatic fields, generated by walking, on particle resuspension in indoor environment. There are many factors that can influence the electrostatic effects on particle resuspension. This work focuses on such factors as particle properties, floor type, walking pattern and indoor relative humidity.

There are several major objectives of this research. First, the basic physical principles underlying particle resuspension are to be analyzed. Particle resuspension forces, generated by human activity on particles, can be decomposed into three types: mechanical vibration induced momentum transfer, aerodynamic drag and electrostatic forces. A parametric study is carried out to compare the magnitudes of different particle resuspension force components introduced by walking and the particle-surface adhesion force, the major force preventing micron-sized particles from resuspension. In order to estimate the magnitude of the electrostatic resuspension force, the principles of human body charging during walking and particle charging under exterior electrostatic field are discussed. Experiments are also designed to measure the real adhesion force between different particles and flooring materials based on the electrostatic detachment method. Comparisons are carried out between the measured values and the theoretical calculation results.

Although controlled large chamber experiments are helpful in determining the particle resuspension coefficients of human walking, due to the cost and complexity of the experiments, the reported experimental results are still very limited. Thus, this study uses a particle resuspension chamber as the major facility to systematically study the walking-induced electrostatic effects on particle resuspension. Experiments are also designed in this study to acquire the floor surface electrostatic field strength that can be generated by human walking in indoor environment. The measured field strength profile will be used for the electrostatic field simulation in the resuspension chamber experiments.

The resuspension experiments intend to identify whether the electrostatic effects can significantly influence particle resuspension phenomena and how different parameters such as particle property and floor type can influence such effects. To testify the validity of the chamber experiments, resuspension coefficients measured from the small resuspension chamber experiments are compared with the results from reported field experiments.

This work also studies the applicability of multizone airflow and contaminant dispersion models in simulating particle resuspension and dispersion in an indoor environment with a heating, ventilation and air-conditioning (HVAC) system.

CHAPTER 2. PARAMETIC STUDIES ON PARTICLE RESUSPENSION FORCES FROM HUMAN WALKING

2.1 Analysis on particle resuspension forces from human walking

This work intends to study the underlying physical mechanisms of indoor particle resuspension due to walking. Particle resuspension phenomena are caused by multi-lifting forces on reservoir particles. Adhesion force between particles and reservoir surfaces as well as gravitational force keeps particles holding positions to the surfaces. Human activity, such as walking or cleaning, introduces disturbing and lifting forces, such as mechanical vibration, airflow drag and electrostatic force on reservoir particles. These forces tend to move particles away from residing surfaces and resuspend particles into the air. The force vectors on surface residing particles are shown in Figure 3.

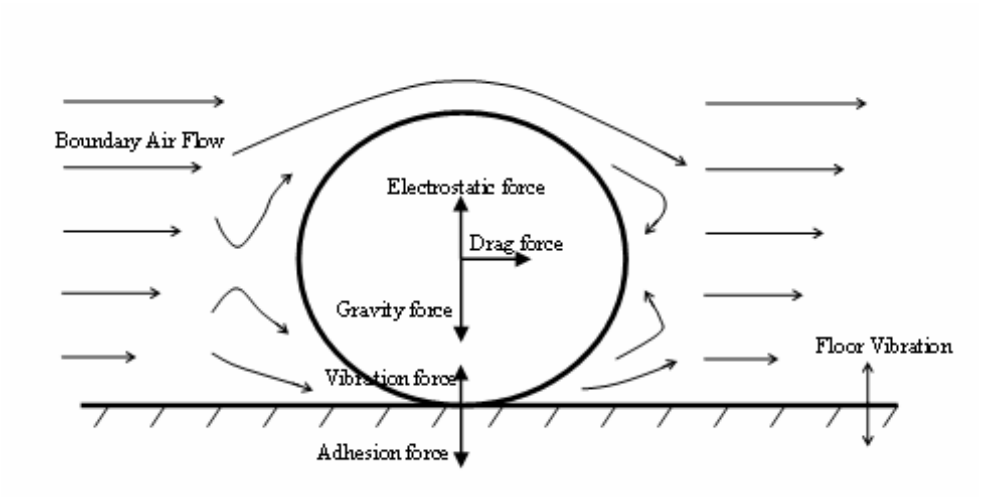

Figure 3 Force analyses on surface residing particles

Although component force analysis of particle resuspension is relatively clear, it is difficult to quantify the magnitude of each force component and compare their relative

influence on particle resuspension. The adhesion force may vary greatly due to difference in particle composition, floor covering materials and environmental parameters, such as humidity. The disturbance forces can also vary significantly in magnitude. Figure 4 displays the array of indoor environment factors that can influence each force component.

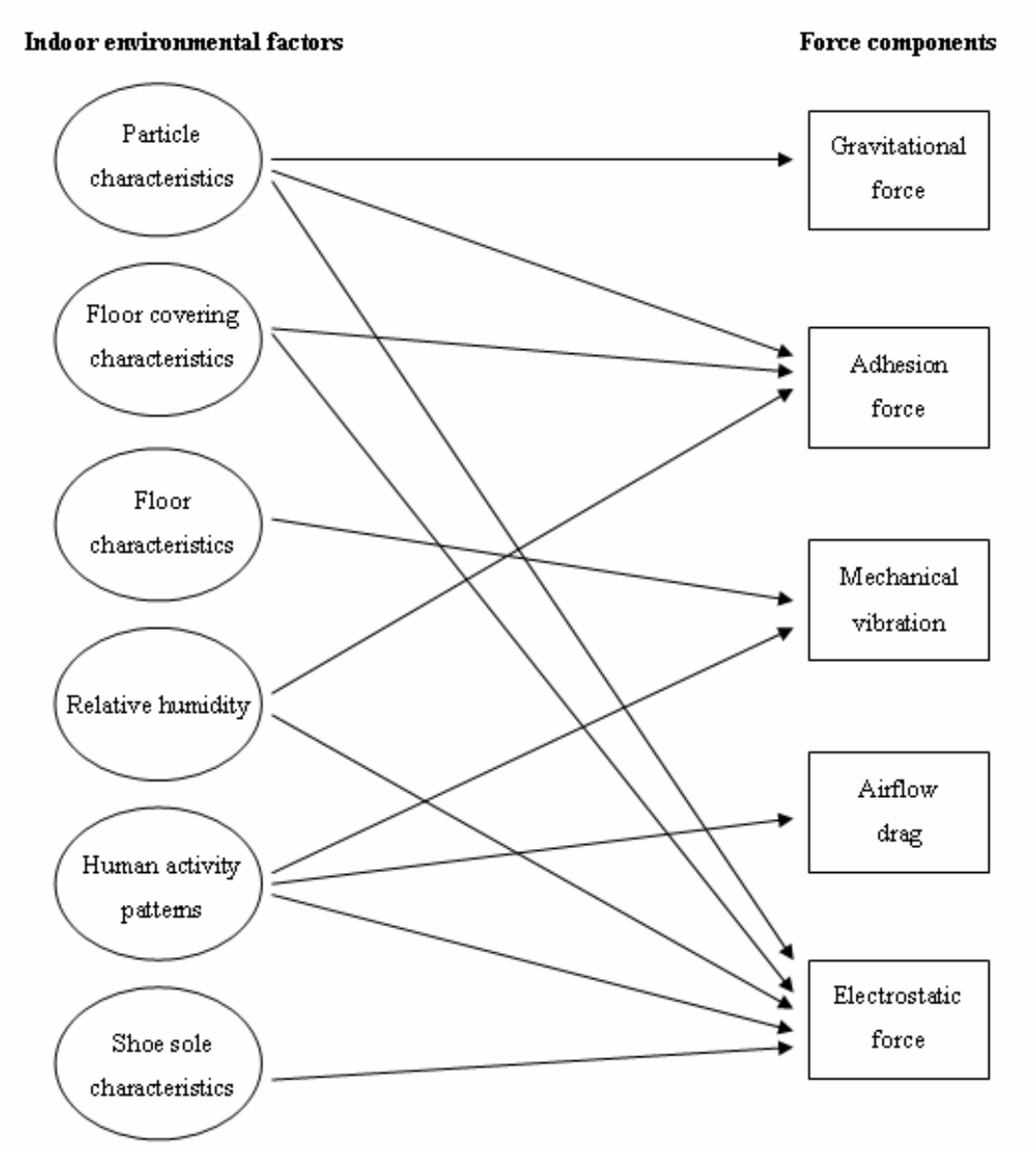

Figure 4 Factors influencing force components on residing particles

2.2 Adhesion force on particles

Micron-sized particles attach firmly to contacted surfaces, mainly due to adhesion forces. The surface nature of the adhesion force distinguishes the adherence behavior of micron-sized particles from gas molecules and millimeter-sized particles. The adhesion forces on micron-sized particles can exceed the gravitational force by orders of magnitude (Hinds 1999).

The main adhesion forces include the van der Waals force, the electrostatic force and the surface tension force due to absorbed liquid films. The main parameters that can influence these forces include: the material, shape, surface roughness and size of the particle; the material, roughness and contamination of the surface; relative humidity; temperature; the duration of contact. Among the three adhesion force types, the van der Waals force is usually the greatest in magnitude.

Equation 10 (Hinds 1999) can be used to calculate the van der Waals force for initial contact between a spherical particle and a flat surface, without consideration of contact area flattening. The symbol A in Equation 10 is Hamaker constant, which depends on the materials involved and ranges from $6\sim150\times10^{-20}$ J for common materials. The separation distance x between particle and substrate, due to irregular contact surfaces, is usually assumed to be 0.4 nm.

$$F_{adh} = \frac{Ad_p}{12x^2} \qquad (10)$$

After the initial contact between a particle and a surface, the particle adhesion force can gradually deform the particle and/or the contacted surface to decrease the separation distance and increase the contact area until a new force equilibrium is reached. Such increase of contact area can increase the adhesion force by up to fifteen-fold in soft metals and more than one hundred-fold in plastics (Tsai et al. 1991). Krishman and Busnaina (1994) studied the time dependent, deformation effect on the adhesion force of micron-size polystyrene latex particles to silicon substrates. Equation 11 shows the contact area A_C, in units of μm^2, as a function of time t by fitting the experimental data.

$$A_c = 0.059 + 0.012\ln(t/\tau) \qquad (11)$$

Where: τ is a time constant for the latex particle and silicon substrate contact, =148 hours.

Relative humidity is another important factor that can influence the particle adhesion force. When the relative humidity is high, particle adhesion force can increase due to absorbed liquid films between particles and contact surfaces. Corn and Stein (1965) carried out direct measurements on the adhesion force between glass and quartz particles (>20 μm) at 25 °C. A useful empirical expression for the adhesion force between hard materials and clean surfaces as a function of relative humidity is shown by Equation 12.

$$F_{adh} = 0.063 d_p [1 + 0.009(\%RH)] \qquad (12)$$

Where: RH is the relative humidity, %.

Based on Equation 10, the van der Waals adhesion force can be calculated and compared with gravitational force for particles with diameters between $0.1 \sim 10.0 \mu m$, as shown in Figure 5. The Hamaker constant A, is assumed to be 1.0×10^{-19} J in the calculation.

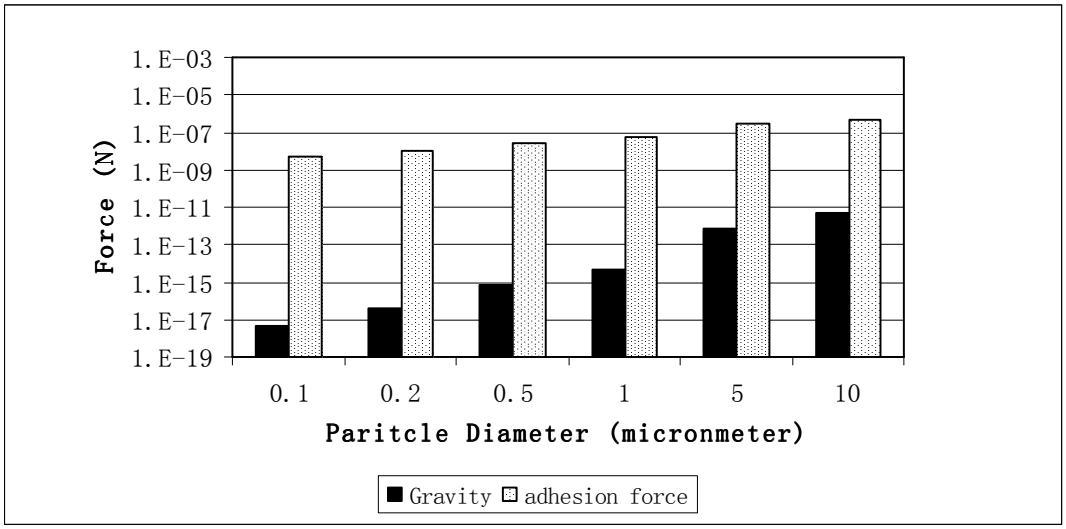

Figure 5 Comparison between adhesion force and gravitational force

Figure 5 shows that, for micron-sized particles, the adhesion force is several orders larger than the gravitational force in magnitude. However, the actual separation distance x between particles and surfaces can be much larger than the values encountered in experiments, due to the irregular morphology, roughness of the contacting surfaces. For this reason, actual particle adhesion forces can be much smaller than the values calculated by the theoretical models. However, the reduced adhesion force can still be considerably larger than corresponding gravitational forces for micron-sized particles.

In a recent report (Matsumoto 2003), researchers suggested that anthrax used on the terrorism attacks on US buildings in 2001 were intelligently weaponized by using a layer of silicon bumps around the anthrax spores. These silicon bumps can reduce the adhesion forces of anthrax particles to any surfaces impacted and thus increase their susceptibility to resuspension. The surface engineering may explain why these particles were easily resuspended and could maintain a high steady state concentration inside buildings for a long period of time.

2.3 Mechanical vibration force on particle resuspension

The floor vibration response due to human activity is the natural frequency or free resonance-like vibration mode of the floor. It is a unique characteristic of each building

and dependent on the building's structure properties. This vibration phenomenon can be modeled as a sinusoidal curve. The floor surface movement is governed by the following classic formulas.

$$\text{Displacement (m): } y = A\sin(2\pi ft) \tag{13}$$

$$\text{Velocity (m/s): } v = y' = 2\pi fA\cos(2\pi ft) \tag{14}$$

$$\text{Acceleration (m²/s): } a = y'' = 4\pi^2 f^2 A\sin(2\pi ft) \tag{15}$$

Where: A is the amplitude of vibration, m; f is the vibration frequency, s^{-1}.

Human perception of floor motion depends strongly on the activity type and level of the occupants. For example, in sporting facilities, the floor can vibrate considerably while nobody senses the motion. However, the same vibration intensity can be intolerable in a concert hall. The Institute of Steel Construction (Murray et al 1997) advises that for offices and residential buildings, people will start to feel uncomfortable if the floor vibrates above 0.5% of the gravitational acceleration. For a typical building, the vibration frequencies are between 4 to 8 Hz.

The maximum normal force tending to remove particles from a surface during floor vibration is shown in Equation 16.

$$F_{v,\max} = m \cdot a_{\max} = \frac{\pi \cdot d_p^3}{6}\rho_p \cdot 4\pi^2 f^2 A = \frac{2}{3}\pi^3 d_p^3 \rho_p f^2 A \tag{16}$$

Based on above information, calculations can be performed to estimate floor vibration force on micron-sized particles. In this calculation, the particles have a unit density. The vibration frequency is 8 Hz and vibration amplitude is 0.005 m. These settings are considered quite conservative for normal situations. The comparison between vibration forces and gravitational forces for different particle size is shown in Figure 6.

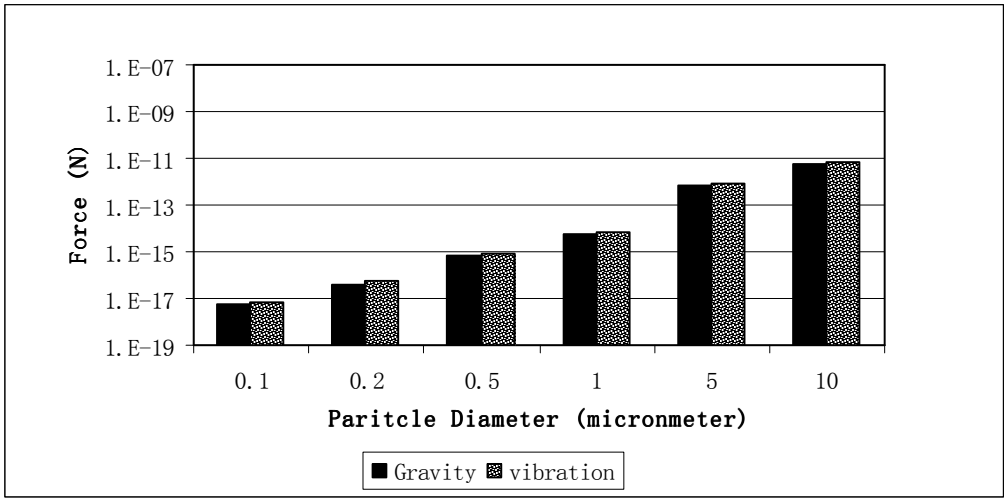

Figure 6 Comparison between vibration force and gravitational force

In Figure 6, the floor vibration force is just a little larger than the gravitational force for micron-sized particles. If there is no adhesion force between particles and a surface, the vibration force alone can resuspend particles from the residing surface into the air. However, an adhesion force normally exists between particles and surfaces, and, as indicated previously, such force can be a few orders larger in magnitude than gravitational force for micron-sized particles. Thus, for aged surface dusts in micron sizes, where the surface adhesion force is well established and much larger than the gravitational force, mechanical vibration alone is suspected to have negligible effect on particle resuspension.

This analysis agrees with the investigative findings reported in the literature. Corn and Stein (1965) concluded that the vibration frequency and displacement to overcome the weight of particles and their adhesion force with the floor need to be so large that would very unlikely be encountered in normal buildings. Walker and Fish (1964) also carried out experiments on the vibration effects on particle resuspension. In their experiments, the maximum removing force generated by vibration is about 90 times of gravity. However, no particles were resuspended. In general there appears to be a minor effect of surface vibration on particle resuspension in indoor environments.

2.4 Aerodynamic force on particle resuspension

Air currents introduced by human activities can add drag force to both the particles residing on the room surfaces and the particles floating in the air. The air drag force F_d on a floating particle of diameter d_p, caused by an air current with velocity v, is given by Equation 17 (Hinds 1999).

$$F_d = \frac{3\pi\mu v d_p}{C_C} \qquad (\mathrm{Re} < 1) \qquad (17)$$

Where: μ is the dynamic viscosity of air, $\approx 1.84 \times 10^{-5}$ at 20°C; C_C is the Cunningham slip correction factor.

The Cunningham slip correction factor C_C is used to take into account the slipping effects between gas and particle surface when particle size is smaller than 1 μm and approaches the mean free size of gas. Calculation of Cunningham slip correction factor is shown in Equation 18.

$$C_c = 1 + \frac{\lambda}{d_p}\left[2.34 + 1.05 \cdot \exp\left(-0.39\frac{d_p}{\lambda}\right)\right] \qquad (18)$$

Where: λ is the air mean free path, mm.

The air mean free path λ is the average distance traveled by air molecules between collisions with each other. It is assumed that particle motion occurs at low Reynolds number (Re<1), which is true for small size aerosols moving at slow velocities. Equation 19 shows the calculation of the air mean free path.

$$\lambda = 10^5 \times \frac{\frac{\mu}{0.499}\sqrt{\frac{\pi}{8}}}{\rho_{Air} \cdot P} \qquad (19)$$

Where: P is the atmosphere pressure, Pa .

Comparison between air drag force and particle gravitational force is shown in Figure 7. The air current velocity is assumed as 0.25 m/s, which is common for indoor air flow near floor surface induced by human walking (Gomes 2004).

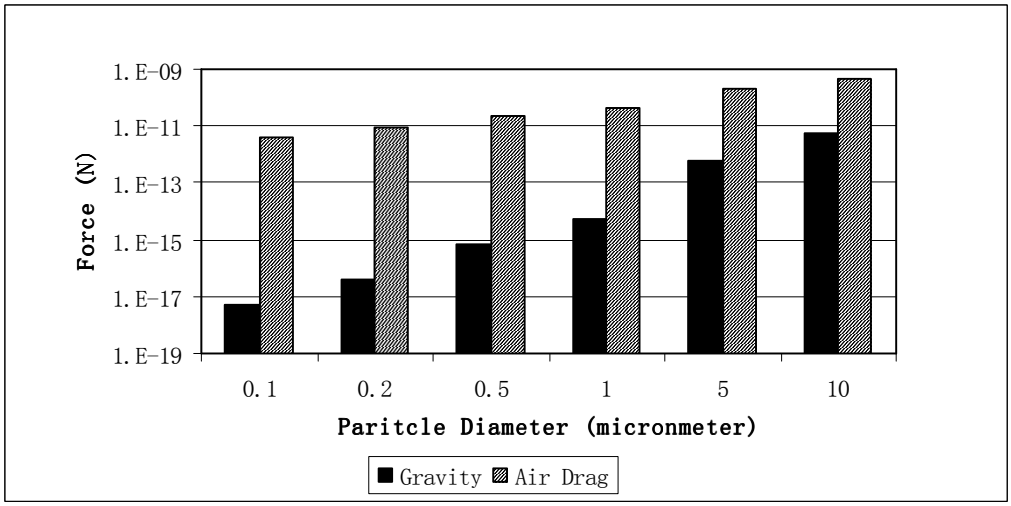

Figure 7 Comparison of particle gravitational force and air drag force

By comparing air drag force with particle gravitational force, it can be concluded that, once micron-sized particles move into the air, the air drag force can keep the particles in suspension status for a long time. According to Corn and Stein (1965), after particles become airborne, room air currents could, theoretically, keep unit density particles as large as 90 μm floating.

The particle drag force model presented above assumes that particles are entrained by an air stream and not affected by solid physical boundaries, such as a wall surface. The presence of a wall or any other solid surface can have a significant effect on the air velocity profile and thus influence the drag force. Velocity of air flow decreases as it gets close to a surface due to the formation of a boundary layer. As the air contacts with a wall,

it has no velocity on the wall surface under no-slipping condition. Thus, for the surface residing particles, the air drag force model is quite different to Equation 17. Equation 20 (Punjrath and Heldman, 1972) is used to calculate boundary layer drag force for surface residing particles.

$$F_d = \left[\frac{\pi d_p^{\,2}}{4}\right]\left[C_{fx}\rho_{Air}U^2/2\right] \qquad (20)$$

Where: C_{fx} is the local shear stress coefficient; U is the velocity of free stream.

When air flow passes the surface of a plate, a boundary layer is formed on the surface. First, a laminar layer is formed from the origin of the boundary layer. As the boundary layer develops downstream, it changes from laminar flow into turbulent flow. The boundary layer property can change the value of local shear stress coefficient C_{fx}. The relationship between C_{fx} and the distance x from the leading edge of boundary layer can be illustrated in Figure 8 (Punjrath and Heldman, 1972).

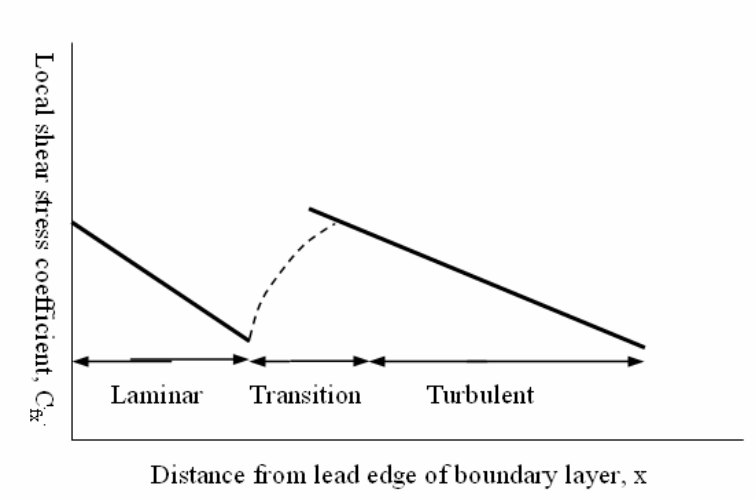

Figure 8 Influence of location on a flat surface on the local skin friction coefficient

Figure 8 shows that there are two extreme large values of C_{fx} within the surface boundary layer. One is at the beginning of the laminar layer and the other is at the transition point from laminar to turbulent. The later value is considered more critical and is the point where surface particles endure the highest drag force within the boundary layer. Schlichting (1968) described the local aerodynamic shear stress coefficient for a turbulent regime along a rough flat plate in Equation 21.

$$C_{fx} = \left(2.87 + 1.58 \log \frac{x}{k}\right)^{-2.5} \qquad \left(10^2 < x/k < 10^6\right) \qquad (21)$$

Where: k is the mean height of rough protrusions on the surface, m.

Based on Equation 20 and 21, the boundary drag force on surface residing particles can be calculated and compared with gravitational force as shown in Figure 9. In the calculation, the free stream air flow velocity U is assumed as 1.0 m/s.

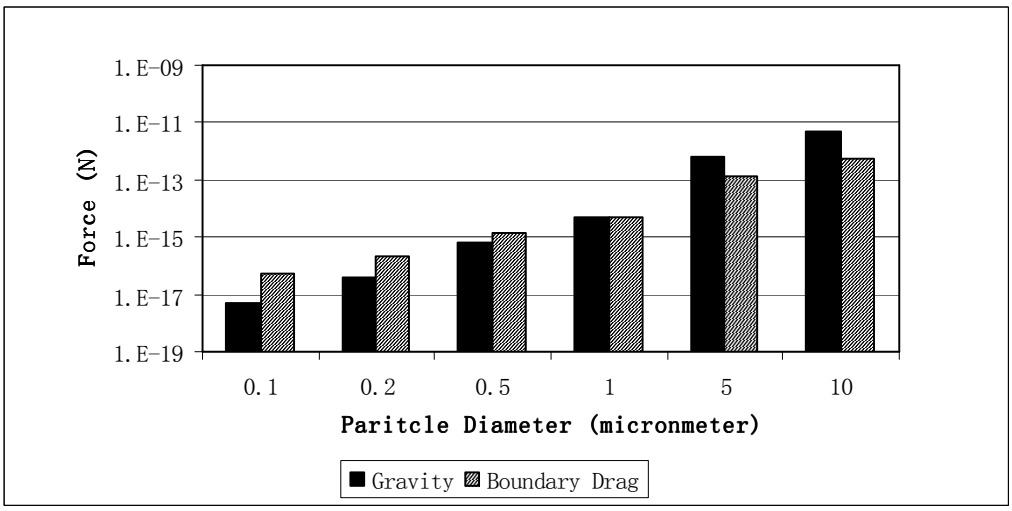

Figure 9 Comparison of particle gravitational force and boundary drag force

Figure 9 shows that the magnitude of boundary drag force changes greatly with the particle diameter relative to the magnitude of particle gravitational force. When particles are smaller than 1 μm, the boundary drag force is larger than the gravitational force in

magnitude. When particles are larger than 1 μm, the boundary drag force becomes smaller than the particle gravitational force. When the boundary drag force is compared with the adhesion force as calculated in Section 2.3, it is difficult to conclude that the boundary drag force alone can overcome the much larger adhesion force and initiate resuspension of micron-sized particles from surfaces.

To partly explain the particle resuspension phenomena caused by aerodynamic force, a particle rolling and sliding theory is proposed in the literature. It is observed that resuspension of particles under air flow is always preceded by particle rolling and sliding (Punjrath and Heldman 1972). The forces required to roll or slide surface particles are much smaller and approximately 1% of those required for static detachment of particles in the normal direction of the surface (Hinds 1999). Once micron-sized particles start to slide or roll on a surface, the adhesion force between particles and the surface is greatly reduced due to decreased contact area. The adhesion force for particles moving along the surface may be equal to or smaller than the adhesion force for freshly deposited particles, and, therefore, much smaller than aged deposited particles. After the surface particles start rolling and sliding downstream, the momentum transfer caused by particle collisions can initiate particle detachment from the surface (Punjrath and Heldman 1972).

The turbulence intensity T_i of free stream can also influence the air drag force on the surface reservoir particles. Some studies (Schubauer and Skramstad 1947, Punjrath and Heldman 1972) found that the critical Reynolds number (Re_x), at which the boundary flow transfer from laminar flow turbulent flow, decreases as the turbulence intensity in the free stream increases. This can influence the location of critical point where the particle sliding and rolling initiates, given a specific free stream air flow velocity.

Barrett and Hollingsworth (2003) concluded that free stream turbulence intensity can also influence the skin-friction coefficient C_f as illustrated in Equation 22.

$$\sqrt{C_f/2} = 0.117\left(L_e^+\right)^{-1/18} T_i^{0.18} \qquad (22)$$

Where: $L_e^+ = 2.25\,\mathrm{Re}_\theta^{3/4}$ is the dimensionless turbulent length scale, based on energy; Re_θ = Reynolds number, based on boundary layer momentum thickness θ.

Besides the collision resuspension theory, many researches focused on the aerodynamic lift force in the surface boundary layer. Several researches (O'Neill 1968; Goren 1970; Cleaver & Yates 1973) tried to get approximate solutions of the motion equations of a fluid around a sphere on a flat surface. While these works have limited applications due to their focus on low particle Reynolds numbers and remain unproven, Hall (1988) set up experiments to measure the mean boundary lift forces (F_L) in turbulent flow on surface residing particles. Hall's work leads to an empirical relationship as shown in Equation 23.

$$\frac{F_L}{\rho \nu^2} \approx 20.9\left(\frac{r u_\tau}{\nu}\right) \qquad (23)$$

Where: ν is kinematical viscosity, m^2/s; r is the radius of particles, m; u_τ is the frictional velocity, $u_\tau \equiv \sqrt{\tau_w/\rho} = \sqrt{C_f \cdot U^2/2}$.

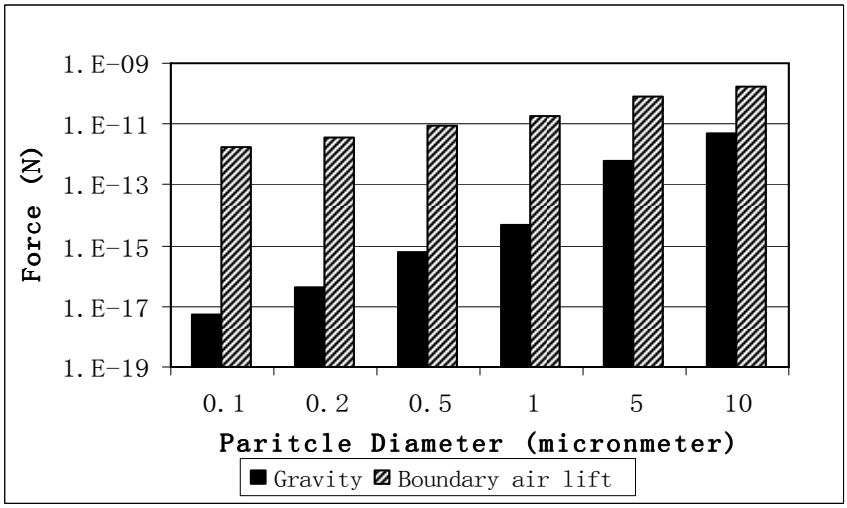

Figure 10 Comparison of particle gravitational force and boundary lift force

Figure 10 shows the comparison between gravitational force and boundary lift force for micron-sized particles based on Equation 23, with a free stream air flow velocity U of 1.0 m/s. It can be observed that the boundary lift forces are much larger than the particle gravitational forces. After the surface adhesion force is greatly reduced by the rolling and

sliding movement of particles, the surface particles are apt to be carried into the air by the boundary lift forces.

Once resuspended into the air, the particles can easily be taken away by the air currents as demonstrated in Figure 7. The movement of floating particles is primarily controlled by the balance between the air convection drag force and particle gravitational force.

In above discussion, two particle resuspension mechanisms due to aerodynamic flow are discussed: particle rolling & collision and boundary lift force. The actual particle resuspension phenomena by aerodynamic effects are very complicated and, due to the focus of this thesis, such effects are not discussed in further details in this work. The surface air flow pattern due to human activity is so complex that more experimental and computational studies are needed to further explain the surface air drag effects on particle resuspension phenomena.

2.5 Electrostatic force on particle resuspension

Human activity can generate electrostatic fields in indoor environments. Electrostatic fields from the human body to particle reservoirs can charge reservoir particles and result in electrostatic forces that cause particle resuspension from residing surface. The resuspension processes induced by transient electrostatic fields are not well understood, compared to the knowledge available for mechanical and aerodynamic resuspension processes of particles. The electrostatic effect on indoor particle resuspension is the focus of this thesis study.

2.5.1 Human body electrostatic charge

A person can accumulate charge through such common functional activities as walking and taking off clothes. Sparkles from taking off clothes and shocks from touching a door knob are common illustrations of electrostatic discharging. Such phenomena are especially obvious in winter when relative humidity of indoor air is extremely low.

The electrostatic charging is mainly caused by frictional contact between two materials of dissimilar composition, for example, between shoes and floor covering. The charge accumulation creates electrical fields in the space around. The amount of static body charge accumulation, and the subsequent electrostatic field strength, depends on many factors such as materials, frictional intensity and indoor environment relative humidity. Insulators can generally create more static charge accumulation than conductors. Figure 11 shows a brief triboelectric series diagram of different materials.

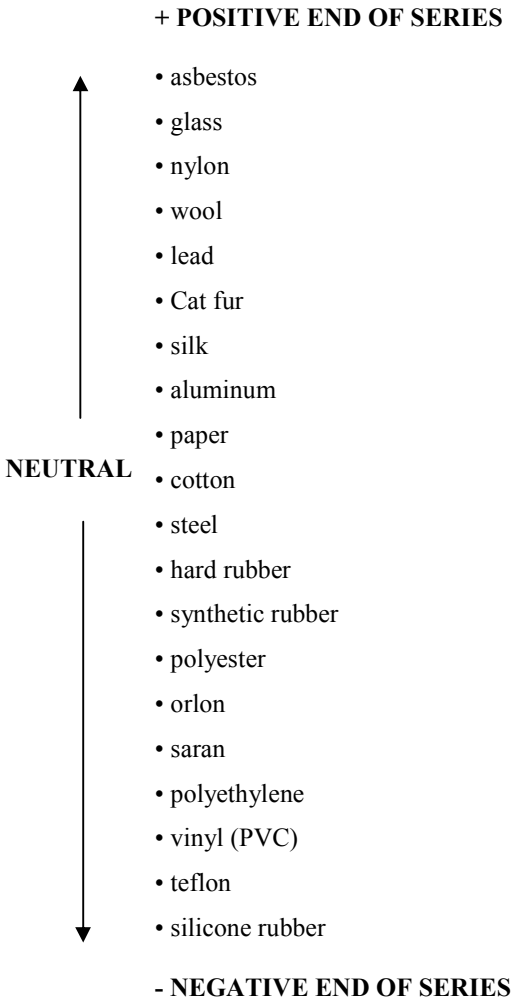

Figure 11 Triboelectric series

Upon frictional interaction, the material closer to the positive end of the series will be charged positively while the other material will be charged negatively. For example, when a person in rubber shoes is walking on a vinyl tile floor, the floor surface is charged negatively while the human body is charged positively.

The friction between rubber shoes and floor can increase the human body electrostatic voltage to levels from 250 to 12000 volts for untreated vinyl floor and from 1500 to 35000 volts for carpets (Reade 1997). Within the short distances between human foot and floor, the voltage results in high electrostatic field strength between the shoe surface and the surface of the floor, the potential particle reservoir. Equation 24 (Jonassen 2001) can be used to describe the electrostatic body voltage (V_b) generated by human walking. This equation is derived from the electric current balance between the charging current and decaying current

$$V_b = R_b n_w \Delta q_{step} \qquad (24)$$

Where: Δq_{step} is the friction-induced average charge separation between shoes and a floor surface by each step of walking, C; R_b is the body resistance to the ground, Ω; n_w is the walking steps in unit time, s^{-1}.

With an electrometer, the separation charge (Δq_{step}) and body resistance (R_b) can be measured. Jonassen (2001) reported an average value of $3.0\times10^{-8} C$ for Δq_{step} and $1.0\times10^{11}\Omega$ for R_b in his experiments. Thus, given a walking frequency of 2 steps per second, electrostatic body voltage can rise to an equilibrium value of 6 kV after continuous walking activity. However, in the field experiments by Jonassen, the maximum human body voltage measured was about 3.5 kV. Jonassen explained this discrepancy by that the effective body resistance would decrease as the human voltage increases. The body resistance value of $1.0\times10^{11}\Omega$ in the calculation of theoretical maximum voltage was measured under a relatively low voltage of 300 V. Thus, Equation

24 provides an upper limit estimation of the maximum body voltage after continuous walking.

Besides the model for equilibrium body voltage after continuous walking, Jonassen (2001) also proposed the model for body voltage after one-step walking. In order to illustrate the one step voltage model, the human body charging process during walking needs to be analyzed first. One human walking step can be approximately divided into two stages: a simultaneous charging and discharging stage, followed by a discharging only stage. After one foot is lifted from the floor and before this foot contacts the floor again, the human body discharges accumulated charge through the other foot contacting the floor, and no significant charging takes place. For simplification, this period is called a discharge only stage. After the lifted foot re-contacts the floor and makes full contact, the human body is charged, while the discharging through contacting feet continues at the same time. This period is call a simultaneous charging and discharging stage. Actually, the two stages may overlap and the so-called discharge only stage may also have charging phenomena, though it may not be significant. This idealized process can be demonstrated in Figure 12.

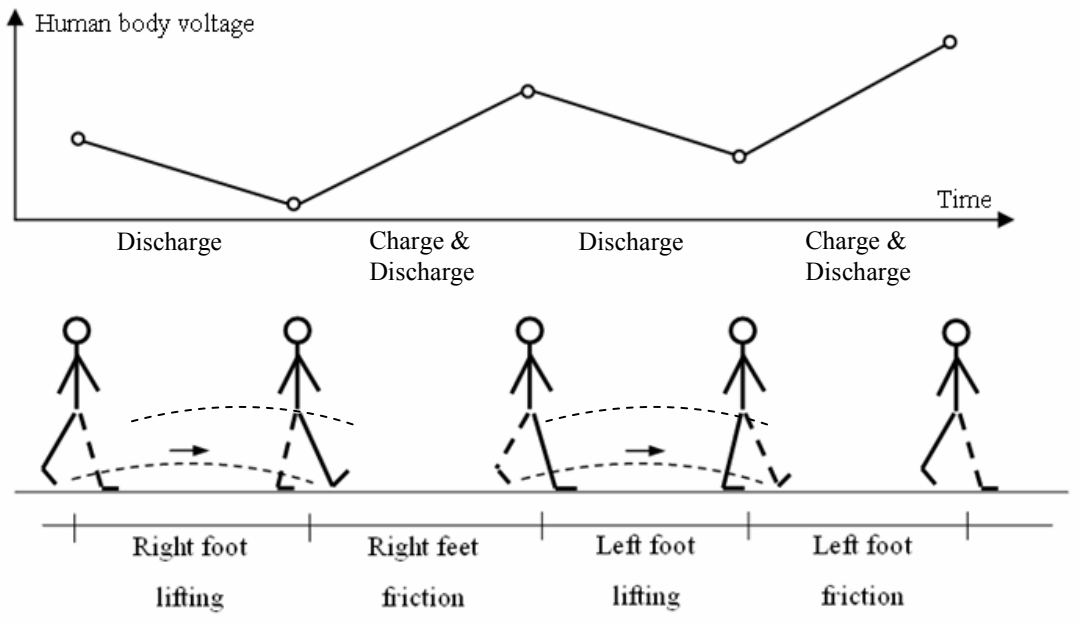

Figure 12 Human walking and charging process
(Dashed leg is left leg and solid leg is right leg)

The one step body voltage model is described by Equation 25.

$$\Delta V_b = \frac{\Delta q_{step}}{C_b} \cdot \frac{R_b C_b}{\Delta t}\left(1 - e^{-\frac{\Delta t}{R_b C_b}}\right) \qquad (25)$$

Where: ΔV_b is the body voltage increase right after a simultaneous charge and discharge stage, with time length Δt ; C_b is the human body capacitance, F.

Jonassen (2001) measured the human body capacitance C_b to be 100 pF with one foot on the floor and assumed 0.1 second for Δt. Then, the calculated human body voltage increase in one step is 180 V. Because of the existence of the discharging process during human walking, it is possible that acquired body charge decays so quickly that no significant electrostatic voltage accumulates during walking process. For the specific example above, $4.5 \times 10^9 \Omega$ is calculated as the critical R_b value, below which the equilibrium human body voltage achieved by continuous walking can not exceed the transient voltage peak within a single step.

2.5.2 Particle charging principles

There are four major particle charging mechanisms: corona charging, triboelectric charging, induction charging and diffusion charging. The particle charging caused by human activity can be a process combining several charging mechanisms while a given mechanism may be more important than others in certain situations.

1) Corona charging of particles

Corona charging can happen when local electric field around a pointed metal object is as high as 3.0×10^6 V/m (Hughes 1997). In the high local electric field, free electrons can be accelerated to such a high speed that they can knock out more free electrons from

initially neutral molecules of N_2 and O_2 in the air. In this way, free electrons and positive ions are generated. When free electrons are attached to neutral molecules in the air, negative ions are generated. The ions have relatively low mobility and can attach to nearby particles suspended in the air. This charging process is called corona charging.

Extremely high local electric fields can often be found near electrodes with sharp features. For example, the sparks between human finger tips and metal door knobs in winter are generated by corona discharging processes. When the finger tips get close to such projected objects as knobs and power switches, extremely high local electric fields ionize the molecules in the air gap between the finger tips and the projected objects.

Corona discharging phenomena are common in the winter, indicating that significant high voltages are generated on people through their activity. When such corona discharging sparks are observed, the human body electrostatic voltage may have reached 2 to 20 kV (Jonassen 1998). During walking, an electrostatic field is formed between shoes and floor surface. If the floor surface particles have projected surfaces, which is common for many mineral particles, such particles can intensify the local field strength around their surfaces and ionize the local air. Due to the small size, corona discharge phenomena of micron-sized particles may not be easily observed by human eyes.

When particles acquire excess surface charge, local electric fields are formed on their surface. When the charges are high enough to generate very strong local electric fields, the air around the charged particles is ionized. The air ionization prevents the highly charged particles from accumulating more charges. Thus, the corona charge principle can be used to set the upper limits of particle charge (q_L), as shown in Equation 26 (Hinds 1999).

$$q_L = \frac{d_p^2 E_L}{4K_E} \tag{26}$$

Where: E_L is the surface electric field strength limit for air ionization, which is $9.0\times10^8 V/m$ for negatively charged particles and $2.1\times10^{10} V/m$ for positively charged

particles. K_E is the electrostatic constant of proportionality or Coulomb force constant, which is $9.0\times10^9 N\cdot m^2/C^2$.

Table 9 lists the charging limits of micron-sized particles, as calculated with Equation 26.

Table 9 Charging limits of micron sized particles

Diameter (μm)	0.1	0.2	0.5	1.0	2.0	5.0	10.0	20.0
Negatively charged particles (C)	1.0E-15	4.0E-15	2.5E-14	1.0E-13	4.0E-13	2.5E-12	1.0E-11	4.0E-11
Positively charged particles (C)	2.3E-14	9.3E-14	5.8E-13	2.3E-12	9.3E-12	5.8E-11	2.3E-10	9.3E-10

2) Triboelectric charging of particles

Triboelectric charging is caused when particles frictionally interact with a solid surface of a different material. In industry, triboelectric charging of particles is widely applied in powder coating application. When powders are transferred through a coating gun system, a type of particle feed nozzle, charge exchanges occur between the particles and the internal surface of the coating gun due to friction. Charged micron-sized particles have better coating performances than uncharged particles since the particles have an additional electrostatic adherence force to the coated surface relative to van de Waals adherence force of uncharged particles.

Human walking can result in some fraction of the particles on a floor surface to be charged directly by the friction between shoe soles and floor surface. Since the shoe material and floor reservoir material charge oppositely due to triboelectric property difference, some of the oppositely charged particles associated with the reservoir may be directly attached to the surface of the shoe soles. It is difficult to quantify the charge amount acquired by particles during this process. For simplification purpose, we assume that particles significantly charged during this friction process attach to the shoe sole surface firmly due to electrostatic attraction force and remain there for a certain time.

Thus the particles directly transferred from the reservoir to the shoe surface and attached by electrostatic adhesion are not considered for the immediate air resuspension from the floor reservoir.

3) Induction charging of particles

When there is an electrostatic field surrounding particles, the particles without any charge tend to distort the nearby field lines to end on the particle surfaces. Electrons or ions move along the voltage gradient established by the distorted field lines and eventually rest on the surface of the particles. When the charge on the particles increases, the particles become less attractive to electrons or the ions with the same charge. Eventually, a charge limit is reached for this charging process. Equation 27 (Hinds 1999) shows the calculation of induced charge for airborne particles as a function of time t.

$$q(t) = \left(\frac{3\varepsilon_r}{\varepsilon_r + 2} \right) \left(\frac{E d_p^{\,2}}{4K_E} \right) \left(\frac{\pi K_E e Z_i N_i t}{1 + \pi K_E e Z_i N_i t} \right) \qquad (27)$$

Where: ε_r is the relative permittivity of particles; E is the field strength, V/m; Z_i is the mobility of the ions, which is about $1.5 \times 10^{-4} m^2/V \cdot s$; N_i is the ion number concentration, $\#/m^3$.

The first two factors of Equation 27 give the induction charge limit, given sufficient charging time. Equation 27 assumes the particles to be charged are suspended in the air containing charged irons. In the industry application of induction charge, the ion concentration in the air can be as high as 10^{13} $\#/m^3$ (Hinds 1999). In this case, the charging time to reach 95% charging limit is no more than 3 s.

The induction charge for surface particles can be different from that for airborne particles. For particles on the floor surface, the charges induced by the electronic field are both from the air and the reservoir surface or other contacting particles, as shown in Figure 13.

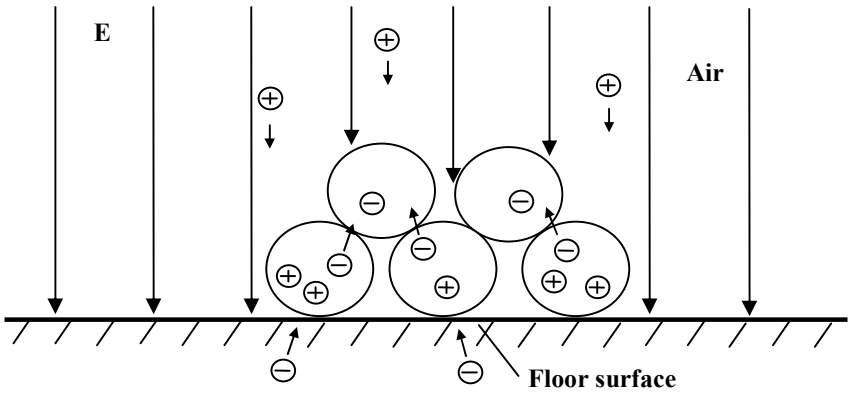

Figure 13 Induction charges on particles residing on insulating floor

For surface residing particles exposed to an electric field E, the saturation charge by induction can be predicted by Equation 28 (Wu et al 2004).

$$q_s = \frac{\pi^3}{18} p\varepsilon_0 d_p^2 E \qquad (28)$$

Where: p is the Pauthenier's coefficient and is defined by Equation 29; ε_0 is the permittivity of free space, $\approx 8.8542\times10^{-12} C^2/\left(N\cdot m^2\right)$.

$$p = \frac{3\varepsilon_r}{\varepsilon_r + 2} \qquad (29)$$

It takes time for particle charge to reach saturation level under electrostatic field. The induction charging speed of surface particles is described by Equation 30.

$$q(t) = q_s \cdot \left(1 - e^{(-t/\tau_q)}\right) \qquad (30)$$

Where: τ_q is the charge relaxation time constant, $= \rho\varepsilon$; ρ is the particle resistivity, $\Omega\cdot m$.

In practice, the saturation charging time can be defined as the time that particles take to achieve 95% of q_s. Equation 31 is used to calculate the saturation charging time t_{charge} of particles.

$$t_{charge} = 3\rho\varepsilon \qquad (31)$$

Where: ρ is particle resistivity, $\Omega \cdot m$; ε is particle permittivity, $C^2/(N \cdot m^2)$.

For alumina particles, ρ is $5.0 \times 10^7 \Omega \cdot m$ and ε is $4.5 \times 10^{-11} C^2/(N \cdot m^2)$ (Wu et al 2004). Thus, the charging time needed for alumina particles to achieve 95% of the saturation induction charge is about 6.64×10^{-3} s. It can be concluded from this value that induction charging is a very quick process.

When the lifted foot of a walking person is approaching the floor, a strong electrostatic field can be formed between the foot and the floor. It is not unusual to observe field strength higher than 1.0 kV/cm. Under such field strength, the floor surface particles can be charged due to the induction effects by acquiring electrons/ions from the air and exchanging electrons with contacting surface or other particles, as shown in Figure 12. Under the influence of electrostatic force, some of the charged particles can overcome the gravitational and surface adhesion forces and be pulled onto the shoe bottom or into the air swirls established by walking, thereby becoming suspended in the air. Therefore, in this study, the induction charge is considered the major mechanism of surface particle charging leading to the phenomena of particle resuspension by electrostatic effects.

4) Diffusion charging of particles

Diffusion charge is very similar to induction charge in that ions or electrons transfer onto particle surfaces and reside there to make particles charged. However, no electrostatic field is needed for diffusion charging of particles. In a diffusion charge process, the collision between ions and particles is due to random Brownian motion, that is, by chance. As mentioned for induction charge, the exposure of floor surface particles to airborne ions is much less than that of air borne particles. Even for airborne particles,

diffusion charging is a minor charging mechanism, as compared to induction charging, for particles larger than 0.5 μm in diameter (Hinds 1999). Thus diffusion charging is not considered a major charging mechanism in the indoor particle resuspension study.

The diffusion charging phenomena are very common in natural environment due to omnipresent air ions, produced by cosmic radiation and radioactive gases emitting from soil. Air ions can attach to the surface of initially neutral particles to make them charged or to neutralize initially charged particles. If this process continues, particles will eventually establish a certain amount of charge. This equilibrium state is called *Boltzmann equilibrium* charge distribution. Equation 32 is a simple empirical relation between the particle diameter and the average equilibrium charge number $\overline{n}$ per particle. This equation shows the minimum limit of charges that a particle can maintain in a natural environment, as compared to the maximum limit derived from corona discharging mechanism.

$$\overline{n} = 2.37\sqrt{d_p} \qquad (32)$$

Equation 32 shows, the average Boltzmann equilibrium charge increases proportionally to the root of particle diameter.

5) Comparisons between different charging mechanisms

To make comparisons between different particle charging mechanisms, the particle charge limits related to different mechanisms are calculated and shown in Figure 14 for micron-sized particles.

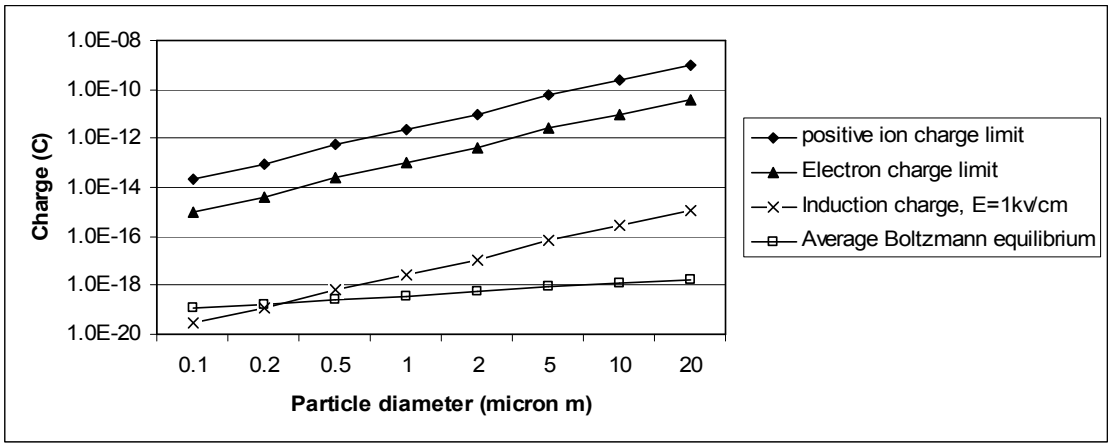

Figure 14 Micron sized particle charge limits
(In the calculation, $\varepsilon = 1.0$)

In Figure 14, for particles larger than 1.0 μm, the induction charge under the field strength of 1 kv/cm lies between the maximum charge limit from corona charging and the minimum charge limit from average Boltzmann equilibrium charge. For particles smaller than 1.0 μm, it is very possible that the induction charge limit is lower than the average Boltzmann equilibrium charge. This means for sub-micron particles, induction charging may have little influence on particle charge. The critical particle diameter, beyond which induction charge limit can exceed the average Boltzmann equilibrium charge, depends on specific values such as ε and E. It is still safe to conclude that, for particles with diameters between 1 and 10 μm, charges acquired from induction can exceed the average Boltzmann equilibrium charge by a few orders of magnitudes.

2.5.3 Electrostatic force on particles

In indoor environment, a human body can be charged by normal human activity such as walking, due to triboelectric difference between shoes and flooring material. The electrostatic body voltage from charge buildup can result in an electrostatic field associated with the human body. Particles on a floor surface can be charged by induction as the foot approaches the floor surface. Inductive charged particles are then removed from the floor surface due to the electrostatic force imposed by the field between the foot

and the floor surface. Some particles entered the air through this process to get resuspended. The electrostatic force F_e acted on charged particles is calculated by Equation 33.

$$F_e = q_p \cdot E \qquad (33)$$

Where: q_p is the charge carried by a single particle, C

The electrostatic force on micron-sized particles, residing on surface, can be estimated by using the induction charge limits (Equation 28, Wu et al 2004) as particle charge values and assuming electrostatic field strength of 1.0 kV/cm. The calculated electrostatic forces are compared with gravitational force for micron-sized particles, as shown in Figure 15.

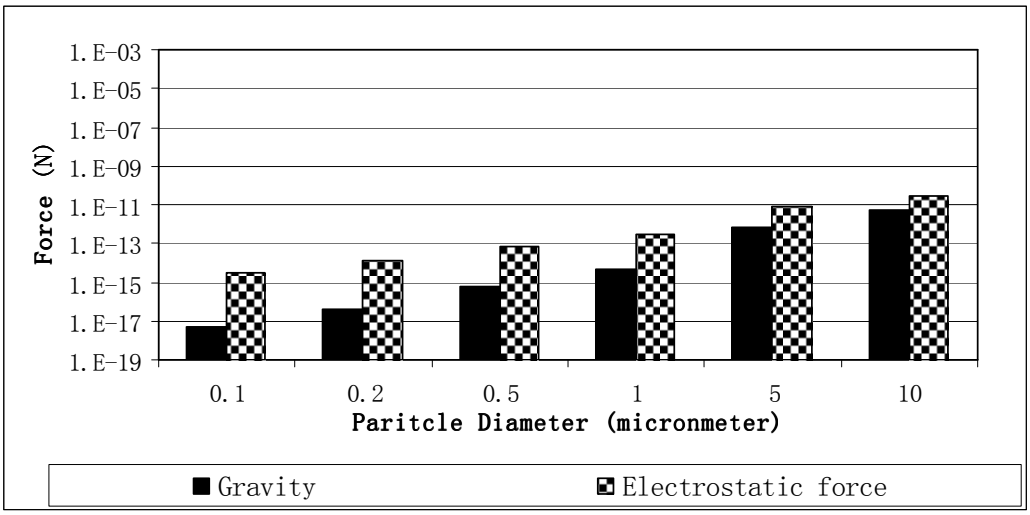

Figure 15 Comparison of particle gravity and electrostatic force

From Figure 15, it can be seen that, for charged particles residing on a floor surface, strong electrostatic fields between a person and a particle reservoir can have a great influence on particle movement. The electrostatic field force can be much larger than the gravitational force of particles, with the difference decreasing as particle diameter increases. This agrees with our observation that smaller particles are more easily affected

by electrostatic attraction than larger particles. Figure 16 shows how a plastic spoon handle, charged by friction with cotton cloth, can attract tiny cock roach dust particles easily.

Figure 16 Roach dusts attaching to the charged plastic spoon handle

2.6 Comparison between force components

Based on above analyses, the magnitudes of particle resuspension force components can be compared with the gravitational force and adhesion force of micron sized particles, as shown in Figure 17.

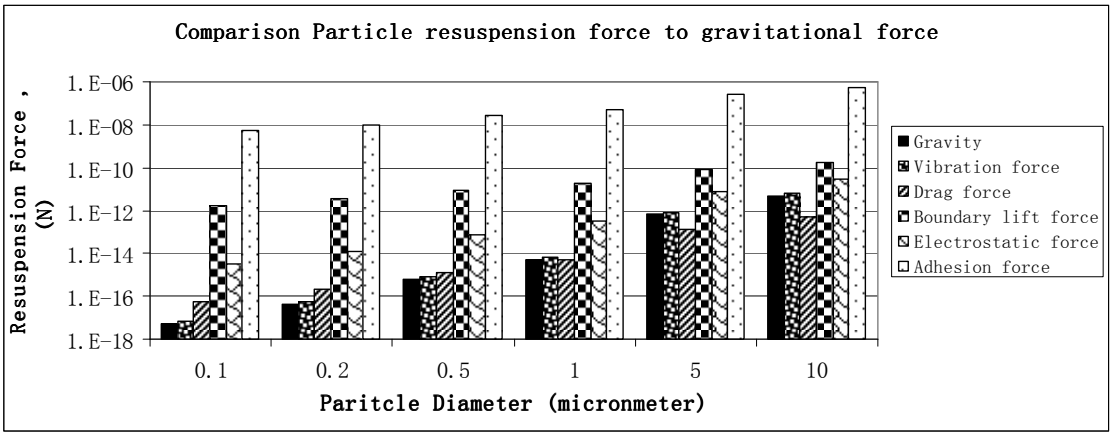

Figure 17 Comparison of force components acting on surface particles

In Figure 17, the four resuspension force components are all larger than the gravitational force for particles with diameter smaller than 1.0 μm. Among the four possible resuspension forces, boundary air lift force has the largest magnitude, followed by electrostatic force, for micronsized particles. As particle size increases, the boundary drag force eventually becomes smaller than the gravitational force while the air boundary lift force and electrostatic force remain 1~2 orders of magnitude larger than the gravitational force. If there is significant human voltage build-up, the resultant electrostatic force can have an important influence on particle resuspension.

The adhesion force of micron sized particles is much larger than any of the resuspension force component calculated. Without considering the boundary air drag force, a direct comparison between combined resuspension force (vibration + air lift + electrostatic forces) and adhesion force is shown in Figure 18.

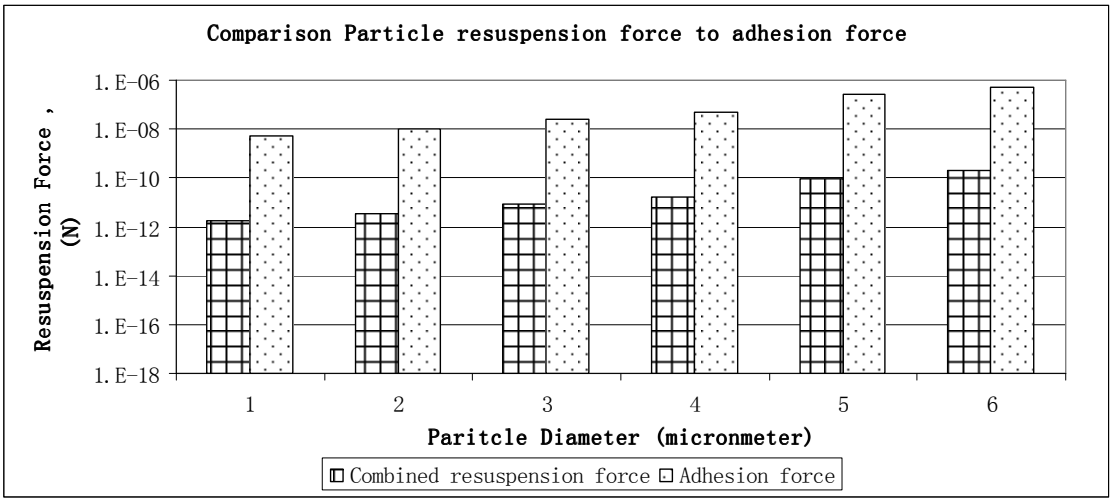

Figure 18 Comparison particle resuspension force to adhesion force

This comparison leads to an intuitive impression that no micron-sized particles could be resuspended by human activity. However, micron-sized particle resuspension is commonly observed, both in our daily life and in the experiments by different researchers (Clayton et al 1993, Kamens et al 1991, Lefcoe and Inculet 1975, Lioy et al 1990, Raunemaa et al 1989, Thatcher and Layton 1995). The main explanation for the theory and reality confliction is that real particle adhesion force has a wide distribution due to reasons such as imperfect contact and limited contact time. Among micron-sized particles on the floor surface, there is a fraction of the reservoir particles with gravitational and adhesion forces that can be overcomed by the resuspension component forces, introduced by human activity. Thus, it is important to study the particle adhesion force distribution as well as each resuspension force component, for a better understanding of particle resuspension phenomena by human activity.

CHAPTER 3. EXPERIMENTS ON PARTICLE ADHESION FORCE

There are two research objectives related with particle adhesion force in this chapter. The first one is to quantify the distribution of particle-to-surface adhesion forces among particles and common flooring materials, by the use of electrostatic detachment method. The quantification of particle adhesion force distribution is required as a fundamental basis for understanding and predicting particle resuspension phenomena. As demonstrated in Chapter 2, there is a significant difference between the magnitudes of theoretically calculated adhesion forces and potential particle re-suspension forces arising from mechanical, aerodynamic and transient electrostatic fields imposed on the particles. Calculations indicate that available disturbance forces are not expected to overcome theoretical adhesion force and to aerosolize micron-sized particles. However, observations indicate that normal human activities do lead to significant particle resuspension from surfaces. The observations suggest that, in any particle reservoir, there is a considerable fraction of surface particles with adhesion forces much smaller than the theoretic calculations. It is suggested that many factors, such as imperfect contact and limited contact time between particles and surfaces, can make adhesion force much smaller than the values predicted by theoretical models. When the adhesion force under imperfect contact is comparable in magnitude to the disturbance forces from human activity, resuspension can happen for micron-sized particles. Thus, the work introduced in this chapter intends to investigate the realistic distribution of particle-surface adhesion force in indoor environments.

The second objective of the work in this chapter is to study the influence of particle type, flooring type and deposition time on the adhesion force. A factorial experiment design is used for this purpose of study.

3.1 Measurement of particle adhesion force

3.1.1 Principles of electrostatic detachment method

Electrostatic detachment method has been used in the study of adhesion force between particles and substrates (Fukuchi and Takeuchi 1998; Nagayama and Takeuchi 2000). The validity of the electrostatic detachment method in adhesion force measurement has been verified with comparison to the more traditional centrifuge method (Fukuchi and Takeuchi 1998).

The basic principle of this method is to charge the particles residing on the surface of a plate by induction and to detach the charged particles from the plate with a controlled electrostatic field. The adhesion force can be determined by measuring the electrostatic field strength and the charge carried by the particles, as shown in Equation 34.

$$F_{adh} \approx F_e = E \cdot q_p \qquad (34)$$

In Equation 34, the gravitational force (F_g) is neglected due to its small magnitude as compared to the adhesion force, and the adhesion force (F_{adh}) is approximated by the electrostatic force (F_e). Figure 19 shows the basic design of the electrostatic detachment method.

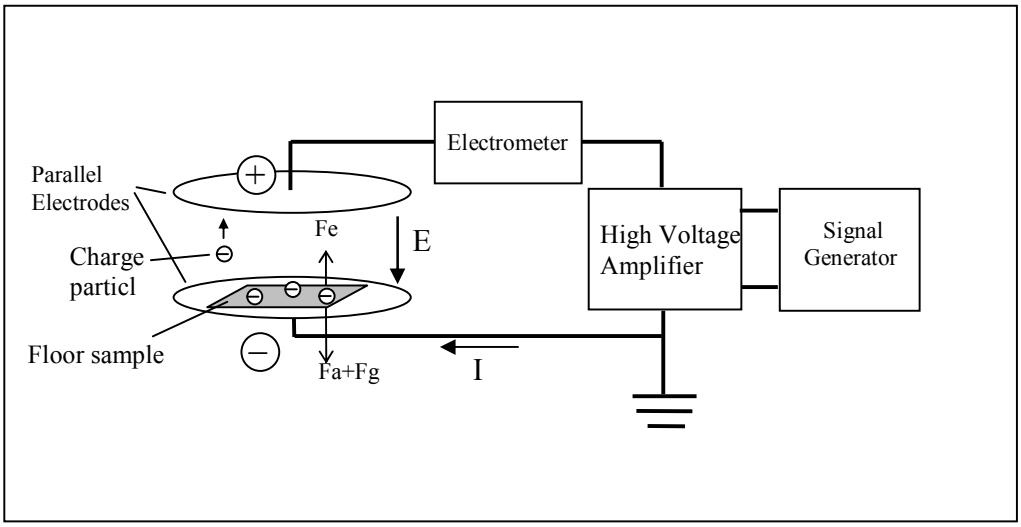

Figure 19 Electrostatic detachment method for particle adhesion force measurement

High voltage is applied on the parallel electrode plates (capacitor) to create an electrostatic field within the space of the two plates. A floor sample with micron-sized particles dispersed on the surface is placed on the lower electrode plate. The direct current (DC) voltage applied to the electrodes is increased at a constant rate from zero to a preset voltage. As the field strength between the two electrodes increases with the increasing voltage, the induction charge on particles residing on the lower plate increases. The increases of both field strength and particle charges lead to the increase of electrostatic detaching force on surface particles. When the electrostatic force is strong enough to overcome the adhesion force, particles begin to jump from the lower plate to the upper plate under the electrostatic force. The transfer of charged particles from one electrode to the other introduces an electric current. The occurrence of the particle detachment is observed by measuring such electric current flowing between the electrodes. The measured current can be expressed in Equation 35.

$$I(t) = C \cdot dV / dt + I_{particle}(t) \qquad (35)$$

Where: $I(t)$ is the total current, A; C is the capacitance of the measuring unit, F; dV / dt is constant voltage changing rate, v/s; $I_{particle}(t)$ is the current caused by charged particle transportation, A.

With Equation 35, given that C and dV / dt are known, $I_{particle}(t)$ can be solved with measured $I(t)$. Then, if the detached particles are of single diameter, the number of particles undergoing plate-to-plate transfer during the experiment can be solved as a function of time, as shown in Equation 36.

$$n(t) = I_{particle}(t) / q_p \qquad (36)$$

Where: $n(t)$ is the number of particles detached per second.

As discussed in Chapter 2, the induction charge for alumina particles is a very quick process. When the capacitor voltage is increased at a slow rate, such as 5 V/s, it is assumed that the particles have achieved saturation charge before the detachment. With this assumption, the charge carried by each particle under electrostatic field can be determined by the induction charge model of Equation 28. The reasonability of this assumption is to be tested in following experiments. With the combined application of Equations 34 to 36, the particle adhesion force distribution function can be determined.

3.1.2 Experiment design for measurement of particle surface adhesion force

Experiments are designed to measure the real particle-to-surface adhesion force distribution. In this experiment, two types of particles are studied: *Bacillus Thuringiensis* spore and alumina particles. These two particle types represent organic and mineral

particles respectively. Two flooring materials are used as the particle contacting surfaces: vinyl tile and rubber tile. These materials are commonly used for indoor flooring and have flat surfaces. The combinations of particles and floor substrates are shown in Table 10.

Table 10 experiments on adhesion force quantification

Experiment #	Particle type	Subplate material
I	Alumina	Vinyl tile
II	Alumina	Rubber tile
III	Spore	Vinyl tile
VI	Spore	Rubber tile

Floor samples are prepared in 9×9 cm^2 plates and placed on the bottom of a particle dispersion box (PDB) which has been cleaned by vacuum. Micron-sized particles are injected into the top space of the PDB by pressurized air. During the injection process, four small fans within the PDB are used to mix the injected particles with the air in the PDB to generate a uniform aerosol mixture of the particles. The suspended particles are left in the PDB to deposit freely onto the surface of floor samples. The density of alumina is 3.95 g/cm^3 and the density of spore is 1.30 g/cm^3. The particle mass load on each sample surface is about 3 mg/cm^2 for alumina and about 1 mg/cm^2 for spore particles. In this way, the surface particle number concentrations between these two types of particles are almost the same. Three days after the particle injection, floor samples are taken out of the PDB for experiments.

Before a detachment experiment, the mass of a floor sample with particles on the surface is measured by an AAA analytical balance (Adam) with a resolution of 0.1 mg. Then, the floor sample is placed on the lower plate of the capacitor as shown in Figure 19. The distance between the two parallel plates is 1 cm. The voltage between the capacitors is increased at a constant rate of 5 V/s. The field strength is initially increased from 0 kV/cm to 4 kV/cm and the capacitor charging current is measured and recorded during the process. After the field strength reaches 4 kV/cm, the applied voltage is reduced to

zero and the floor sample is taken out to measure the mass change due to particle transfer. The particles transferred to the upper plate are wiped off. Then the floor sample is placed back into the capacitor. This procedure is repeated for another two times, with terminal field strength of 6 kV/cm and 8 kV/cm respectively.

All the experiment procedure is carried out in a lab with an area of about 25 m^2. Because relative humidity is a very important factor to influence particle adhesion force (Hinds 1999), a DH 540EL dehumifier (Goldstar) is used in the lab to maintain a relative humidity level of 40%±2.5%. Though the temperature of the lab is not specifically controlled, it is about 20 ºC during the experiments.

Both the alumina and spore particles are polydisperse. The size distributions of alumina particles are measured with a Spectro .3 Optical Particle Counter (CLiMET) and the size distribution of spore particles are measured with a Mastersizer 2000 optical particle counter (Malvern). The particle size distributions are shown in Table 11 and Table 12.

Table 11 Alumina particle size distribution

Diameter*(μm)	Number differential (%)
0.35	10.85%
0.45	5.01%
0.53	1.81%
0.63	6.65%
0.83	16.18%
1.15	8.42%
1.45	14.14%
1.8	6.74%
2.1	3.39%
2.6	12.11%
3.4	8.69%
4.5	3.64%
5.25	1.01%
6.25	1.03%
8.5	0.19%
10	0.12%
	100.00%

* The mean diameter of the diameter bin

Table 12 Spore particle size distribution

Diameter*(um)	Number differential (%)
0.58	19.27%
0.67	23.03%
0.78	19.94%
0.91	13.65%
1.06	9.03%
1.24	5.73%
1.44	3.50%
1.68	2.09%
1.95	1.25%
2.28	0.77%
2.65	0.50%
3.09	0.35%
3.60	0.25%
4.19	0.18%
4.88	0.13%
5.69	0.10%
6.63	0.07%
7.72	0.05%
9.00	0.04%
10.48	0.02%
12.21	0.02%
14.22	0.01%
16.57	0.01%
	100.00%

* The mean diameter of the diameter bin

3.1.3 Validation of particle induction charging model

Before the induction charge model of Equation 28 can be used to determine the particle adhesion force, the reliability of this model needs to be validated. In this study, the measured mass of transferred particles is compared with the mass calculated from measured transfer charge and particle induction model, in order to validate the charging model. In other words, transferred particles are assumed to be charged to saturation values under electrostatic field. As the charge transfer between the two capacitor plates are measured, the corresponding particle transfer mass, based on induction charging

model, can be calculated and compared with measured mass transfer for validation purpose.

1) Equivalent monodisperse diameter

A conception of equivalent monodisperse diameter is introduced here for comparison convenience. When particles are monodisperse, it is straight forward to calculate the particle transfer mass based on Equation 36. However, in the experiments, both spore and alumina are polydisperse particles, so additional calculations are needed to account for the polydisperse particle charging. For monodisperse particles with diameter d, Equation 37 and Equation 38 are used to calculate particle total charge (Q) and total mass (M).

$$Q = q_d \cdot n = \left(\frac{\pi^3}{18} p\varepsilon_0 d^2 E \right) \cdot n = \left(\frac{\pi^3}{18} p\varepsilon_0 E \right) \cdot d^2 \cdot n \tag{37}$$

$$M = \rho_p \frac{\pi}{6} d^3 \cdot n \tag{38}$$

Where: q_d is the charge per particle of diameter d.

For polydisperse particles, the total mass and total charge are calculated by Equation 39 and Equation 40.

$$Q = \sum_{i=1}^{n} q_{d_i} \cdot n_i = \sum_{i=1}^{n} \left(\frac{\pi^3}{18} p\varepsilon_0 {d_i}^2 E \right) \cdot n_i = \left(\frac{\pi^3}{18} p\varepsilon_0 E \right) \cdot \sum_{i=1}^{n} {d_{S,d_i}}^2 n_i = \left(\frac{\pi^3}{18} p\varepsilon_0 E \right) \cdot d_S^2 \cdot n \tag{39}$$

$$M = \sum_{i=1}^{n} \rho \frac{\pi}{6} {d_i}^3 \cdot n_i = \rho \frac{\pi}{6} \sum_{i=1}^{n} {d_{Vi}}^3 \cdot n_i = \rho \frac{\pi}{6} d_V^3 \cdot n \tag{40}$$

Where: d_{S,d_i} is the area diameter of particles with diameter d_i; d_S is the particle number weighted area diameter; d_{V,d_i} is the volume diameter of particles with diameter d_i; d_V is the particle number weighted volume diameter.

The values of d_S and d_V for spore and alumina particles can be calculated based on the measured particle size distributions as shown in Section 3.1.2. With the introduction of equivalent monodisperse particle diameter, polydisperse particles can be represented by monodisperse particles and be compared with other polydisperse particles when particle charge/mass ratio is of concern. The relationship between polydisperse particles and equivalent monodisperse particles are shown through Equation 41 to Equation 46.

$$Q_{poly} = \left(\frac{\pi^3}{18} p\varepsilon_0 E \right) \cdot d_S^2 \cdot n \tag{41}$$

$$Q_e = \left(\frac{\pi^3}{18} p\varepsilon_0 E \right) \cdot d_e^2 \cdot n_e \tag{42}$$

$$Q_{poly} = Q_e \tag{43}$$

$$M_{poly} = \rho \frac{\pi}{6} d_V^3 \cdot n \tag{44}$$

$$M_e = \rho \frac{\pi}{6} d_e^3 \cdot n_e \tag{45}$$

$$M_{poly} = M_e \tag{46}$$

Where: Q_{poly} is the total charge of polydisperse particles; Q_e is the total charge of equivalent molodisperse particles; d_e is the equivalent diameter; n_e is the number of equivalent particles; M_{poly} is the total mass of polydisperse particles; M_e is the total mass of monodisperse particles.

From above equations, the equivalent diameter and number of equivalent monodisperse particles can be calculated by Equation 47 and Equation 48.

$$d_e = d_V^3 / d_S^2 \tag{47}$$

$$n_e = n \cdot d_S^6 / d_V^6 \tag{48}$$

The definition of equivalent diameter (d_e) and equivalent number (n_e) are introduced specifically for the study of electrostatic charging of polydisperse particles. Equation 47 and Equation 48 mean that n polydisperse particles with d_V and d_S can be represented by n_e monodisperse particles with a diameter of d_e. When polydisperse particles have the same total volume (mass) as equivalent monodisperse particles, both particles should have the same total surface area. Since induction charge is proportional to particle surface area, this also means that equivalent monodisperse particles (d_e) will have the same induction charge as polydisperse particles (d_V, d_S), given their total masses are equal. In the following analysis, all the polydisperse particles will be represented by their equivalent monodisperse diameter when the induction charge/mass property is under comparison. The calculated characteristic particle diameters for both the alumina and the spore particles used in the study are shown in Table 13.

Table 13 Characteristic diameters of polydisperse particles

Particle type	Mean diameter $\bar{d}$ (μm)	Area diameter d_S (μm)	Volume diameter d_V (μm)	Equivalent diameter d_e (μm)
alumina	1.287	2.107	1.976*	1.738
spore	0.912	1.095	1.553	3.121

* shaping factor d_{Vi}/d_{Si} is 0.7752 for individual particle (Wu et al 2005)

2) Comparison between measured and calculated surface particle mass transfer

With the introduction of equivalent diameter of polydisperse particles, it is possible to compare polydisperse particles with monodisperse particles for the induction charge property. As mentioned above, the induction charge model can be validated by comparing the measured particle transfer mass with the calculated particle transfer mass, based on measured charge transfer and induction charge model.

In the particle electrostatic detachment experiments, as the voltage on the capacitor increases at a constant rate (5V/s), the capacitor charging current is measured with a 6514

electrometer (Keithley) that can detect a current as low as $1.0\times10^{-16}A$. A current measurement sample of alumina-vinyl detachment experiment is shown in Figure 20.

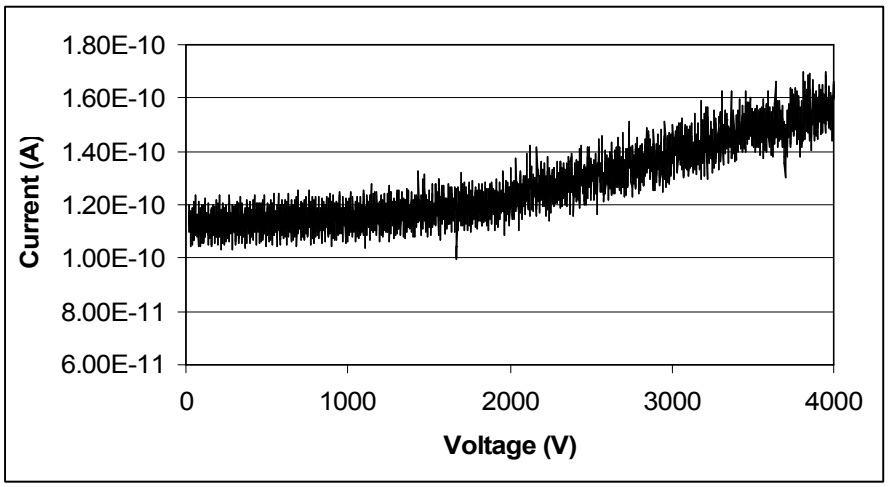

Figure 20 Measured charging current in Alumina-Vinyl detachment experiment

In Figure 20, the measured charging current has a very clear trend while some rapid oscillation shows around the general trend line. When the voltage on the capacitor is low (<1000 volts), the charging current is approximately constant at $1.15\times10^{-10}A$. This is because the field strength is still not strong enough to induct enough charges onto the particles to generate strong electrostatic force to overcome the adhesion force. As the voltage increases, some particles get enough induction charge and overcome the adhesion force under the influence of electrostatic force. The detached particles move to the upper plate of the capacitor to generate a particle transfer current over the original charging current. As the voltage further increases, the particle transfer current is even obvious in magnitude.

With the measured charging current of the detachment experiments, the particle mass transfer can be calculated based on the particle charging model and induction charge model. The comparisons between calculated mass transfer and measured particle mass transfer are shown from Figure 21 to Figure 24.

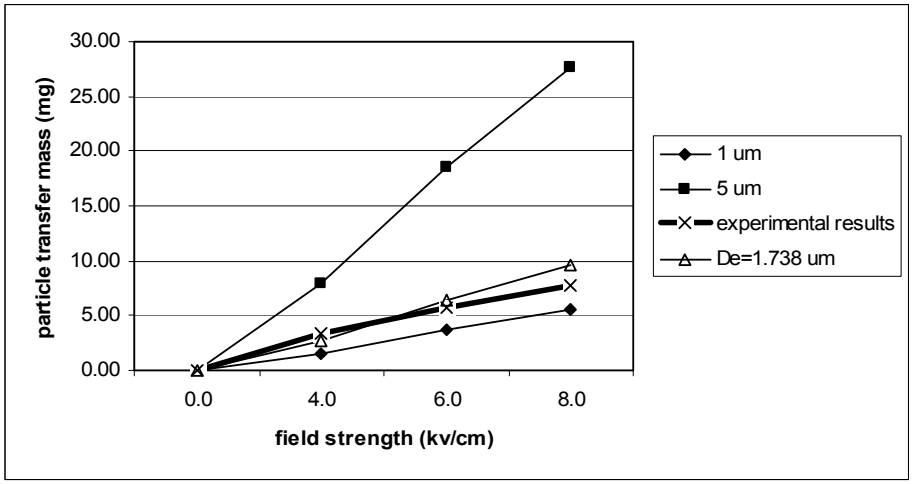

Figure 21 Mass comparisons for alumina on vinyl tile

In Figure 21, lines of 1 μm and 5 μm represent the calculated transfer mass of monodisperse particles with diameter of 1 μm and 5 μm respectively, given the measured transfer charge and induction charge model. The line of "$D_e = 1.738 \mu m$" is calculated for monodisperse particles with the equivalent diameter of the alumina particles under test. These three calculated lines are compared with the experimentally measured particle transfer mass in the plot. Figure 21 shows that the measured transfer mass line lies between the lines of 1 μm and 5 μm, and is very close to the equivalent diameter line. From this comparison, it can be concluded that the particle induction charge model is applicable in this study and the alumina particles can be considered as being charged to saturation before being pulled away from vinyl surface.

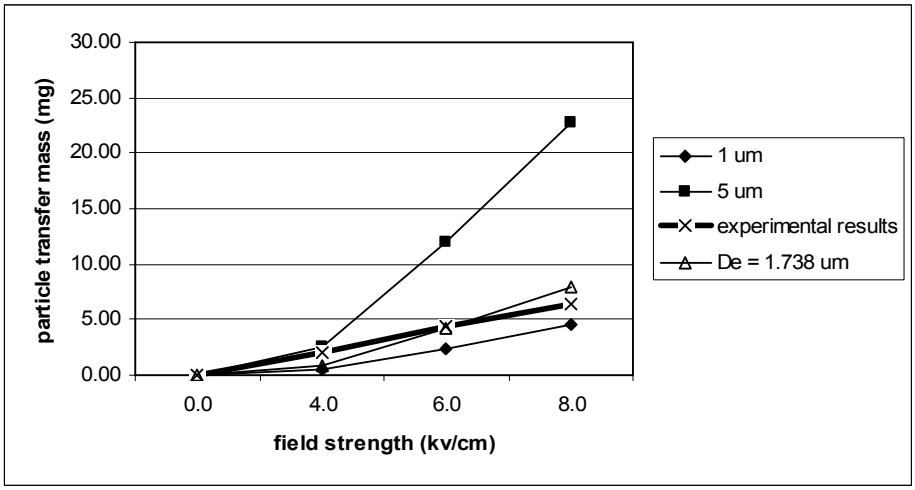

Figure 22 Mass comparisons for alumina on rubber tile

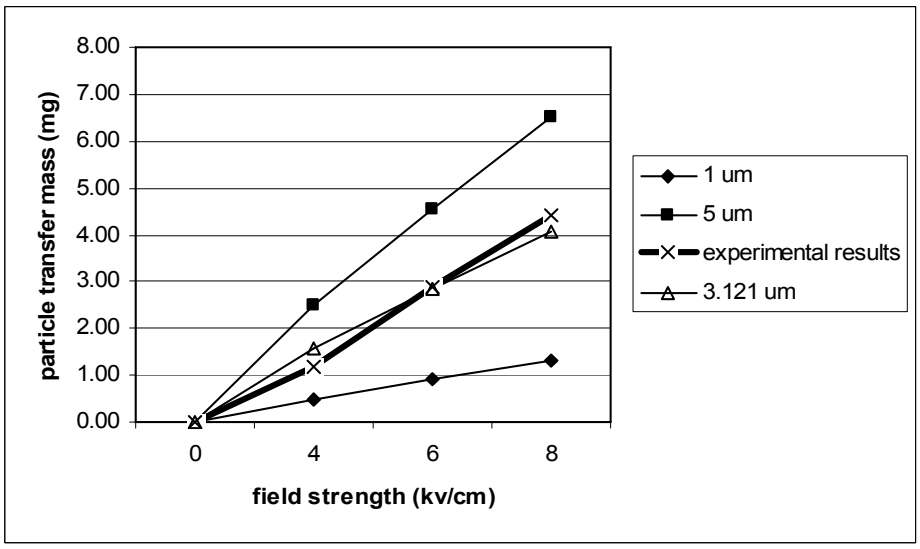

Figure 23 Mass comparisons for spore on vinyl tile

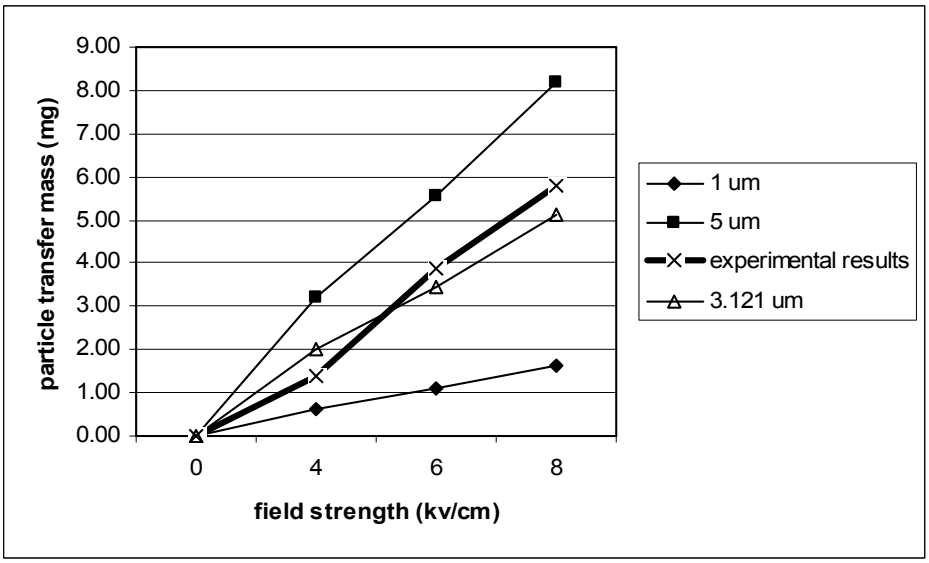

Figure 24 Mass comparisons for spore on rubber tile

Figure 22 to Figure 24 show the similar comparison results as Figure 21. Thus for different combinations of particle types and substrate surface types, the induction charge model as shown in Equation 28 can be validated and thus can be used for the following particle adhesion force calculation.

3.1.4 Measurement of particle adhesion force

With the measured particle transfer mass, the validated particle induction charging model can be used to calculate the particle adhesion force distribution. The average adhesion force per particle measured from the experiments $F_{adh,\exp}$ can be calculated as shown by Equation 49 with particle number weighted area diameter d_S.

$$F_{adh,\exp} \approx F_e = E \cdot q_p = E \cdot \left(\frac{\pi^3}{18} p \varepsilon_0 d_S^2 E \right) = \frac{\pi^3}{18} p \varepsilon_0 d_S^2 E^2 \tag{49}$$

Figure 25 shows the measured adhesion force distributions for the alumina and the spore particles.

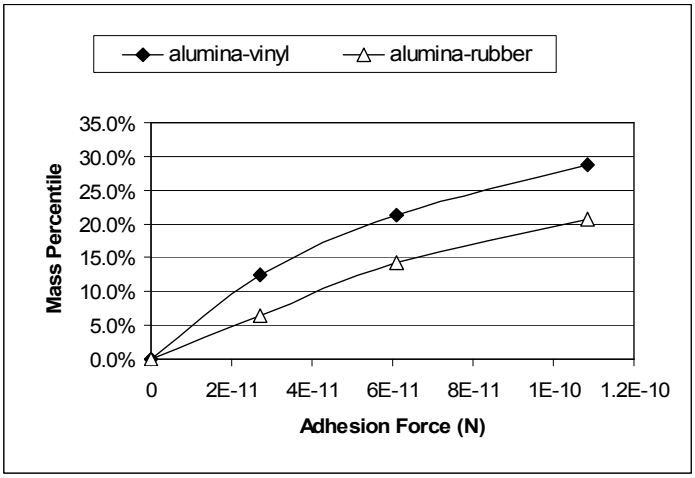

(a) Alumina particles

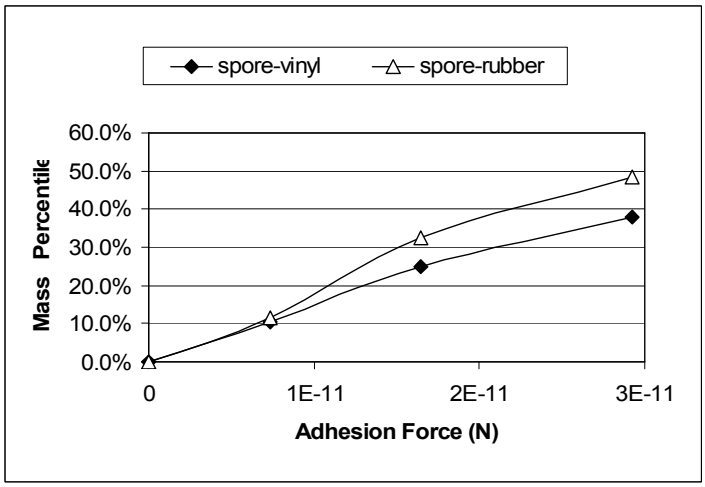

(b) Spore particles

Figure 25 Particle adhesion force distribution

The theoretical adhesion force $F_{adh,theo}$ of the polydisperse particles can be calculated by Equation 50 (Hinds 1999) with particle number weighted mean diameter $\bar{d}$.

$$F_{adh,theo} = \frac{A}{12x^2}\bar{d} \qquad (50)$$

Where: A is Hamaker constant, which depends on the materials involved and ranges from $6\sim150\times10^{-20}$ J for common material; x is the separation distance between particles and substrate, usually assumed to be 0.4 nm due to irregular contact surfaces.

Table 14 shows the measured adhesion force distributions for alumina and spore particles, as well as the theoretically calculated adhesion force from Equation 50 and the gravitational force.

Table 14 Comparison between calculated and experimental adhesion force

Particle type	Flooring material	Transfer mass percentile*	Measured F_{adh} * (N)	Calculated F_{adh} (N)	G (N)
Alumina	Vinyl	28.75%	1.08×10^{-10}	6.70×10^{-8}	1.56×10^{-13}
	Rubber	20.73%			
Spore	Vinyl	37.93%	2.93×10^{-11}	4.75×10^{-8}	2.50×10^{-14}
	Rubber	48.33%			

*at field strength of 8kv/cm

Table 14 shows that, for both alumina and spore particles, there is a significant portion of particles with adhesion forces that are much smaller than the theoretically calculated adhesion forces, but much larger than the gravitational force. The major reason for this is considered to be imperfect contact between particles and indoor surfaces, which in turn makes the indoor particles more possible to be resuspended by human activity.

It can also be observed that, on such flat surfaces as vinyl and rubber tiles, the adhesion force of alumina is generally larger than that of spore particle, given similar particle size distribution. For alumina, about 25% of all the particles on the surface have adhesion forces less than the value of 1.08×10^{-10} N. For spore particles, about 40% of all the particles have adhesion forces less than the value of 2.93×10^{-11} N. This result may suggest that spore particles are easier to be resuspended than alumina particles with similar size distribution.

Figure 26 is a photo of the surface alumina particles, taken with an electronic scanning microscope (Fei Quanta 200 ESME). This photo shows that the irregular shape of particles and particle clustering greatly reduce the contact area between particles and flat surface. The reduced adhesion force makes surface particles apt to be resuspended under such exterior disturbance such as human activity.

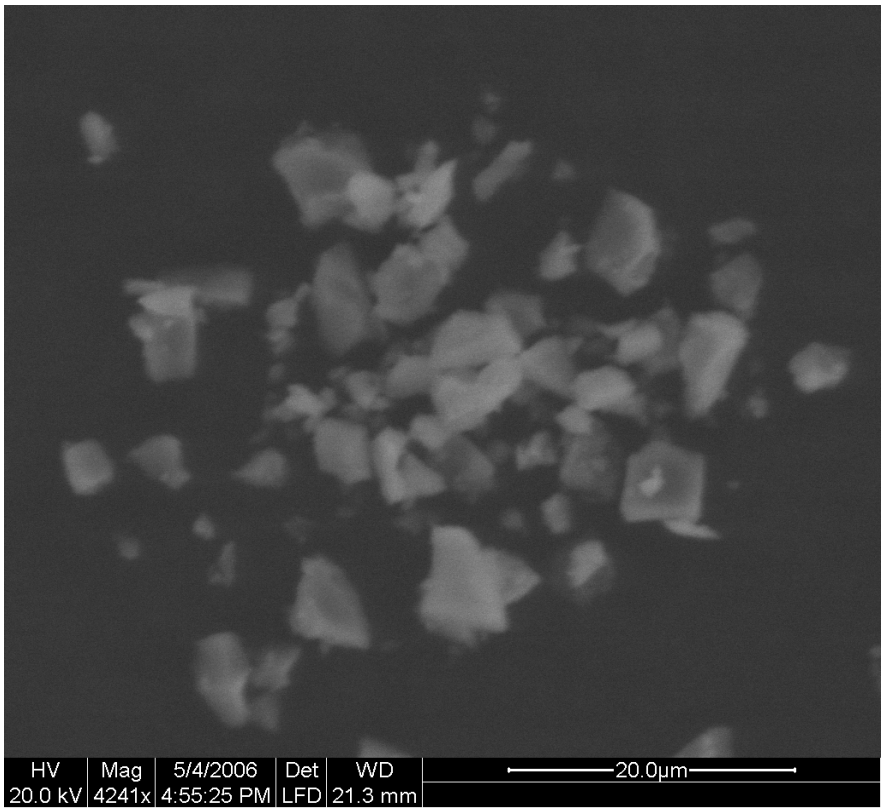

Figure 26 Surface alumina particles under SEM

3.2 Factorial analysis of particle adhesion force

3.2.1 Design of the factorial experiments

As demonstrated in Section 3.1, the real particle surface adhesion force can be a few orders of magnitude lower than the theoretical prediction. The work in this section focuses on the influence of a few factors, such as particle type, flooring type and contact time, on particle-to-surface adhesion force. In order to study these effects, a factorial experiment is designed.

Three types of flooring material are studied in this work: nylon carpet, vinyl tile and rubber tile. These materials are widely used in indoor environment. The particles to be studied are alumina and spore particles, the same as used in Section 3.1. Particles are dispersed onto surfaces of floor samples, each with an area of $9 \times 9 cm^2$. Two surface contact time lengths are considered: 1 day and 10 days. For each type of particles, 18 floor samples are prepared to accommodate the study on 3 flooring types and 2 contact time lengths, with 3 repetitions for each combination of flooring material and contact time length. With this arrangement, there are 36 floor samples in total to be tested in the experiments, as listed in Table 15.

Table 15 Arrangement of floor-particle samples

Batch number	Particle type	Floor type	Contact time	Number of samples
I	Alumina	Round loop carpet	1 day	3
			10 days	3
		Vinyl tile	1 day	3
			10 days	3
		Rubber tile	1 day	3
			10 days	3
II	Spore	Round loop carpet	1 day	3
			10 days	3
		Vinyl tile	1 day	3
			10 days	3
		Rubber tile	1 day	3
			10 days	3

The consideration of surface particle load on floor samples is the same as that in the experiments of Section 3.1, which is about 3 mg/cm^2 for alumina and about 1 mg/cm^2 for spore particles. One day after the particles are dispersed into the particle dispersion box (PDB), half of the 18 floor samples (3 for each flooring material), are randomly picked out for electrostatic detachment experiments. The other 9 floor samples are tested 10 days after the dispersion to study the contact time effects on adhesion force distribution.

This is a three-factor factorial design. For simplicity, the response variable is the mass tranfer ratio after the field strength is increased to 8 kV/cm. There are two research questions of interest for this study. The first one is how particle type and flooring type can influence particle adhesion force. The second one is to test the contact time effects on particle adhesion force. As in the adhesion force measurement experiments, the relative humidity of the lab is controlled at 40%±2.5% with a room temperature about 20 ºC.

3.2.2 Effects of particle type and flooring type on adhesion force

Although this is a three-factor factorial experiment, the three way interaction among the three factors is not easy to interpret and is not of the research interest here. Thus, the 36 tests are classified into two groups based on the factor of contact time length, in order to study the effects of particle type and flooring type. The first group includes the 18 tests on floor samples one day after the experiments, while the second group includes the 18 tests on floor samples 10 days after the experiments. The experimental results from these experiments are recorded in Table 16.

Table 16 Particle mass tranfer ratio under field strength of 8 kV/cm

alumina	1 day	v6*	v2	v4	r5	r2	r9	c7	c1	c9
		37.9%	32.4%	41.9%	39.8%	45.8%	37.4%	35.4%	29.1%	29.5%
	10 days	v10	v3	v8	r4	r2	r6	c4	c5	c3
		34.0%	26.9%	16.3%	31.9%	27.1%	22.3%	27.6%	28.9%	23.5%
Spore	1 day	v4	v3	v2	r2	r1	r4	c4	c9	c3
		42.3%	48.7%	43.3%	55.3%	54.9%	58.3%	34.8%	30.4%	35.9%
	10 days	v11	v7	v5	r10	r8	r3	c2	c8	c5
		41.6%	44.0%	42.0%	44.4%	42.1%	50.4%	21.4%	13.2%	17.0%

* v denotes vinyl; r denotes rubber; c denotes carpet.

The statistical model for each time group of floor sample tests is shown in Equation 51.

$$y_{ijk} = \mu + \tau_i + \beta_j + (\tau\beta)_{ij} + \varepsilon_{ijk} \quad \begin{cases} i = 1,2 \\ j = 1,2,3 \\ k = 1,2,3 \end{cases} \tag{51}$$

Where: y_{ijk} is the mass transfer ratio of the kth replicate of particle i on floor j; τ_i is the effect of particle type i; β_j is the effect of flooring type j; $(\tau\beta)_{ij}$ is the interaction between particle type i and flooring type j; ε_{ijk} is the random error.

1) Analysis on the floor samples tested 1 day after dispersion

The statistical software Minitab is used to analyze the test results. A two way analysis of variance (ANOVA) is carried out with particle type and flooring type as the two factors and particle mass transfer ratio as the response. The Minitab output is shown in Figure 27.

Two-way ANOVA: Jumping ratio versus Particle, Floor

Source	DF	SS	MS	F	P
Particle	1	0.031043	0.0310434	23.90	0.000
Floor	2	0.077281	0.0386407	29.76	0.000
Interaction	2	0.012414	0.0062072	4.78	0.030
Error	12	0.015584	0.0012986		
Total	17	0.136323			

S = 0.03604 R-Sq = 88.57% R-Sq(adj) = 83.81%

Figure 27 ANOVA analysis on adhesion force I

The p value for 'Interaction' is 0.03, which is smaller than normally used significance level of 0.05. This means the interaction between flooring type and particle type on particle adhesion force is very significant. The p values for factor 'Particle' and factor 'Floor' are also smaller than 0.05, which means the particle type and flooring type each can have great influence on particle adhesion force. That is to say particle adhesion force changes significantly as particle type and flooring type change.

In order to further interpret the experimental results, a main effect plot of the average responses at each factor level combination from Minitab is shown in Figure 28.

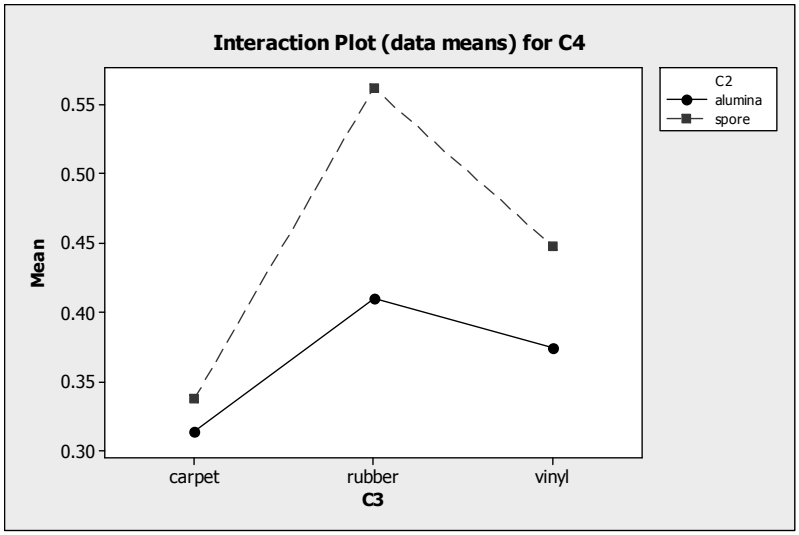

Figure 28 Main effect plot for particle adhesion force

In the plot, the mean mass transfer ratios of alumina on each floor surface are connected by a solid line while those of spores are connected by a dashed line. The nonparallel property of the dashed line and the solid line shows the strong interaction between particle type and flooring type. It can be observed, for rubber floor, the mass transfer ratio of spore is much larger than that of alumina. Such large increase is more obvious on rubber surface than on nylon carpet or vinyl surface, which demonstrates the interaction effects between flooring type and particle type. Although the particle size distributions of these two types of particles are similar, the alumina particles have a stronger adhesion force to the floor surface and thus have smaller mass transfer ratios than the spore particles. When the three floor materials are compared, the carpet gives the strongest adhesion forces to particles while the rubber floor adhere particles most loosely to its surface.

2) Analysis on the floor samples tested 10 days after dispersion

For floor sample group tested 10 days after dispersion, the two-way ANOVA (Figure 29) and main effects plot (Figure 30) are used again for the analysis.

Two-way ANOVA: Jumping Ratio versus Particle, Floor

Source	DF	SS	MS	F	P
Particle	1	0.033378	0.0333784	13.58	0.003
Floor	2	0.072308	0.0361539	14.71	0.001
Interaction	2	0.073758	0.0368792	15.00	0.001
Error	12	0.029496	0.0024580		
Total	17	0.208941			

S = 0.04958 R-Sq = 85.88% R-Sq(adj) = 80.00%

Figure 29 ANOVA analysis on adhesion force I

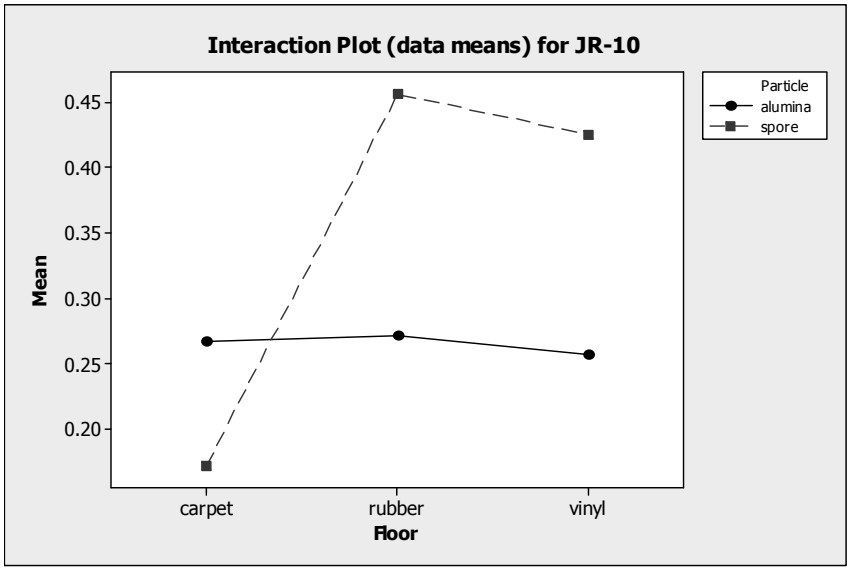

Figure 30 Main effect plot for particle adhesion force

The analyses of particle mass transfer ratio after 10 days of deposition show a very similar trend of those after 1 day deposition. There is significant interaction between particle type and flooring type when the particle adhesion force is considered. Again, alumina particles show larger adhesion forces on rubber tiles and vinyl tiles than spore particles. However, on carpet floor, the adhesion bond between carpet and spore is stronger than that between carpet and alumina after a contact as long as 10 days.

3.2.3 Time effects on adhesion force

Because the strong interaction between particle and flooring type on particle adhesion force, the time effects on adhesion force are to be tested on each combination of particle and flooring material. This means 6 comparisons are to be carried out to test the time effects on adhesion force. The two contact time levels to be studied are one day and ten days after initial particle dispersion. The one day group represents freshly deposited particles while the other group has ten days to allow possible increase in adhesion force due to time effect. The mean and standard deviation of particle mass transfer ratio are recorded in Table 17.

Table 17 analysis of time effects on adhesion force

Particle type	Flooring type	1-day mass transfer ratio		10-day mass transfer ratio		P-value by one-way ANOVA
		Mean	Standard deviation	Mean	Standard deviation	
Alumina	Vinyl	37.4%	4.8%	25.7%	8.9%	0.117
	Rubber	41.0%	4.3%	27.1%	4.8%	0.020
	Carpet	31.3%	3.5%	26.7%	2.8%	0.148
spore	Vinyl	44.8%	3.4%	42.5%	1.3%	0.355
	Rubber	56.2%	1.9%	45.6%	4.3%	0.018
	Carpet	33.7%	2.9%	17.2%	4.1%	0.005

From Table 17, it can be seen that there is a general decrease trend of particle mass transfer ratio as the contact time between particles and surfaces increases. This means the adhesion forces between particles and surfaces increase as contact time increase. The p values from one way ANOVA also show that most of the experiments detect significant time effects on particle adhesion force. A practical meaning of this finding is that freshly deposited particles are much easier to be resuspended from surfaces than particles with a long time of contact. Besides the particle type and flooring type, contact time of particles is also an import factor that needs to be specified in order to determine particle adhesion force and thus particle resuspension coefficients.

CHAPTER 4. HUMAN GAIT AND BODY VOLTAGE MEASUREMENT

A charged human body can generate an electrostatic field between the shoes and the floor surface. The electrostatic field can charge particles on the floor surface. The electrostatic force on the charged particles can counteract the adhesion force between the particles and the surface and can even cause the particles to detach from the surface. In this way, the walking-created electrostatic field can have an impact on particle resuspension. .In order to study such electrostatic effects, it is important to determine the electrostatic field strength between a human foot and floor surface. It is difficult to measure such transient field strength near the ground directly. Thus, in this study, it is suggested to measure the human gait and body voltage during walking separately. The transient electrostatic field can be calculated by coupling these two measurements. This chapter describes the body voltage measurements and the coupling of the human gait and body voltage.

4.1 Walking gait measurement

4.1.1 Description on human gait measurement

The foot motion during human walking is measured with the Motion Analysis Eagle System (Motion Analysis), in the Biomechanics Laboratory at the Pennsylvania State University. The Motion Analysis Eagle System is a 3D optical motion capture system, with eight Eagle Digital Cameras to capture and digitize human motion, represented by reflective markers attached to human body. Figure 31 is a demonstration of the testing system software interface, which shows how the system captures and analyzes the motion of a male subject playing golf.

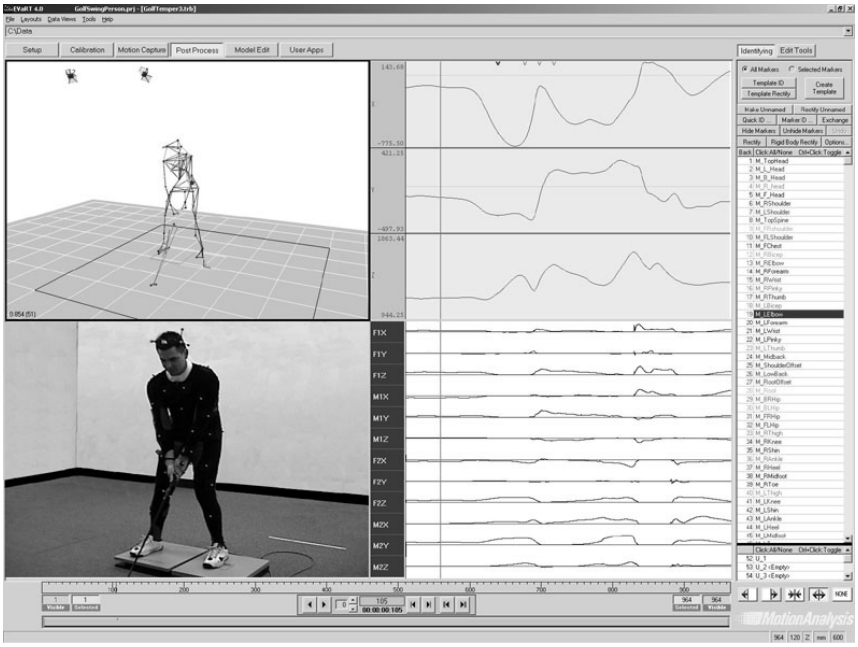

Figure 31 demonstration of motion analysis eagle system
(From www.motionanalysis.com)

In this research, the major concern is the vertical distance between a shoe bottom and a floor surface during human walking. For the purpose of simplification, the human foot motion during walking is described by three points on the shoes as shown in Figure 32. These three points are called toe point, metatarsal point and heel point.

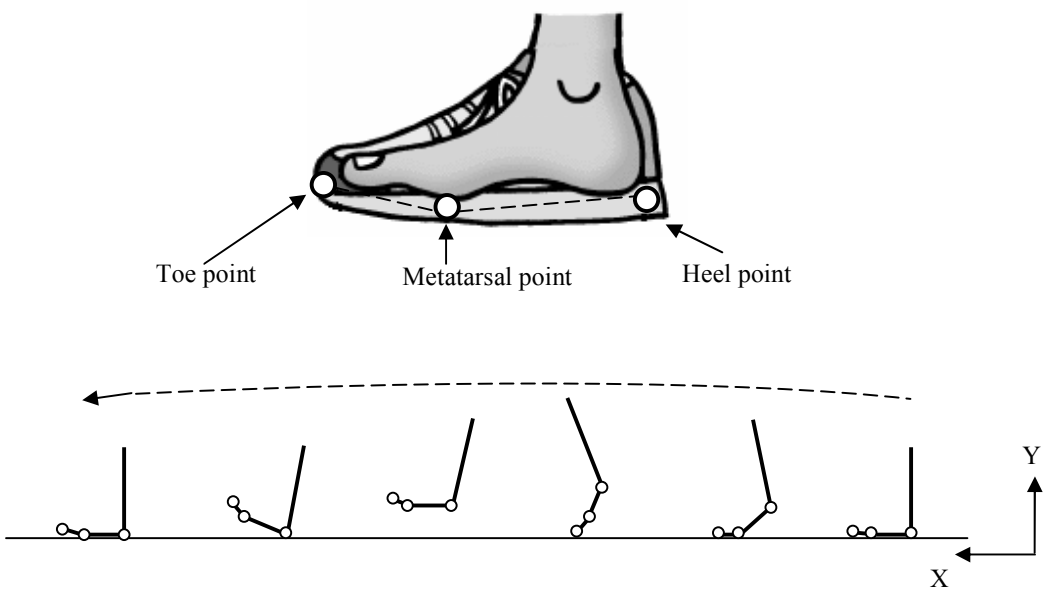

Figure 32 Three points to measure the shoe bottom position to the floor surface

As shown by Figure 32, the average distance between shoe bottom and floor surface can be determined by the locations of these three points during human walking.

4.1.2 Testing procedure for human subjects

Four human subjects, two male and two female were recruited for the human gait testing. Before this experiment is conducted, the use of human subjects was reviewed and approved by the Office for Research Protections (IRB #22583) at the Pennsylvania State University. Consent forms have been signed and collected from the recruited human subjects. The ages of these human subjects are between 20 and 35. The human subjects were coded as A, B, C and D in the experiment. Some body physical information of these human subjects is listed in Table 18.

Table 18 Body physical information of human subjects

Code	Gender	Height (cm)	Weight (kg)	Shoe size (cm)
A	Male	178.5	75.8	27.0
B	Male	166.5	60.8	25.5
C	Female	174.0	64.4	25.0
D	Female	154.0	64.4	23.5

Before the test, reflective markers are placed on the sneakers of human subjects to identify the three points as mentioned in Figure 32. During the test, the human subjects walking through a testing trail at their casual pace as the Motion Analysis Eagle System captures their optical walking image and transfers the human motion into analyzable digital files. These digital files include such information as human feet real time coordinates, relative to the ground.

4.1.3 Testing results and analysis

Three walking trials are recorded for each human subject. The test results show that the foot motions for the same human subject from three trials are very similar. Thus, the testing results from one trial are randomly chosen for each human subject to represent their foot motion during walking, as shown from Figure 33 ~ Figure 36. In these Figures, Y-value denotes the vertical distance of the marker points to the ground during human walking and X-value denotes the horizontal traveling distance of the marker points during human walking.

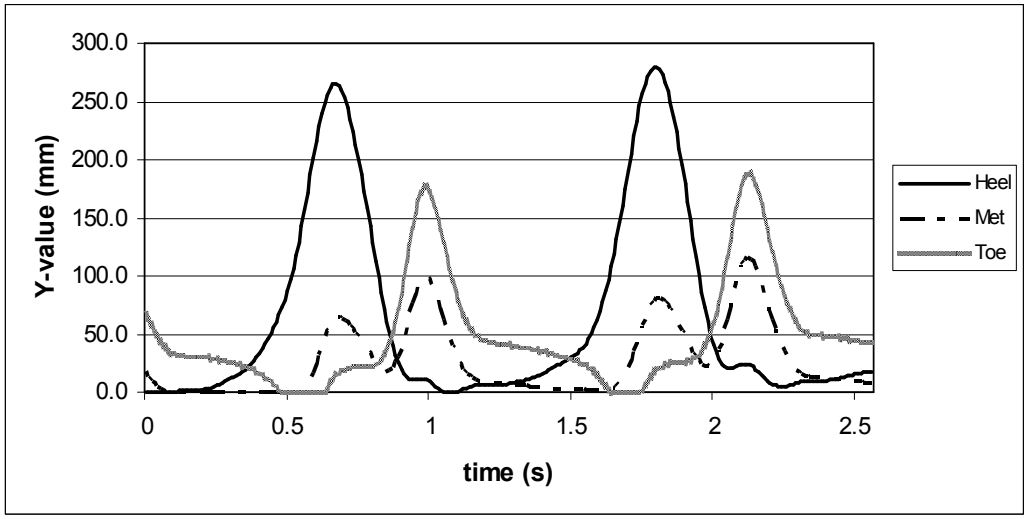

(a) Vertical coordinates of human foot

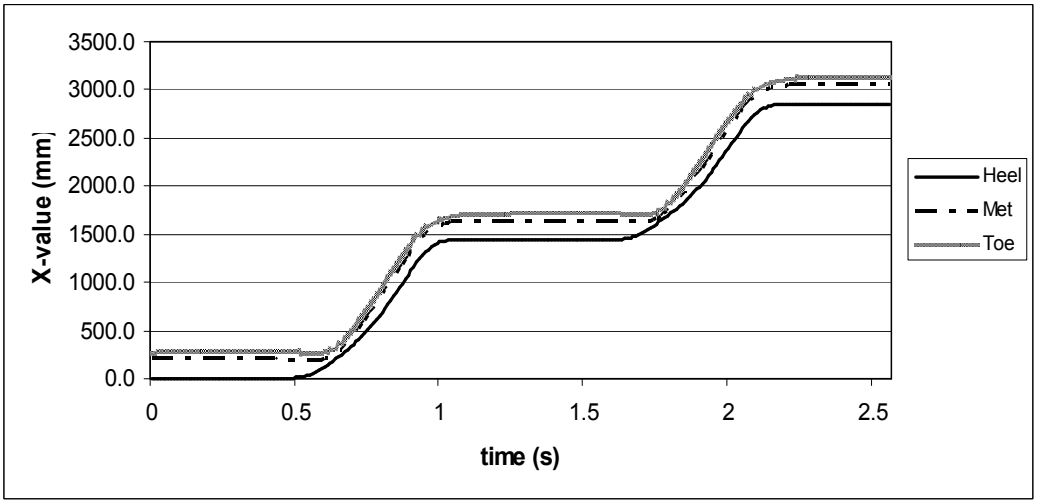

(b) Horizontal coordinates of human foot

Figure 33 Foot motion profile of Human subject A

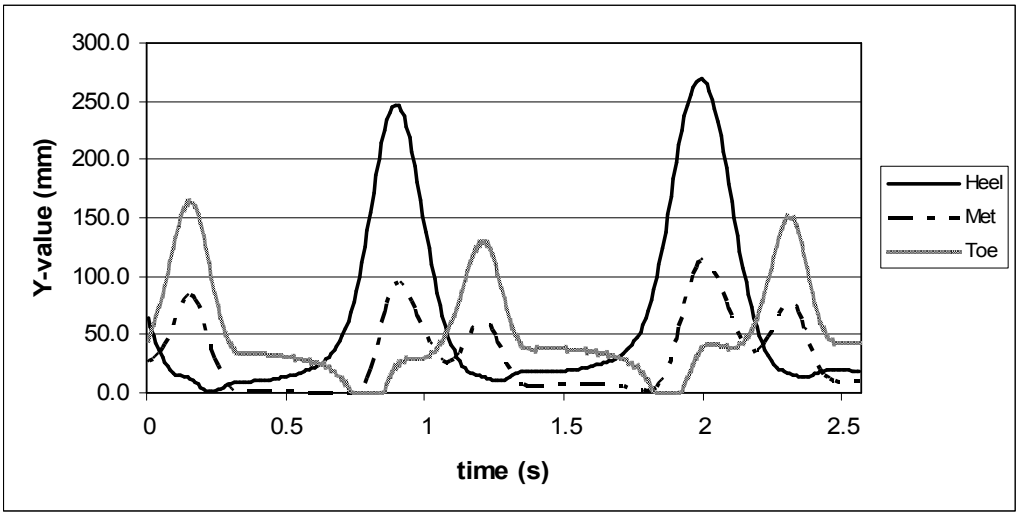

(a) Vertical coordinates of human foot

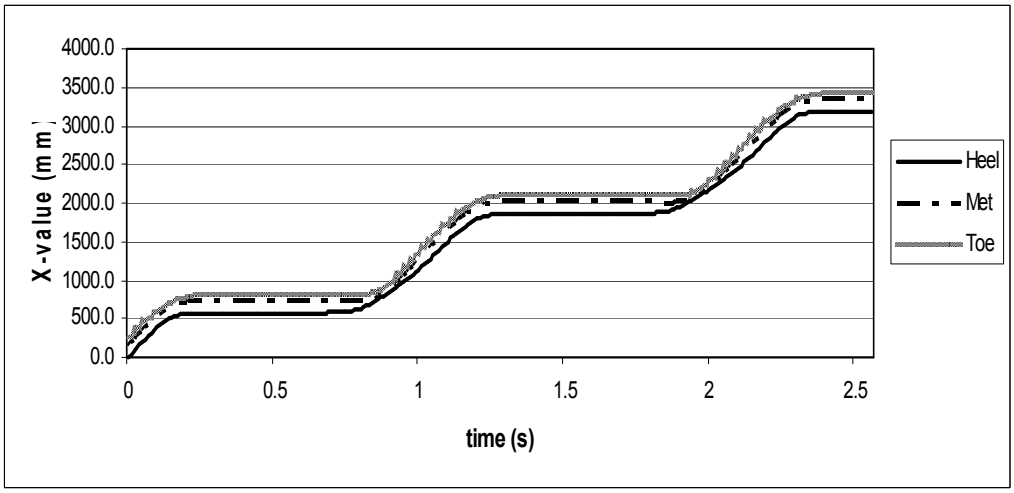

(b) Horizontal coordinates of human foot

Figure 34 Foot motion profile of Human subject B

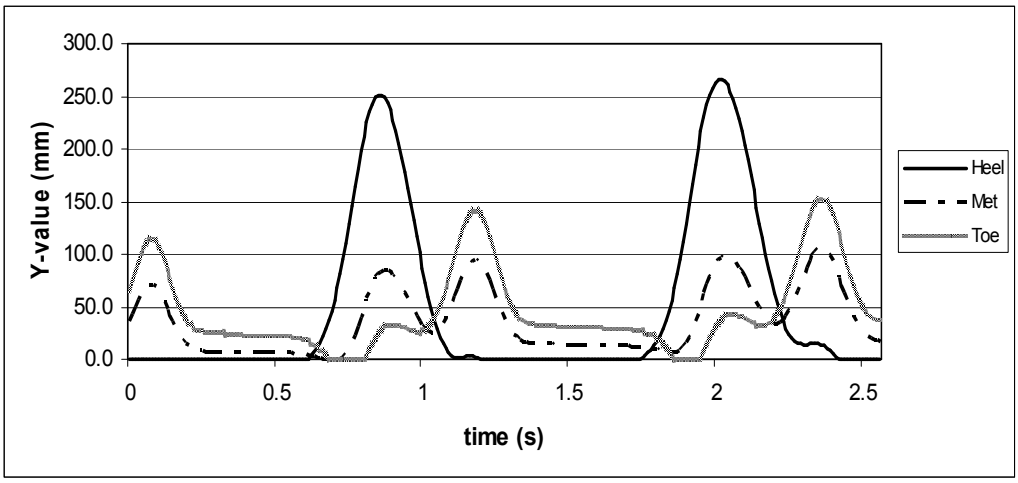

(a) Vertical coordinates of human foot

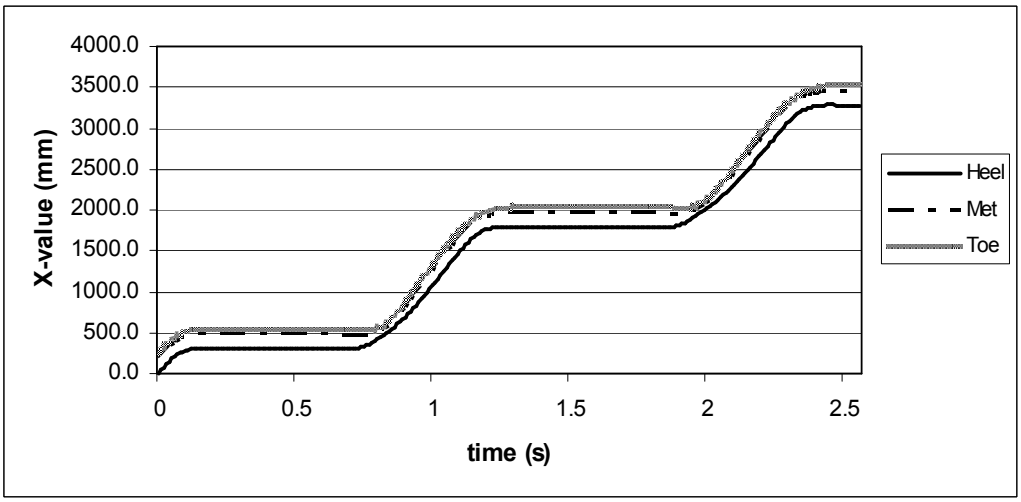

(b) Horizontal coordinates of human foot

Figure 35 Foot motion profile of Human subject C

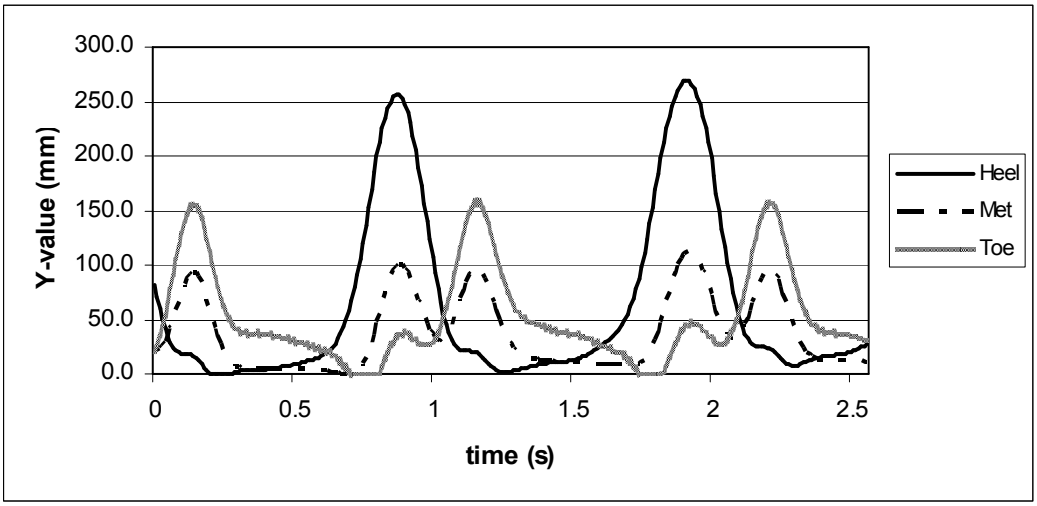

(a) Vertical coordinates of human foot

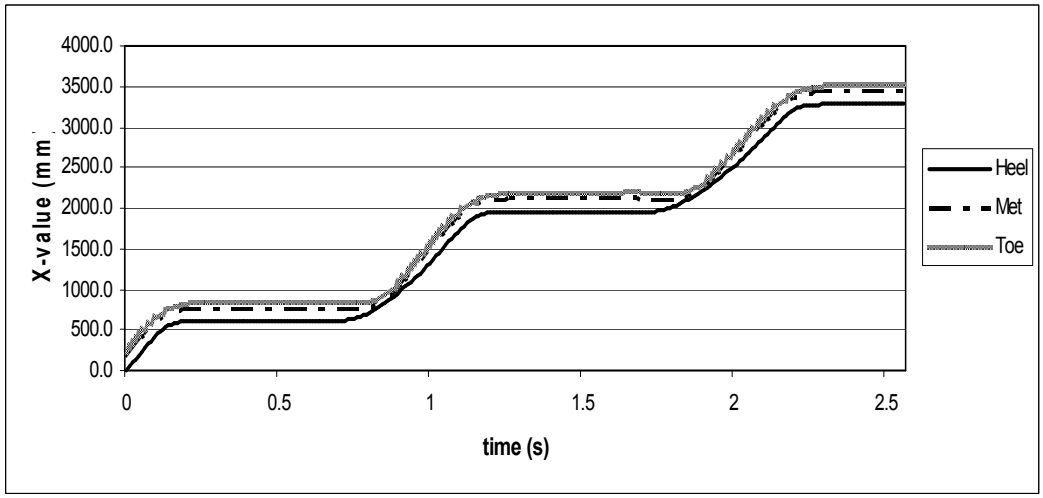

(b) Horizontal coordinates of human foot

Figure 36 Foot motion profile of Human subject D

From Figure 33 to Figure 36, it can be observed that the foot motion patterns for all human subjects are similar although small difference can be observed due to difference in personal walking habits. The highest distances between human foot and the floor are about 25.0 cm, achieved by the heel points. The strides range between 1.1 m to 1.3 m. Walking is composed of many foot movement cycles. In this study, the most important parameter of human walking is the vertical distance between human foot and floor

surface. Analysis on the measurement results shows that the vertical distance profiles for each human subject are very similar. Thus a random pick of a walking profile is used in the following analysis to represent a normal gait.

For this study, the foot movement cycle can be divided into three continuous phases: lifting heel, forward moving, foot landing, as shown in Figure 37.

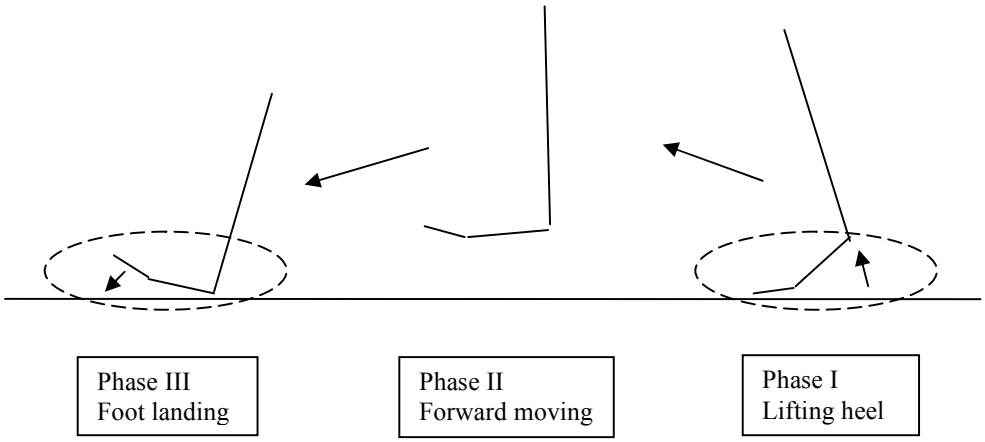

Figure 37 Decomposition of foot motion cycle of human walking

In Figure 37, it can be seen that Phase I and Phase III of human foot motion happen within a fixed location as denoted by the dashed circles, while, in Phase II, the human foot is moving from the Phase I location to the Phase III location. In this study, the electrostatic effects on particle resuspension are mainly considered in Phase I and Phase III. There are three major reasons for this consideration.

1) The foot motion in Phase I and Phase III happens within fixed locations. This means the electrostatic field generated between human shoes and floor surface can persist for a relatively longer time for such surface areas. In Phase II, from the measured data, human foot only takes about 0.1 second to pass a distance of 30 cm, which is the dimension to describe the length of the fixed areas in Phase I and III. The time for foot landing and re-lifting at a fixed location is about 0.5 second (not including the time that the whole shoe bottom rest on the floor surface).

2) Foot lifting and landing motion introduces much stronger air flow between shoe bottom and floor surface than the forward moving motion of human foot. These kinds of air flow are similar to jets impinging on a surface (Gomes 2005). As the electrostatic

force, formed under shoe bottom, can either directly pull particles away from surface or loosen their adhesion bonds with surface, air jets can more easily carry particles away from floor surface under the electrostatic field influence. Thus, the air jets occurring in Phase I and Phase III can magnify the electrostatic effects on particle resuspension.
3) The third reason is that the average distances between shoe bottoms and floor surfaces in Phase II are generally larger than those in Phase I and III. The larger distance leads to weak electrostatic field strength above the floor surface.

After all these considerations, the electrostatic effects are mainly studied in the foot landing and heel lifting phases of walking.

4.2 Measurement on human body voltage during walking

4.2.1 Description on human body voltage measurement

A body charge can easily be established in the indoor environment when the relative humidity is lower than 35% (Harriman et al 2001). Such dry air is often found in winter indoor environment when heating is used.

In this study, human body voltage is measured in the Indoor Environment Chamber of Noll Lab, at the Pennsylvania State University. The indoor environmental parameters of air temperature and relative humidity can be strictly controlled within this chamber. In the experiments, the room temperature is controlled at 25 °C and the relative humidity is controlled around 20%. These conditions are used to simulate the dry indoor air conditions in winter when electrostatic phenomena are obvious.

Three types of flooring materials and two types of human shoes are tested in this experiment, as shown in Table 19. The flooring materials are commonly found in indoor environment. The shoe sole materials are widely used for leather shoes, sneakers, flippers and etc.

Table 19 Types of flooring material and shoe sole in the test

Types of flooring material	• Vinyl tile • Cut pile nylon carpet • Loop pile nylon carpet
Types of shoe sole	• Hard rubber • EVA (Acetate)

The body voltage profiles during walking of four human subjects are tested in this experiment. Before the test can be started, each human subject needs to rest for half an hour in the chamber in order to dry body and clothes.

Each human subject has three walking test trials for a certain combination of floor sample and shoes. Given there are 3 floor samples and two types of shoes, each human subject needs to finish 18 test trials, with a repetition of 3 for each combination of floor and shoes. In each test trial, a human subject wears a pair of designated shoes and walks on a piece of designated floor material (1.2 m × 1.8 m) for 30 seconds. An electrometer is connected to the subject's body through a wrist wire. The connection of the measurement system is shown in Figure 38.

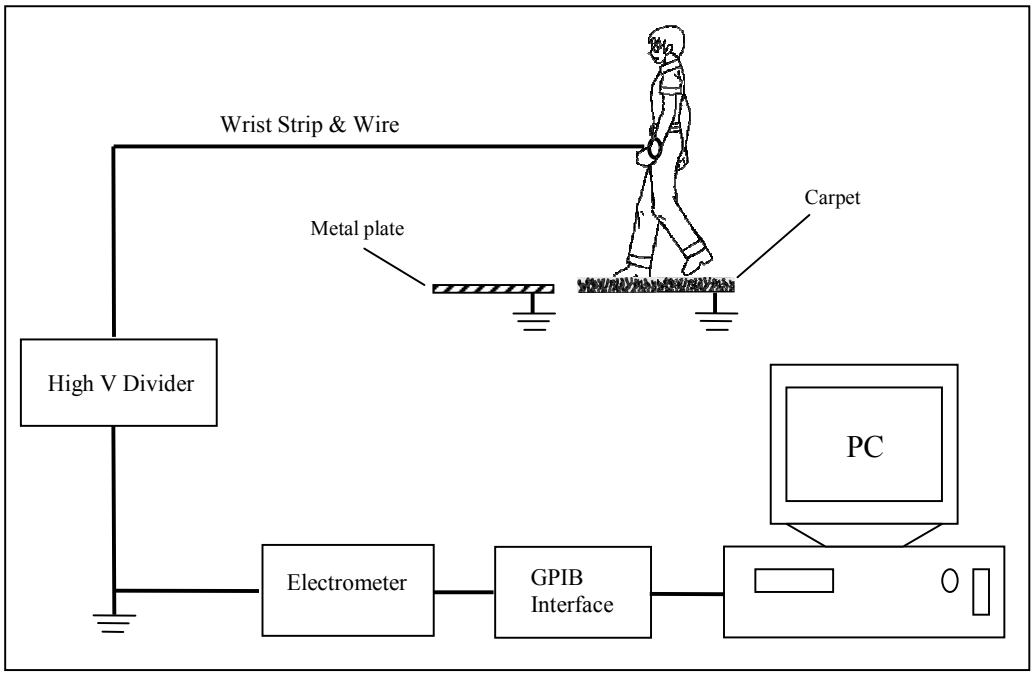

Figure 38 Measurement system of human body voltage during walking

When a human subject is walking on the surface of the floor covering, the electrometer measures the voltage of human body to the ground ($V_{body-ground}$). This voltage is actually the combination of two voltages, the voltage of human body to floor surface ($V_{body-floor}$) and the voltage of floor surface to the ground ($V_{floor-ground}$), as shown in Equation 52.

$$V_{body-ground} = V_{body-floor} + V_{floor-ground} \tag{52}$$

Because we are actually interested in $V_{body-floor}$, these two voltages need to be separated from the measured $V_{body-ground}$. Thus, after 30 seconds of continuous walking, the human subject will step on a grounded metal plate and a body discharge process will begin. The initial body voltage of the discharge process equals the $V_{body-floor}$.

Another import point to be noticed is the body voltage oscillation during walking. As introduced before, the human body gets charged to certain balanced level very quickly in winter indoor environment. While there is a dynamic balance level of body charge in continuous walking, the body capacitance changes due to different contact between human feet and the floor during walking. For example, the human body capacitance with 2 feet on the ground is about 2 times the value with one foot on the floor and the other away from the floor (Harriman et al 2001). Even with one foot on the floor, the capacitance also changes as the distance between the other foot and the floor surface changes. As the distance increases, the human body capacitance decreases and the human body voltage increases. Thus the body voltage shows oscillation pattern during human walking. The human body voltage reaches lowest value when both feet are on the floor; the human body voltage reaches the highest value when one foot rises to its highest level during walking.

Figure 39 shows a typical measurement plot from the test. A human subject wears a pair of shoes with rubber sole and walks 30 seconds continuously on a cut pile nylon carpet. Before the walking, the human subject stands still on the grounded metal plate to neutralize body voltage. After the 30-second walking, the human subject step onto a grounded metal plate again to discharge. For this discharging process, the subject only

stands on one foot in order to measure the body to floor surface voltage with one foot $V_{body-floor,1foot}$.

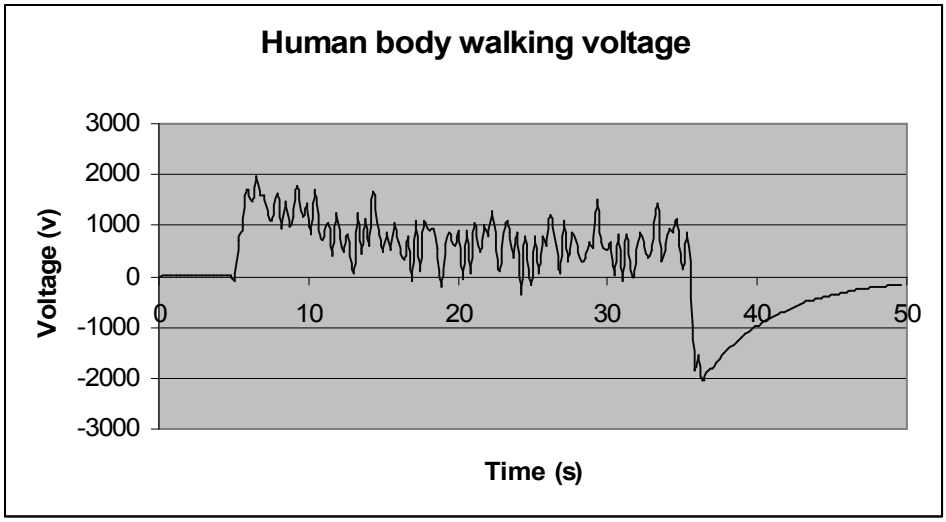

Figure 39 Body voltage recording for a walking trial

Before walking, the human subject's body voltage is around zero volts. During the 30 second walking process, the body voltage shows an obvious oscillation pattern at the same frequency of walking steps, about 1~2 steps per second. The difference between peaks and vales of the oscillation is about 1000 volts. After 30 second walking, the human subject steps onto the grounded metal plate and a peak value ($V_{body-floor}$) of -2000 volts is reached. With the information from Figure 39, the maximum and minimum body voltage during walking can be estimated with Equation 53 to Equation 55.

$$V_{body-ground,\min} = V_{body-floor,1\,foot} + V_{floor-ground} \quad (53)$$

$$V_{body-ground,\max} = V_{body-floor,2\,feet} + V_{floor-ground} \quad (54)$$

$$V_{difference} = V_{body-floor,2\,feet} - V_{body-floor,1\,foot} \quad (55)$$

Where: $V_{difference}$ = 1000 volts, $V_{body-floor,1\,foot}$ = -2000 volts, $V_{body-ground,\min}$ = 0 volts and $V_{body-ground,\max}$ = 1000 volts.

The solution of above equation series shows that $V_{body-floor,1\,foot}$ equals -2000 volts and $V_{body-floor,2\,feet}$ equals -1000 volts. Thus, during this walking process, the human body voltage to the floor surface changes between -2000 volts and -1000 volts at the same frequency of walking cycle.

4.2.2 Test results and analysis

As shown in above section, the values of maximum body to floor voltage and minimum body to floor voltage can be calculated from the measurements on each walking trial. The results are concluded in Table 20.

Table 20 Human body voltages during walking

Carpet type	Shoe sole type	Peak and vale	Human subject body voltage (V)				
			A (male)	B (male)	C (female)	D (female)	Average
Vinyl tile	Rubber	Maximum	287	987	813	1240	832
		Minimum	-433	120	93	240	5
	EVA	Maximum	2353	3620	3087	1433	2623
		Minimum	953	1420	1587	333	1073
Cut pile nylon carpet	Rubber	Maximum	-687	-373	-633	-993	-672
		Minimum	-53	-53	-133	-160	-100
	EVA	Maximum	2420	3980	4933	3187	3630
		Minimum	1020	1647	3067	1187	1730
Loop pile nylon carpet	Rubber	Maximum	-20	53	-480	90	-89
		Minimum	193	-40	-40	27	35
	EVA	Maximum	1520	1853	1647	1027	1512
		Minimum	587	787	713	460	637

From Table 20, a few important conclusions can be drawn as below.

I) The test results of human body voltage agree with the triboelectric series (Figure 11). When two materials with different position in the series are contacted, the material closer to the positive end of the series tends to get positive charges while the material closer to the negative end tends to get negative charges. When the shoe sole is acetate (EVA) that ranks more positive in the series than any flooring material in the test, human bodies are charged positively during walking. Hard rubber lies in the neutral zone of the triboelectric series, which means it tends to produce the least amount of static electricity when it gets contacted with materials at either end of series (Long 2005). This trend is also observed from Table 20, which shows the human body voltages from hard rubber friction with floor surface is much smaller than the values from EVA friction. In some cases, the human body charge with rubber shoes can oscillate between negative and positive charge instead of a unipolar charge.

II) The body voltage profiles vary significantly between different human subjects, though the general trend as mentioned in Conclusion I is obvious. Even though many factors such as air temperature, relative humidity and shoe sole material and carpet material are well controlled, there are still many factors, such as body physical properties, wearing and walking style, which can influence body voltage profiles. In this study, it is not the focus to track down all those factors. Thus average body voltage profiles are calculated for all human subject measurement results to guide the chamber electrostatic field strength simulation, as described in the following section.

III) Based on the average voltage profiles, the EVA shoe sole can generate significant body voltages on all three flooring materials, while shoe sole of hard rubber can only generate significant body voltage on the flooring materials of vinyl and cut pile nylon carpet. Here, the significant voltage level is considered as an average peak body-to-floor surface voltage higher than 500 volts.

4.3 Carpet surface field strength introduced by human walking

With the measurement results for both walking gait and body voltage, the electrostatic field strength between human shoes and floor surface can be determined. As discussed in Section 4.1, the electrostatic field effects from human walking act on floor surface residing particles mainly during two processes: foot lifting and foot landing. During these two processes, local electrostatic field strength remains high values between shoe bottom and floor surface on a fixed location, for a relatively long period of time in a walking cycle. As discussed in Section 4.2, $V_{body-floor}$ increases to its peak value when one foot lifting away from the floor surface and decreases to its vale value when both feet land completely on the floor surface. Thus the human body voltage is a function of the distance between human foot and the floor surface. For simplicity, a linear model is used to relate human body voltage with the distance between the lifting foot and the ground as shown in Equation 56.

$$V_{body-floor} = V_{\min} + k \cdot d \qquad (56)$$

Where: d is the average distance between the shoe bottom and the floor surface, m; $V_{\min}$ is the minimum body voltage during walking and is actually the body voltage when both feet contact the floor; k is a regression constant.

With the measured results both from Section 4.1 and Section 4.2, two points are available to determine the body voltage linear model for each combination of shoe sole and floor material. When both feet of a walking person are on the floor surface, d equals 0 and $V_{body-floor}$ equals $V_{\min}$. When one foot of a walking person is lifted away from the floor surface and reaches its highest point, d has the maximum value and $V_{body-floor}$ equals ($V_{\min} + k \cdot d_{\max}$). With these two points, the linear model can be determined. In Table 21, the human body voltage functions are listed for each combination of shoe sole and flooring material.

Table 21 human body voltage linear function model

Shoe sole vs. floor material*	**Linear model****
EVA vs. vinyl tile	$V_{body-floor} = 1073 + 8244.7 \cdot d$
EVA vs. cut pile nylon carpet	$V_{body-floor} = -100 + 10106.4 \cdot d$
EVA vs. loop pile nylon carpet	$V_{body-floor} = 637 + 4654.3 \cdot d$
Rubber vs. vinyl tile	$V_{body-floor} = 5 + 4398.9 \cdot d$
Rubber vs. cut pile nylon carpet	$V_{body-floor} = -100 - 3042.6 \cdot d$

* The combination of rubber and loop pile nylon carpet is not listed due to insignificant voltage generation.

** d is in the unit of m; $d_{\max}$ is 0.188 m and is the average values from all trials.

With the information of Table 21, the field strength on floor surface during human walking can be calculated by Equation 57.

$$E = \frac{V_{body-floor}}{d} \qquad (57)$$

In Equation 57, it can be noticed as d approaches to its maximum value, the field strength E decreases to its minimum value. For example, if the shoe sole material is EVA and the floor material is vinyl tile, the field strength is 139.5 V/cm when the lifting foot reaches its highest point of 18.8 cm. The field strength of 139.5 V/cm is too weak to have any influence on surface particles. When d is 0.5cm, the field strength is 2228 V/cm, which is large enough to have some electrostatic influence on surface particles. As d approaches zero, above model seems to give infinitely large field strength. However, this could not happen in reality. The air broken field strength is about 30 kV/cm and this value can not be observed during human walking. In this study, the maximum field strength is calculated only at the minimum distance of 3 mm to the ground. When the distance is below 3 mm, the measurement error of human body voltage and human gait can be too large to apply the models in Table 21 and it can be assumed that, for such a small distance, the electrostatic charged particles can only jump to the bottom surface of human shoes and are not able to enter the room air to cause resuspension. Thus, the range of d is from 3 mm to 188 mm for the models in Table 21.

As analyzed in Section 4.1, the gait profiles of the four human subjects are similar. Thus one trial of one human subject is randomly chosen to represent human walking. With the statistical software Minitab, trial 2 of human subject C is chosen as the representative human gait. As discussed in Section 4.1, the major electrostatic and airflow combined effects, on a fixed location on carpet surface, occurs during the period from foot landing to foot lifting. Such a period is extracted from the gait profile of trial 2 of human subject C and the corresponding electrostatic field strength between shoe bottom and floor surface are calculated as demonstrated in Figure 40.

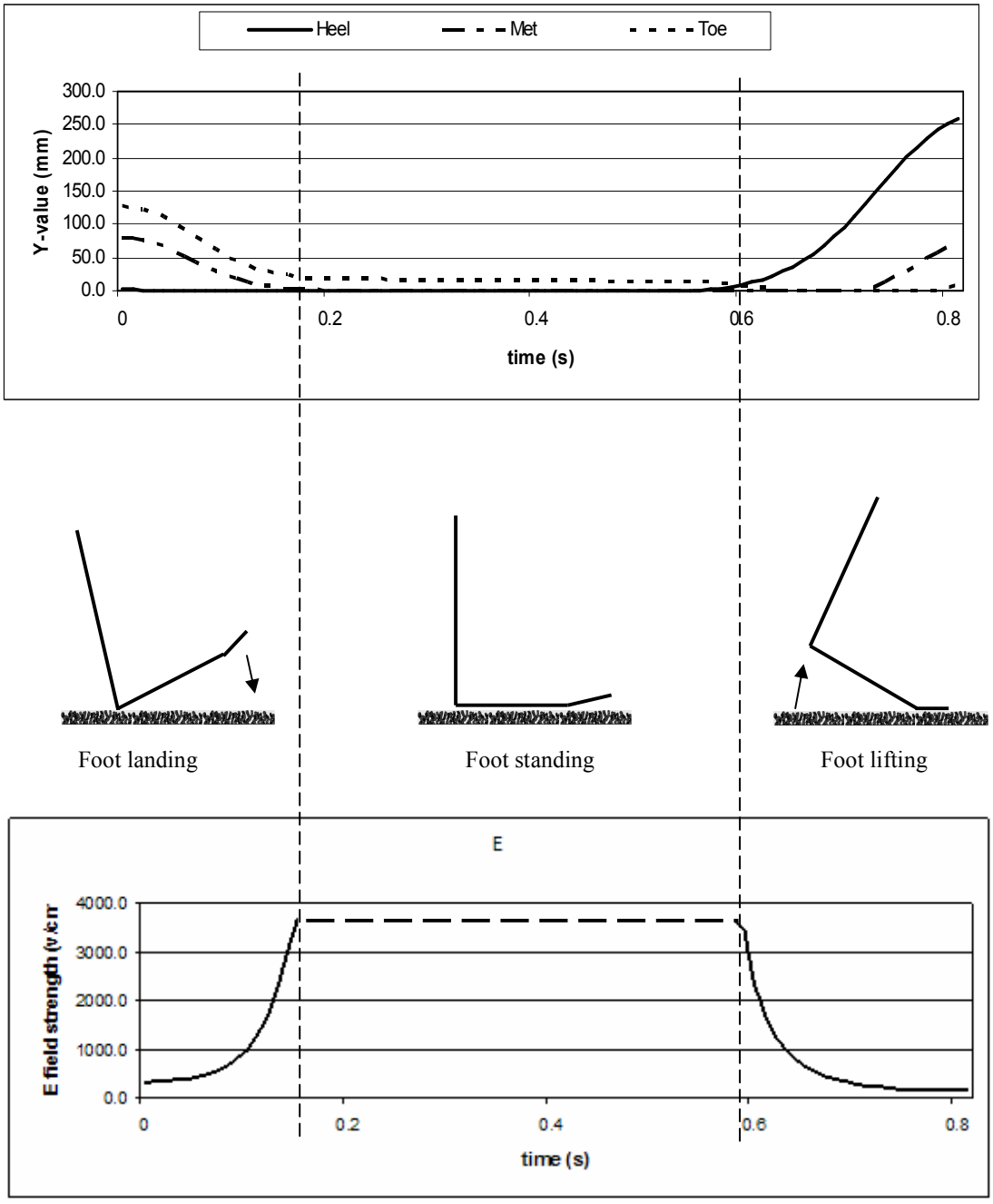

Figure 40 Human gait and floor surface electrostatic field strength

In Figure 40, the field strength on floor surface varies with the foot motion and human body voltage variation. When the heel makes first contact with the floor surface and the foot is landing, the field strength is increasing. This period lasts for 0.15 second

from 0.0 s to 0.15 s. When the foot makes full contact with the floor surface and is standing still, the field strength is very strong at a peak value about 3700 v/cm. The field strength is represented with dashed line in this period because the model in Table 21 is not valid for this period. However, since no particles can jump from the floor surface into the air under the shoe bottom due to the full contact, the real electrostatic field in this area is not a concern in this study. This period lasts for 0.43 second from 0.15 s to 0.58 s. In Phase III, the heel began to lift and the foot is lifting away from the surface. In this period, the field strength is decreasing as the foot is lifting upwards. The period lasts for 0.23 second from 0.58 s to 0.81s and ends when the foot toe detaches the floor surface.

This combined electrostatic field and air flow effects on particle resuspension is to be simulated in the particle resuspension chamber, at the Aerosol Lab of the Pennsylvania State University. As analyzed above, for 0.38 second out of the 0.81 second foot-landing-lifting cycle, such combined effects exist to influence the surface particles. In the chamber experiments, the electrostatic effect on particle resuspension will be studied for the 0.38 second period of time in one foot cycle. The electrostatic field strength profile for the 0.38 second period of time is shown in Figure 41 and is to be used in following chamber simulation study.

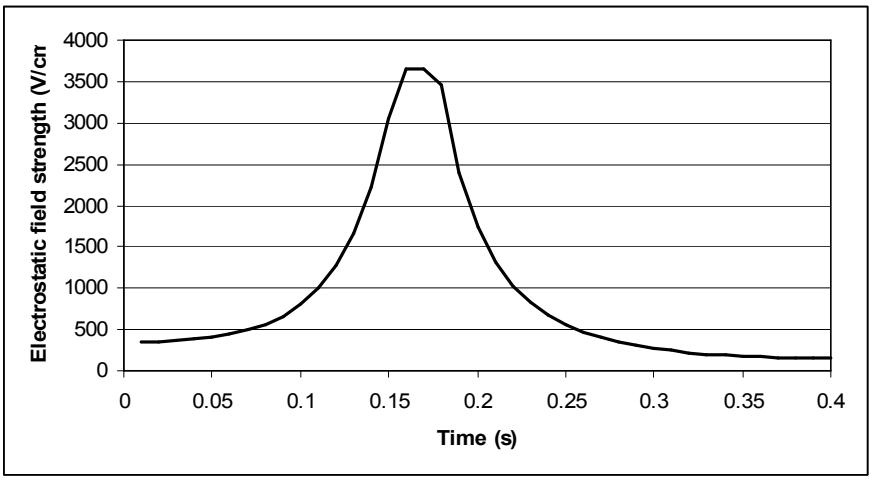

Figure 41 Electrostatic field profile of the 0.38 second period

CHAPTER 5. EXPERIMENTAL STUDY ON PARTICLE RESUSPENSION UNDER ELECTROSTATIC FIELD

As introduced in Chapter 1, a number of field experiments have been carried out to study indoor particle resuspension by human activity. However, due to the large number of uncontrolled variables in the field experiments, the measured resuspension coefficients can vary in a large range of magnitudes. It is hard to make direct comparisons between these results. These results are often so specific for the experimental conditions from which they are acquired and are not easily applied to other situations. Besides, the cost of field experiments on particle resuspension is very high. Due to these significant shortcomings, chamber experiments are used in this research to study the electrostatic effects, introduced by human walking, on particle resuspension phenomena.

5.1 Particle resuspension chamber system

The particle resuspension chamber system is composed of different equipments and control software. Before demonstrating the operation of the whole system, the most important components of this system are introduced below.

(1) Particle resuspension chamber

A particle resuspension chamber, as shown in Figure 42, was first constructed to study particle resuspension by aerodynamic force and vibration force (Gomes 2005), in the Aerosol Lab at the Pennsylvania State University. The main frame of the chamber is a quadrate metal box with dimension $400 \times 200 \times 200 mm^3$. As shown in the figure, the chamber has a pyramidal air inlet (the left side) and a pyramidal air outlet (the right side). The floor sample with particles on its surface is placed onto a movable plate in the center of the chamber floor. The vibration is simulated by a vibrator underneath the center plate. The air flow near the floor sample surface is generated air puff delivered through six

bronze pipes around the center plate. The air flow rate and blowing time of these pipes can be controlled to simulate the near ground airflow introduced by human walking.

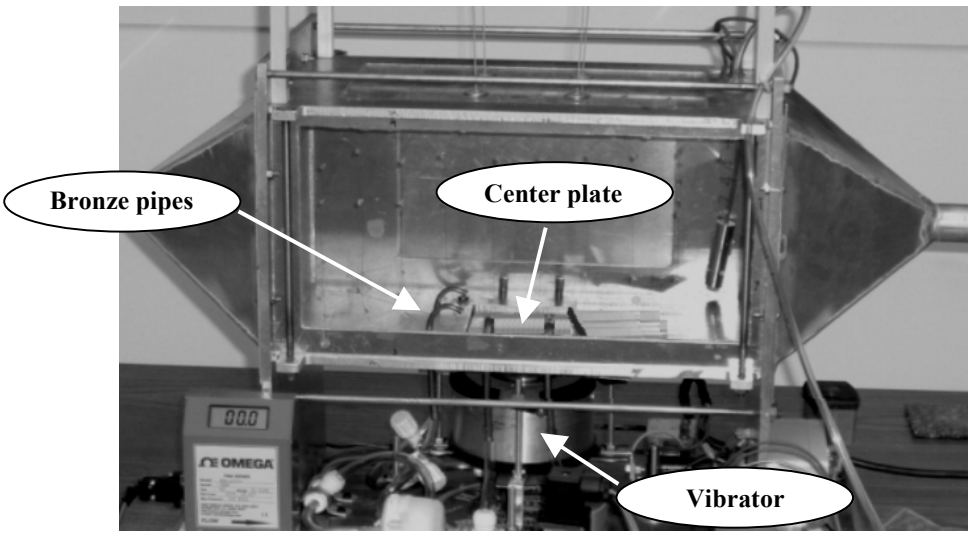

Figure 42 Particle resuspension chamber (I)

In this study, the chamber is further improved to be capable of simulating electrostatic field over the floor sample, as introduced by human walking. The improvement to the chamber is shown in Figure 43. An aluminum plate, parallel to the chamber floor, is fixed above the movable center plate, where the floor sample undergoing resuspension study is placed. The aluminum plate is then connected through a high voltage cable to a high voltage amplifier (AMS-10B2, Matsusada). The high voltage amplifier amplifies the voltage signal sent out by a Labview DAQ system.

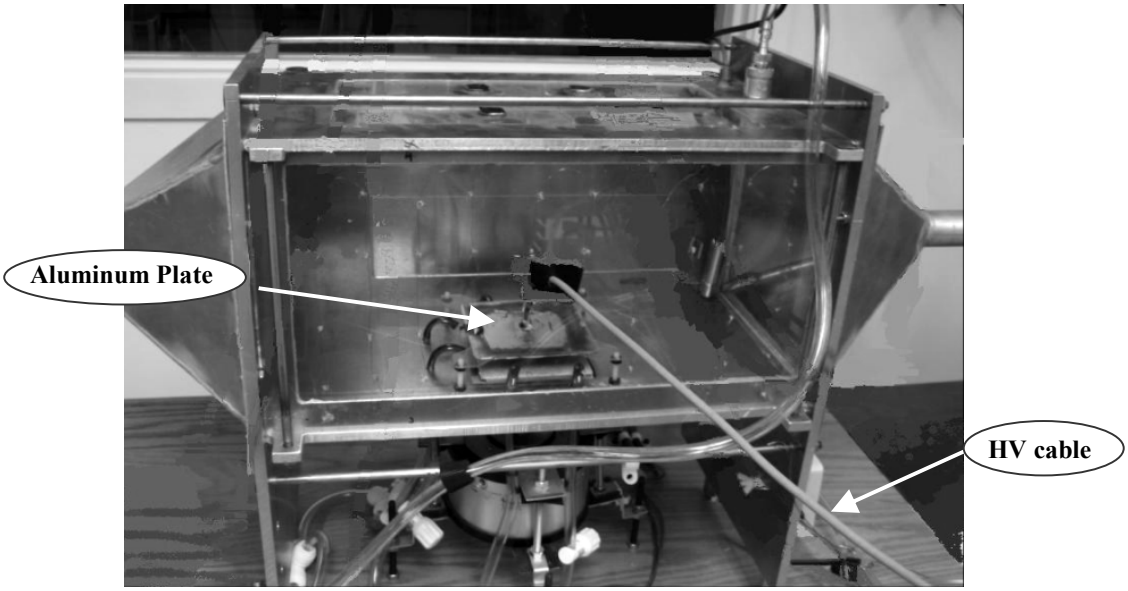

Figure 43 Particle resuspension chamber (II)

The metal walls of the chamber are all grounded during the experiment. Thus, when the high voltage signal is sent to the metal plate above the floor sample, a transient electrostatic field is generated on the surface of the floor sample. The high voltage pulse has duration of 0.38 seconds and is so controlled that the generated transient electrostatic field profile is similar to the one derived from the field measurements, as described in Figure 41.

(2) Particle dispersion box

Particle dispersion box (PDB), as shown in Figure 44, is used to disperse particles evenly onto the surface of floor samples. Particles are injected into the air space of the PDB by pressurized air though a nozzle. Four small fans are installed at the four corners of PDB to mix the suspended particles evenly with the air during the dispersion process. The PDB is 76×76×42 cm^3 in size and can be used to prepare at most 24 floor samples simultaneously.

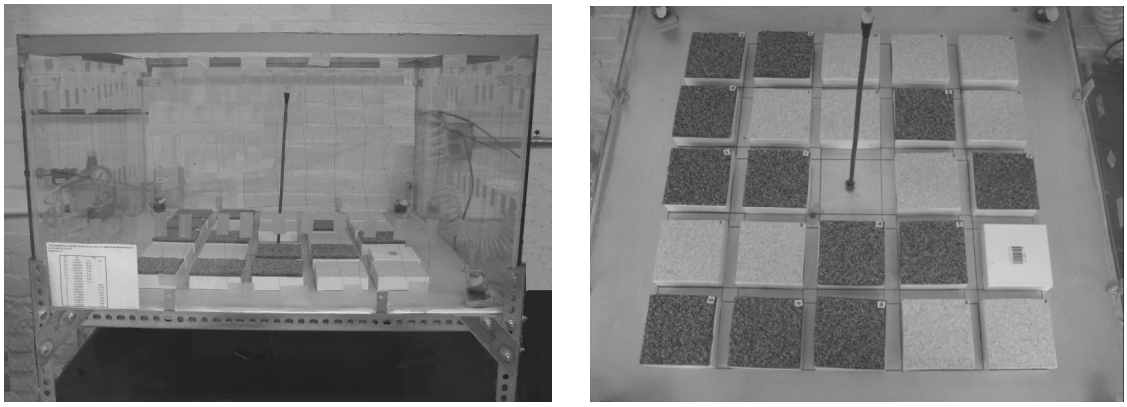

(a) Front view **(b) Top view**

Figure 44 Particle dispersion box

(3) Environmental chamber

The environmental chamber (S-8, Therotron), as shown in Figure 45, is used to maintain the temperature and humidity of the air, supplied to the particle resuspension chamber through the pyramidal inlet. The supply air is used to carry away the resuspended particles during resuspension experiments for airborne particle concentration measurement. The control range of the environmental chamber is -70ºC ~180ºC for temperature and 30% ~ 90% for relative humidity. The deliverable flow rate of controlled air is about 120 L/s.

Figure 45 Environmental chamber

(4) PM-300 optical particle counter

The optical particle counter (PM-300, Sensors Inc), as shown in Figure 46, is used to measure the airborne particle concentration in the particle resuspension chamber. This instrument measures the concentration of particles ranging from 0.3 μm to 2.0 μm in discrete size bins, at a sampling rate of 1 second. The maximum measurement capability of particle concentration is 10^{10} #/L. The sampling air flow rate is 4.0 L/min.

Figure 46 PM-300 optical particle counter

(Picture from www.sensors-inc.com)

(5) Spectro .3 optical particle counter

The Spectro .3 Particle Counter (CLiMET), shown in Figure 47, is used to provide a wider range of particle concentration measurement. This instrument provides a measurement range from 0.3 μm to 20.0 μm. The sampling interval is 12 seconds. The sampling air flow rate is 7.0 L/min.

Figure 47 Spectro .3 particle counter

(Picture from www.climet.com)

(6) Partlab 1.0

PartLab 1.0 is a visual instrument program specifically developed for the particle resuspension research in the Aerosol Lab. It is programmed with the LabView (version 7.1, National Instrument) graphical programming software. Figure 48 shows the interface of PartLab 1.0. This program communicates with a DAQ board (PCI-6259, National Instrument) and GPIB interface (PCI, National Instrument) to realize the functions of control and data acquisition. With this software, three different disturbances can be simulated and generated in the resuspension chamber. Partlab 1.0 can also help to define disturbance cycle and total time length of disturbance. The environmental parameters of the resuspension chamber such as temperature and relative humidity are monitored and recorded by this software.

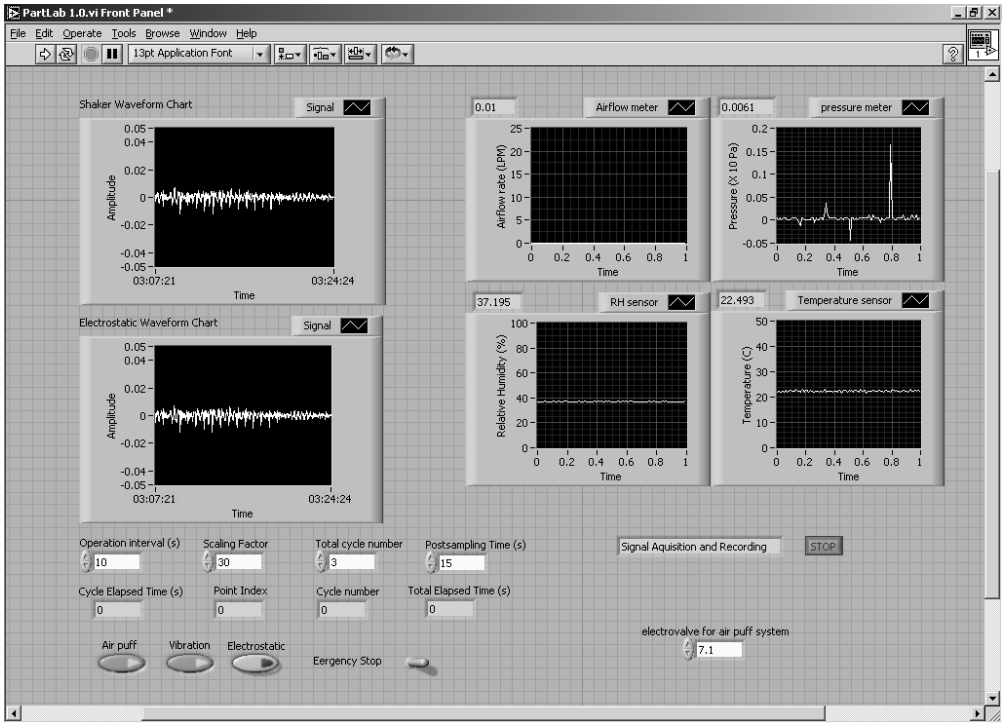

Figure 48 Interface of PartLab 1.0

(7) High voltage amplifier

The high voltage amplifier (AMS-10B2, Matsusada), shown in Figure 49, is used to amplify the low voltage signals from DAQ board into high voltage profiles, simulating human body electrostatic voltage in the particle resuspension chamber. The maximum voltage output is ±10 kV. The slew rate is 30V/μm, giving the instrument a very fast response to variation of input signals.

Figure 49 High voltage amplifier

(8) Operation of resuspension chamber system

The particle resuspension chamber system is a combination of above components for the purpose of particle resuspension study. The operation flow chart of the chamber system is demonstrated in Figure 50.

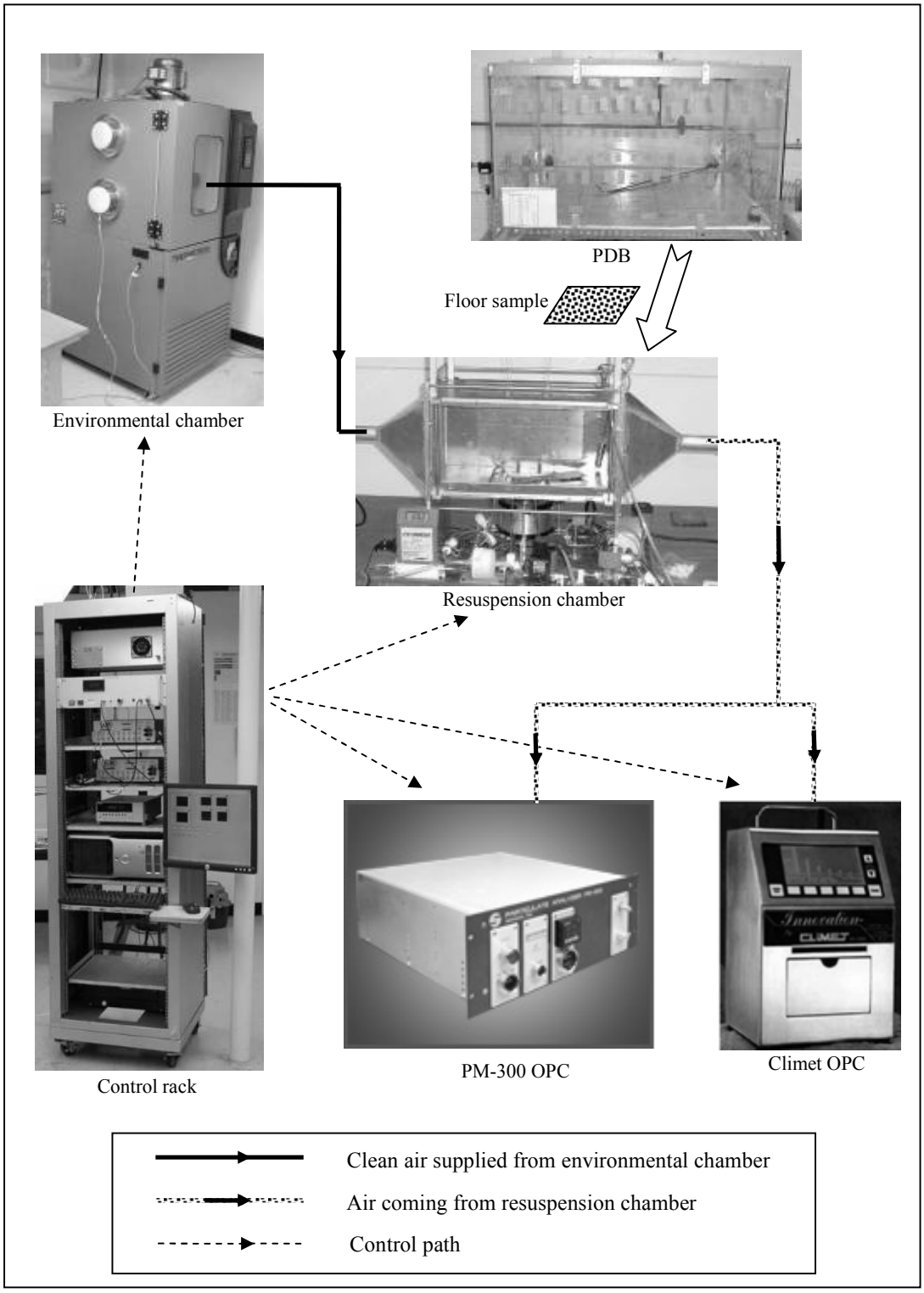

Figure 50 Operation flow chart of resuspension chamber system

In Figure 50, a floor sample with deposited particles on its surface is taken out from the PDB and placed onto the center plate of the chamber. Except for the air inlet and outlet at each end of the chamber, the chamber is sealed from outer environment.

Air with controlled temperature and relative humidity is supplied from the environmental chamber. The supplying air is filtered before it enters the resuspension chamber. The flow rate of supplying air is 34.0 L/min. The average supply air flow velocity passing the chamber space is about 1.4 cm/second. This speed is too small to generate any significant particle resuspension from floor sample by itself. Such slow air flow forms a displacement flow from one end of the chamber to the other end. This flow can be approximated as laminar flow and can help to pressurize the chamber and carry the resuspended particles to the chamber outlet for measurement purpose.

Disturbance of aerodynamic, vibration and electrostatic forces can be generated on the floor sample within the chamber to resuspend the particles on its surface. This disturbance generation is controlled by the control rack. After the surface particles enter the air, the continuous supply air of the chamber carries the airborne particles away. Then the clean supply air becomes contaminated and flows out of the chamber through the outlet at the other end of the chamber. The out-flowing contaminated air is sampled by two OPCs: one is PM_300 and the other is Climet .3. OPC PM_300 gives a concentration reading every one second, while OPC Climet .3 gives an average concentration reading every 12 seconds. In the following analysis, the sampling results from OPC PM_300 are used due to its fast sampling frequency. The sampling data from OPC Climet .3 are used as a back-up in case there is a reading failure of OPC PM_300.

In this resuspension experiment, each transient electrostatic field lasts 0.38 second with air puff from the six pipes at the same time to simulate the disturbance to floor surface particles of one step during human walking. The electrostatic field strength profile is measured by experiments and demonstrated in Figure 41. The flow rate of the air puff system is 19 L/min, which is used to simulate the air flow introduced by human walking (Gomes 2005). The mechanical disturbance is not considered and thus not simulated in this research.

After the 0.38 second of resuspension disturbance, there is an interval of 23.62 seconds before another disturbance of 0.38 second is started. Thus, there is a cycle of 24

seconds in the chamber system and the disturbance time only lasts 0.38 second in each cycle. When the disturbance starts, the airborne particle concentration increases abruptly. After the disturbance stops, the airborne concentration decrease gradually as the continuing supplying displacement air flow of chamber pushes the contaminated air out of the chamber. By the end of the 24-second cycle, it is considered that all the resuspended particles have been carried out of the chamber through the chamber outlet and the chamber air is clean again for the start of another turn of particle resuspension. This assumption is validated by the experimental observations.

As the particle adhesion force experiments, all the particle resuspension experiments are carried out in the 25 m^2 lab. The lab relative humidity is maintained a relative humidity level of 40%±2.5%.

5.2 Experiment design on the study of the electrostatic effects

Experiments are designed with the resuspension chamber to study the electrostatic effects on particle resuspension. In the experiments, the effects of four factors on particle resuspension are studied: flooring type, particle type, electrostatic field profile and electrostatic field direction.

There are two possible electrostatic directions. When the shoes contain positive charge after friction with floor surface, the field direction is from the shoe bottom to the floor surface. For simplicity of representation, the electrostatic field with this direction is named positive field in this study. Likewise, the field is called negative field when the shoes carry negative charge after friction with the floor surface.

In the study, a complete factorial design on flooring type, particle type and electrostatic field profile is used within each field direction to study the electrostatic effects on particle resuspension. The two factorial designs are introduced below.

5.2.1 Factorial design with positive electrostatic field

For the resuspension experiments designed in this section, all field directions are positive. There are four types of particles and two types of flooring materials to be studied as shown in Table 22.

Table 22 Particle type and floor type for factorial design with positive field

Particle type		Flooring type
Organic	**Mineral**	
• Spore • Dust mite	• Alumina • Quartz	• Vinyl tile • Nylon round loop carpet

As shown in Table 22, the particles are classified into two groups: one is mineral particles and the other is organic particles.

As introduced in Chapter 4, in the field measurements of human body voltage profiles, different combinations of shoe types and floor materials can give different electrostatic field profiles. However, most of the measurements give positive fields between human shoe bottoms and floor surfaces. The shoes with sole material of EVA generate more significant field strength than the hard rubber soles. The combination of EVA sole and vinyl floor generate a stronger field than the combination of EVA sole and nylon round loop carpet. In the experiment design, three profiles of electrostatic field are used. One of the three profiles is a control profile, which means zero field strength is applied in the experiments. The other two profiles are named high field strength profile and medium field strength profile, abbreviated as high profile and medium profile. The profile determined from the combination of EVA sole and vinyl tile is used as the high profile. The profile determined from the combination of EVA sole and nylon round loop carpet is used as the medium profile.

All three field strength profiles will be applied across the combination of particles and flooring types in following experiment design. It may look strange to apply high profile of field strength onto nylon carpet sample since this profile is not measured on the surface of nylon carpet. As only two sole materials are measured in the field experiments

in Chapter 4, it is possible that some other shoe sole material can achieve the high profile on the surface of nylon carpet. Because the focus in this experiment is how the field profiles can influence resuspension instead of which specific combination can achieve such profiles, both the high profile and medium profile are tested across the flooring types. The complete factorial design for positive field is shown in Table 23.

Table 23 Factorial experiment design for positive field

Carpet	Particle	Field profile	Replication
• Vinyl tile • Nylon round loop carpet	• Spore • Dust mite • Alumina • Quartz	• High • Medium • Control	3

As shown in Table 23, with a replication of 3 for each combination of carpet, particle and field profile, the total number of resuspension experiments for this design is $2 \times 4 \times 3 \times 3 = 72$.

5.2.2 Factorial design with negative electrostatic field

Most of the field measurements on electrostatic fields generated by human walking give positive voltage profiles. As discussed before, due to the limited types of testing materials, this does not mean that the occurrence of negative field strength is not common. The effects of negative field on particle resuspension also need to be studied in order to determine whether there is an effect of field direction on particle resuspension. For this purpose, the directions of the positive high profile and medium profile, as introduced in Section 5.2.1, are reversed to get the negative high profile and medium profile, while the absolute magnitude of the profiles are the same. In the experiment design with negative electrostatic field, only two types of particles (spore and alumina) and two field profiles (high and control) are chosen for the experiments. This simplification can greatly reduce the number of required experiments, while it can still address the concern on the effects of field direction in this part of design. The complete factorial design for positive field is shown in Table 24.

Table 24 Factorial experiment design for positive field

Carpet	Particle	Field profile	Replication
• Vinyl tile • Nylon round loop carpet	• Spore • Alumina	• High • Control	3

As shown in Table 24, with a replication of 3 for each combination of carpet, particle and field profile, the total number of resuspension experiments for this design is $2 \times 2 \times 2 \times 3 = 24$.

5.3 Experimental results and analysis

5.3.1 Calculation of resuspension fractions from experiments

As introduced before, resuspension fraction is a standardized measure of particle resuspension rate, based on actual particle resuspension area. In the particle resuspension chamber experiments, because the whole area of floor sample is uniformly disturbed by controlled forces, the measurement results from the chamber system can be directly used to calculate the particle resuspension fractions. Thus, resuspension fractions from the experimental study will be calculated and compared with the values acquired from literature.

The OPC read airborne particle number concentration in the chamber continuously during the particle resuspension experiments. As described above, each resuspension cycle is 24 seconds with disturbance of 0.38 second. The measured airborne concentration can be used to calculate the total particle mass resuspended into the air and calculate the particle resuspension fraction. Assuming uniform particle concentration of the air flowing out of the chamber, the calculation of resuspension fraction is shown by Equation 58.

$$\text{Re}\,suspension\ fraction = \frac{\sum_i \sum_j C_{Ai,j} \cdot \dot{V} \cdot \Delta t \cdot \frac{\pi}{6} d_{pi}^3 \cdot \rho_p}{\Delta m} \tag{58}$$

Where: i is the order number of particle size bin; j is the order number of sampling interval, $j = 1,2,\ldots 24$ for one simulation cycle; $C_{Ai,j}$ is the airborne particle concentration of ith size bin measured at jth sampling interval by OPC, $\#/L$; $\dot{V}$ is the airflow rate of chamber supplying air, 34 L/min; Δt is the sampling interval of OPC, $\frac{1}{60}$ min; d_{pi} is the diameter of particles in ith size bin, m; Δm is the total particle mass on the floor sample, kg.

The total particle mass on a floor sample is measured with an analytical balance AAA 160L (Adam Equipment). The balance gives a resolution of 0.1 mg. Before a floor sample with deposited particles is placed into the chamber, the total mass of the floor sample is measured and recorded as m1. After the resuspension experiment, the floor sample is taken out of the chamber. Then the remaining particles on the floor sample are cleaned by a vacuum and high pressure air. After cleaning, the floor sample is measured again by the scale and recorded as m2. The difference between m1 and m2 gives the value of Δm , the total particle mass on the floor sample. It needs to be noticed that the particle resuspension fraction is highest for the first disturbance and drops greatly through flowing disturbances because of exhaust of resuspensible particles. In this study, the resuspension fractions from the first disturbance are used for following analysis.

5.3.2 Resuspension fractions under positive fields

(1) Resuspension fraction for alumina particle

For alumina particles, the resuspension fractions from chamber experiments are concluded in Table 25. There are 18 experiments in total.

Table 25 Alumina resuspension fractions

Electrostatic field profile	Flooring type	replication number	Resuspension fraction	Mean resuspension fraction	Standard deviation
High	vinyl	1	1.51E-05	1.57E-05	2.36E-06
		2	1.37E-05		
		3	1.83E-05		
	Nylon carpet	1	2.87E-05	2.71E-05	6.06E-06
		2	3.22E-05		
		3	2.04E-05		
Medium	vinyl	1	9.49E-06	9.58E-06	1.57E-06
		2	1.12E-05		
		3	8.06E-06		
	Nylon carpet	1	6.86E-05	6.24E-05	5.50E-06
		2	5.82E-05		
		3	6.03E-05		
Control	vinyl	1	6.12E-06	8.45E-06	2.50E-06
		2	1.11E-05		
		3	8.16E-06		
	Nylon carpet	1	3.77E-05	4.06E-05	4.62E-06
		2	4.59E-05		
		3	3.81E-05		

Table 25 shows the mean resuspension fractions of alumina particles for each field profile and flooring type combination. In order to study the effects of different factors on resuspension fraction, the statistical analysis of ANOVA is applied on the experimental results acquired from the factorial experiment design. The software used to implement this analysis is Minitab v14. The Minitab outputs are shown in Figure 51.

General Linear Model: Resuspension Fra versus E-field Profile, Floor

```
Factor           Type   Levels  Values
E-field Profile  fixed       3  Control, High, Medium
Floor            fixed       2  Nylon carpet, vinyl


Analysis of Variance for Resuspension Fraction, using Adjusted SS for Tests

Source                  DF     Seq SS     Adj SS     Adj MS       F      P
E-field Profile          2  0.0000000  0.0000000  0.0000000   20.66  0.000
Floor                    1  0.0000000  0.0000000  0.0000000  270.98  0.000
E-field Profile*Floor    2  0.0000000  0.0000000  0.0000000   37.54  0.000
Error                   12  0.0000000  0.0000000  0.0000000
Total                   17  0.0000000


S = 4.136135E-06   R-Sq = 97.00%   R-Sq(adj) = 95.74%
```

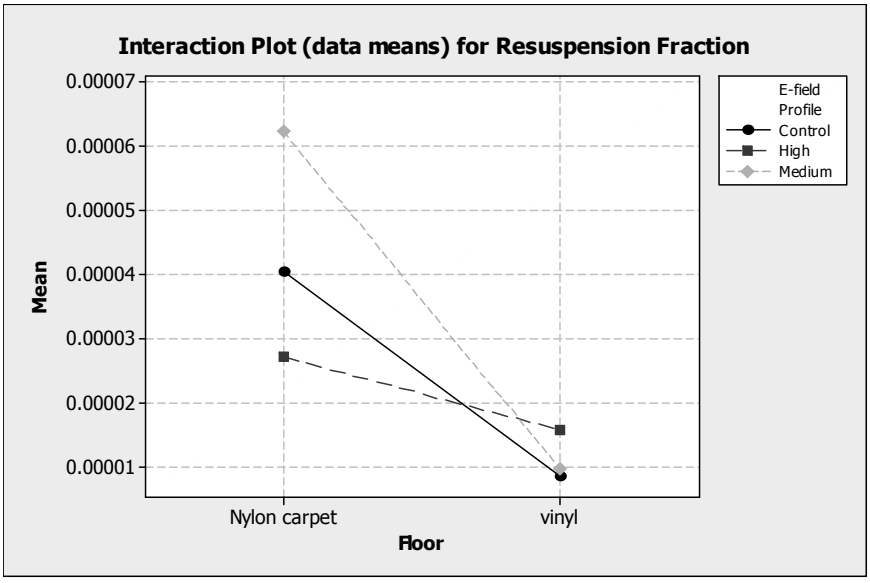

Figure 51 Statistical analysis of alumina resuspension fractions

In the analysis, the p values of the factors and interactions, as denoted by an oval in Figure 51, are most important for the interpretation. P values range from 0.0 to 1.0 and a small p value means the corresponding factor or interaction is significant. In this study, a value of 0.10 is used as the significance level. When a p value is smaller than 0.10, the corresponding factor or interaction is considered as significant. In Figure 51, the p values for both factors (field profile and floor type) and their interaction are all about 0.00, which are much smaller than the critical value of 0.10. Thus, it can be concluded that

field profile, floor type and their interaction have significant influence on alumina particle resuspension fraction.

To help the interpretation, an interaction plot is also drawn with Minitab as shown in Figure 51. In Figure 51, the resuspension fractions for nylon carpet are generally larger than those for vinyl tile. This is because the surface configuration of the carpet can disturb air flow boundary layer and increase the turbulence of air flow. In this way, for the same magnitude of air puff disturbance, the air flow has a more significant effect on particle resuspension on the carpet surface than on the flat vinyl tile surface. The non-parallel property of effect lines shows that there is interaction between field profile and floor type on alumina particle resuspension. For vinyl tiles, the medium profile does not change the resuspension fraction much from the control experiments while the high profile significantly increases the resuspension fraction. For nylon carpet, the high profile decreases alumina particle resuspension while the medium profile increases the resuspension fraction.

Above analysis shows that electrostatic field does have significant effects on alumina resuspension. Under high profile, the resuspension fraction of alumina on vinyl tile is increased by 85.8% as compared to the control group experiments without any electrostatic field strength. However, the experimental results for nylon carpets are more complicated than for vinyl tile. This can be explained by the multi-way effects that electrostatic field can have on surface particle resuspension. First of all, the electrostatic force can loosen or totally destroy the adhesion bond between particles and surface, and thus contribute to resuspension. On the other hand, the electrostatic field can also attract some jumped particles onto the surface of charged shoe bottoms and thus decrease the amount of particles entering the air. So the final effect on the particle resuspension is the combination of these two counteracting processes. Given the high air flow turbulence above carpet surface, particle resuspension fractions from the combined effects can be non-uniform trend with regard to the field strength increases. In this experiment, it shows that the high profile field on the surface of carpet cause more particles attached to the metal surface and leads to a resuspension fraction lower than that of control experiment. However, the dynamic balance under medium field strength makes more particles to eventually enter into the air than the control experiments.

In the experiments, particles are observed to attach the surface of the metal plate when the electrostatic field profile is high, as shown in Figure 52, even though high field strength beyond 1 kV/cm lasts less than 0.1 second in each disturbance cycle. However, such attachment phenomena are not so obvious for medium field strength. In the experiments of Roberts et al (1996), particles smaller than 10 μm show strong tendency to attach to shoe soles. It can be conjectured that such attaching phenomena have strong connections with the electrostatic attraction effects.

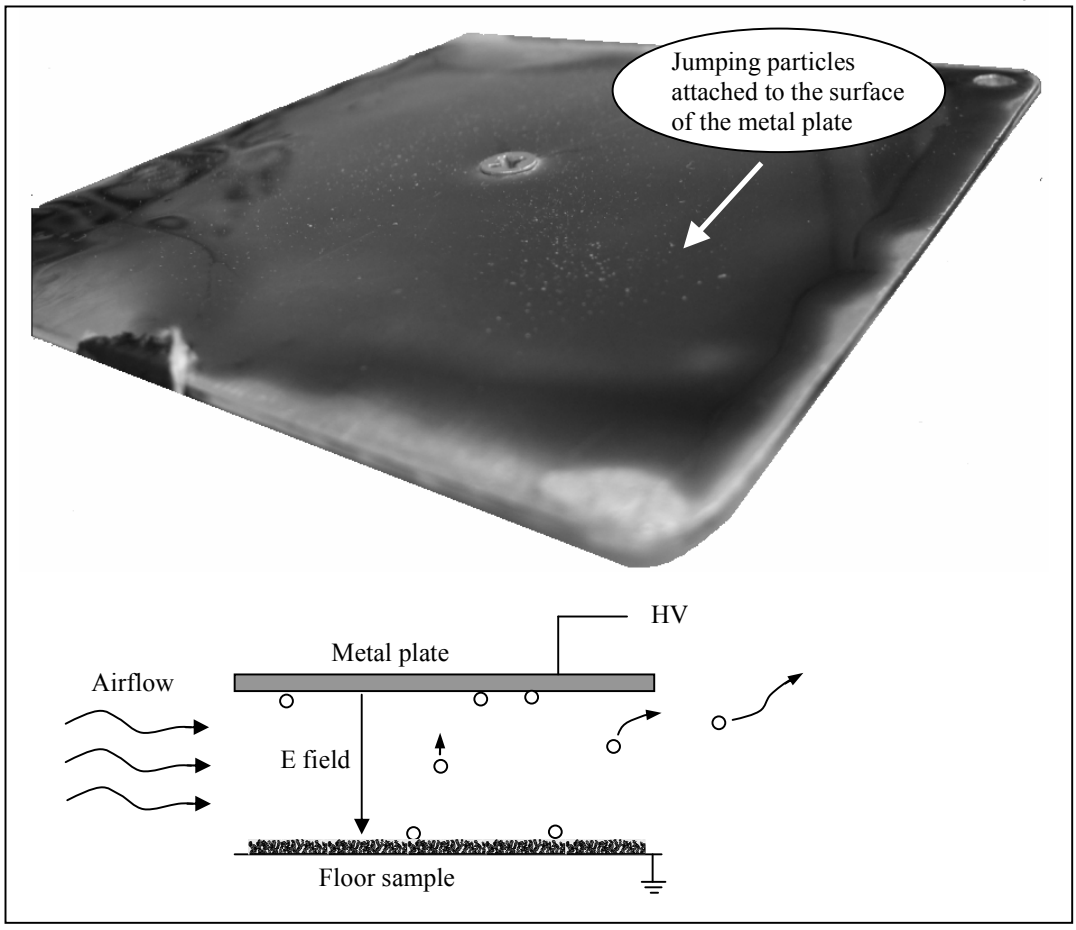

Figure 52 Surface particle attachment under high field profile

(2) Resuspension fraction for silica sand particle

For silica sand particles, the resuspension fractions from chamber experiments are concluded in Table 26. There are 18 experiments in total.

Table 26 Silica sand resuspension fractions

Electrostatic field profile	Flooring type	replication number	Resuspension fraction	Mean resuspension fraction	Standard deviation
High	vinyl	1	8.35E-05	7.35E-06	2.08E-05
		2	6.2E-05		
		3	4.2E-05		
	Nylon carpet	1	6.02E-05	4.58E-06	1.85E-05
		2	2.8E-05		
		3	2.84E-05		
Medium	vinyl	1	3.7E-05	5.17E-06	1.43E-05
		2	6.03E-05		
		3	3.44E-05		
	Nylon carpet	1	1.98E-05	3.38E-06	9.44E-06
		2	3.86E-05		
		3	2.77E-05		
Control	vinyl	1	4.99E-05	5.13E-06	5.65E-06
		2	4.19E-05		
		3	3.9E-05		
	Nylon carpet	1	5.09E-05	5.91E-06	1.42E-06
		2	5.12E-05		
		3	4.86E-05		

ANOVA is carried out with Minitab on the experiment design shown in Table 26. The Minitab output is shown in Figure 53.

General Linear Model: Resuspension Fraction versus E-field Profile, Floor

```
Factor           Type   Levels  Values
E-field Profile  fixed       3  Control, High, Medium
Floor            fixed       2  Nylon carpet, vinyl


Analysis of Variance for Resuspension Fraction, using Adjusted SS for Tests

Source                  DF     Seq SS     Adj SS     Adj MS     F      P
E-field Profile          2  0.0000000  0.0000000  0.0000000  1.82  0.204
Floor                    1  0.0000000  0.0000000  0.0000000  2.82  0.119
E-field Profile*Floor    2  0.0000000  0.0000000  0.0000000  1.99  0.180
Error                   12  0.0000000  0.0000000  0.0000000
Total                   17  0.0000000


S = 0.0000135399   R-Sq = 46.53%   R-Sq(adj) = 24.25%
```

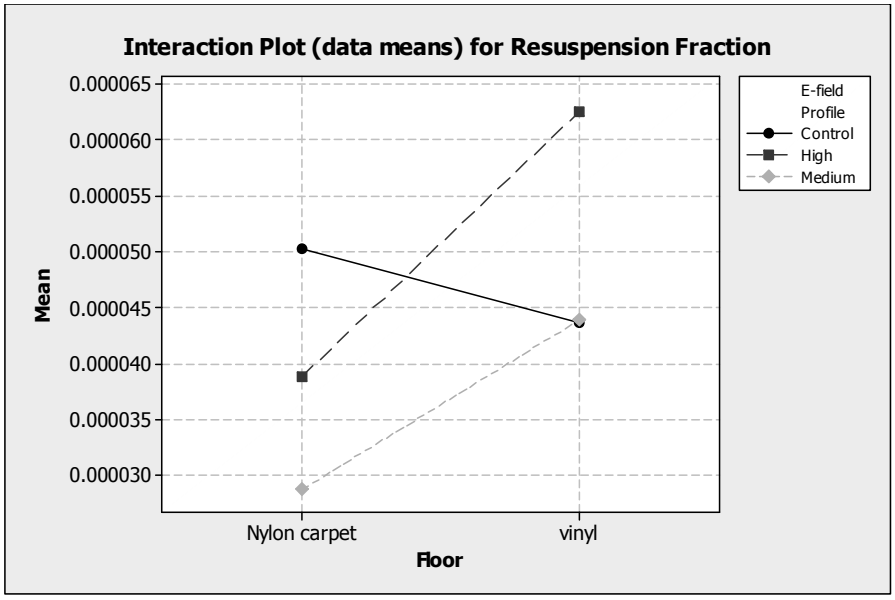

Figure 53 Statistical analysis of silica sand resuspension fractions

The Minitab output shows that none of the p values is smaller than 0.10. It can not be concluded that any of the factors and interaction is statistically significant. However, the p values are still close to 0.10 and a further explore on the interaction plot, as also shown in Figure 53, can help interpret the realistic meaning of the experimental results.

In the interaction plot, the resuspension fractions of silica sand on vinyl file show a pattern similar to that of alumina particles. That is, on vinyl tile surface, resuspension fractions of silica sand increase under high electrostatic profile while they do not change

much from the results of control experiments for medium profile. The resuspension fractions in control experiments are increased by about 43.3% when high profile electrostatic field is applied upon the vinyl tile surface. For nylon carpet, both the high and medium profiles decrease the particle resuspension fraction due to the overwhelming electrostatic attraction effects as discussed for alumina particles.

(3) Resuspension fraction for spore particle

For the organic particles of spore, the resuspension fractions from chamber experiments are concluded in Table 27. There are 18 experiments in total.

Table 27 Spore resuspension fractions

Electrostatic field profile	Flooring type	replication number	Resuspension fraction	Mean resuspension fraction	Standard deviation
High	vinyl	1	2.81E-05	2.54E-05	4.79E-06
		2	2.81E-05		
		3	1.98E-05		
	Nylon carpet	1	9.80E-06	1.07E-05	2.81E-06
		2	8.52E-06		
		3	1.39E-05		
Medium	vinyl	1	2.73E-05	2.27E-05	4.04E-06
		2	2.11E-05		
		3	1.97E-05		
	Nylon carpet	1	2.52E-05	2.15E-05	3.24E-06
		2	2.01E-05		
		3	1.92E-05		
Control	vinyl	1	2.23E-05	1.72E-05	4.46E-06
		2	1.38E-05		
		3	1.57E-05		
	Nylon carpet	1	1.85E-05	1.39E-05	4.01E-06
		2	1.23E-05		
		3	1.10E-05		

ANOVA is carried out with Minitab on the experiment design shown in Table 27. The Minitab output is shown in Figure 54.

General Linear Model: Resuspension Fra versus E-field Profile, Floor

```
Factor           Type   Levels  Values
E-field Profile  fixed       3  Control, High, Medium
Floor            fixed       2  Nylon carpet, vinyl


Analysis of Variance for Resuspension Fraction, using Adjusted SS for Tests

Source                  DF     Seq SS     Adj SS     Adj MS       F      P
E-field Profile          2  0.0000000  0.0000000  0.0000000    4.20  0.041
Floor                    1  0.0000000  0.0000000  0.0000000   11.76  0.005
E-field Profile*Floor    2  0.0000000  0.0000000  0.0000000    4.99  0.026
Error                   12  0.0000000  0.0000000  0.0000000
Total                   17  0.0000000


S = 3.948668E-06   R-Sq = 71.52%   R-Sq(adj) = 59.66%
```

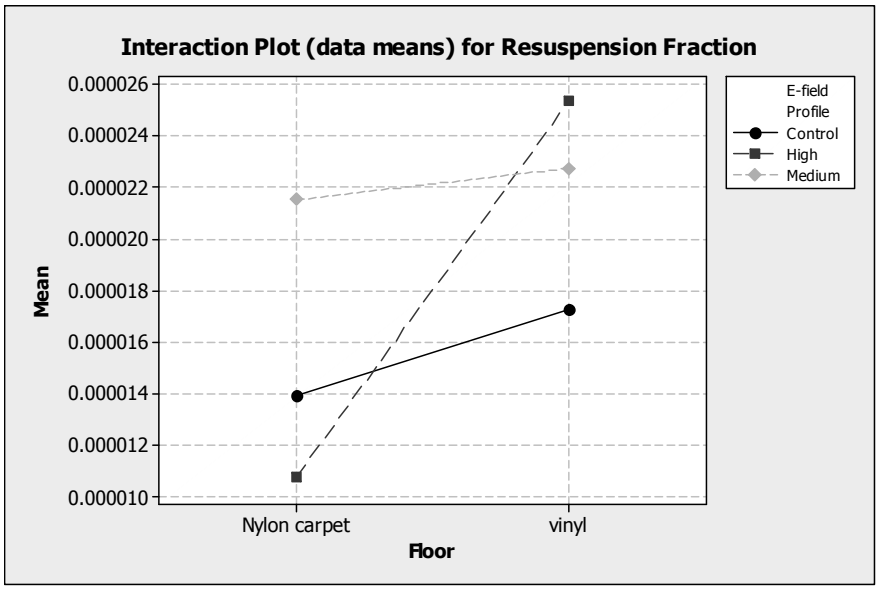

Figure 54 Statistical analysis of spore resuspension fractions

In the Minitab outputs, all the p-values are smaller than the significance level of 0.10. Thus, it can be concluded that field profile, floor type and their interaction all have significant influence on spore particle resuspension fraction.

The interaction plot shows that significant increase of resuspension fractions can be observed for spore particles on the vinyl surface, for both high profile (47.7% increase) and medium profile (32.0% increase). Again, the pattern on carpet surface is not so

obvious to conclude, as the medium profile increase the resuspension fraction while the high profile decrease the value.

(4) Resuspension fraction for dust mite particles

For the organic particles of dust mite, the resuspension fractions from chamber experiments are concluded in Table 28, with 18 experiments in total.

Table 28 Dust mite resuspension fractions

Electrostatic field profile	Flooring type	replication number	Resuspension fraction	Mean resuspension fraction	Standard deviation
High	vinyl	1	1.15E-04	1.15E-04*	1.33E-05
		2	9.62E-05		
		3	1.22E-04		
	Nylon carpet	1	3.56E-05	3.79E-05	3.42E-06
		2	3.62E-05		
		3	4.18E-05		
Medium	vinyl	1	1.16E-04	6.73E-05*	2.63E-05
		2	6.73E-05		
		3	7.45E-05		
	Nylon carpet	1	5.76E-05	5.36E-05	6.33E-06
		2	5.69E-05		
		3	4.63E-05		
Control	vinyl	1	6.82E-05	7.61E-05	7.57E-06
		2	8.33E-05		
		3	7.68E-05		
	Nylon carpet	1	8.30E-05	8.03E-05*	1.77E-05
		2	5.01E-05		
		3	7.77E-05		

* Unusual observations denoted by Minitab are not counted for mean.

ANOVA is carried out with Minitab on the experiment design shown in Table 28. The Minitab output is shown in Figure 55.

General Linear Model: Resuspension Fra versus E-field Profile, Floor

```
Factor           Type   Levels  Values
E-field Profile  fixed       3  Control, High, Medium
Floor            fixed       2  Nylon carpet, vinyl


Analysis of Variance for Resuspension Fraction, using Adjusted SS for Tests

Source                  DF     Seq SS     Adj SS     Adj MS       F      P
E-field Profile          2  0.0000000  0.0000000  0.0000000   12.96  0.002
Floor                    1  0.0000000  0.0000000  0.0000000  111.74  0.000
E-field Profile*Floor    2  0.0000000  0.0000000  0.0000000   74.35  0.000
Error                    9  0.0000000  0.0000000  0.0000000
Total                   14  0.0000000


S = 5.605272E-06   R-Sq = 96.93%   R-Sq(adj) = 95.23%
```

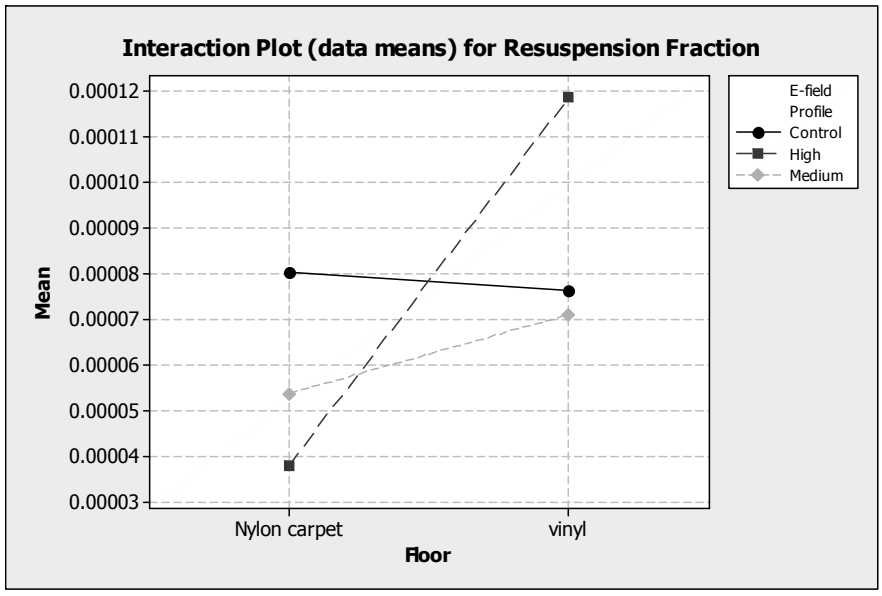

* Three resuspension fractions are reported as unusual observations and are treated as missing values in the analysis. These observations are Medium-Vinyl-1, Control-Nylon carpet-2 and High-Vinyl-2.

Figure 55 Statistical analysis of dust mite resuspension fractions

As denoted in Figure 55, three resuspension fractions are reported by Minitab as unusual observations so these observations are not included in the analysis. All the p-values are smaller than the significance level of 0.10. Thus, it can be concluded that field profile, floor type and their interaction all have significant influence on dust mite particle resuspension.

The interaction plot shows that significant increase (55.1%) of resuspension fractions can be observed for dust mite particles on the vinyl surface for high profile, as compared to control experiments. However, for dust mite particles on the surface of carpet samples, the attraction effect of electrostatic field overcomes the particle lifting effect so the resuspension fractions decrease.

For all the resuspension experiments under positive profiles, the particle resuspension fractions are concluded in Table 29.

Table 29 Particle resuspension fractions under positive electrostatic field

	Vinyl tile			**Nylon carpet**		
	High profile $\left(\times 10^{-5}\right)$	**Med. Profile** $\left(\times 10^{-5}\right)$	**Control** $\left(\times 10^{-5}\right)$	**High profile** $\left(\times 10^{-5}\right)$	**Med. profile** $\left(\times 10^{-5}\right)$	**Control** $\left(\times 10^{-5}\right)$
Alumina	1.57	0.96	0.85	2.71	6.24	4.06
Silica sand	6.25	4.39	4.36	3.89	2.87	5.02
Spore	21.53	19.32	14.66	9.13	18.28	11.84
Dust mite	11.52	6.73	7.61	3.79	5.36	8.04

Table 29 shows that the particle resuspension fractions range between 8.5×10^{-6} and 2.2×10^{-4}. Comparison shows that organic particles (spore and dust mite) have resuspension factors larger than mineral particles (alumina and silica sand), especially on the vinyl surface. With similar particle size distribution, alumina particles have a much larger adhesion force distribution, as shown in Chapter 3, and larger gravitational forces due to larger density. These factors lead to smaller resuspension fractions of mineral particles as compared to organic particles, given the same magnitude of resuspension forces. In the chamber experiments, the organic particles have resuspension fractions between 3.79×10^{-5} and 2.15×10^{-4}, while the mineral particles have resuspension fractions between 8.5×10^{-6} and 6.25×10^{-5}. These values are very close to the resuspension fractions acquired from controlled field experiments as reviewed in Chapter 1, a range of $5.0\times10^{-4} \sim 3.2\times10^{-3}$ for organic particles and a range of

$8.5\times10^{-6} \sim 3.1\times10^{-4}$ for mineral particles. This validated the reliability of particle resuspension chamber in simulating particle resuspension by human walking activity.

Gomes (2007) carried out research on particle resuspension with the same chamber system as in this study, but with a focus on aerodynamic and vibration force induced by walking. The resuspension fractions from the control experiments in this study, which also have aerodynamic effects but not electrostatic effects, are similar to the experiments carried out by Gomes for particle resuspension chamber study. The resuspension fractions for this study range between $8.5\times10^{-6} \sim 1.466\times10^{-4}$. The average resuspension rates reported by Gomes range $1.0\times10^{-10} \sim 1.0\times10^{-4}$ min^{-1}. As the resuspension rate of 1st disturbance normally 3 times the average value and a cycle length is of 16 seconds (Gomes 2007), the converted resuspension fraction range from Gomes' experiments is $8.0\times10^{-11} \sim 8.0\times10^{-5}$. Thus, the resuspension fractions acquired from this study overlap the range from the similar experiments. This further demonstrates the repeatability of the chamber experiments. The wider range of resuspension coefficients in Gomes' experiments is mainly due to a wide range of aerodynamic disturbance profiles in the experiments. Besides, this comparison also shows that aerodynamic force is a major factor in particle resuspension because this factor can change particle resuspension coefficient by orders of magnitude while the electrostatic influence is limited within one order of magnitude.

From all these analysis under positive field profiles, it can be concluded that there is strong interaction effects between floor type and electrostatic field on particle resuspension. On vinyl tile, the electrostatic field generally tends to increase the particle resuspension from floor surface because electrostatic force can counteract particle surface adhesion force and gravitational force. For the four types of tested particles, the resuspension fraction can be increased by 43% to 87%. These phenomenons are especially obvious for high electrostatic field profile. However, on carpet surface which can increase the turbulence of air flow boundary layer, as the electrostatic attraction effects can overwhelm the adhesion loosing effects on surface particles, the particle resuspension phenomenon are often weakened by introduction of electrostatic field. In this situation, more particles can attach to the surface of human shoes and be delivered to other area by human walking transportation. Thus, even though the local particle

resuspension is not increased, the contamination dispersion can still be aggravated by the electrostatic effects during human walking.

5.3.3 Resuspension fractions under negative fields

The effects of positive electrostatic field on surface particle resuspension are studied in above section. A natural development of the next research question is whether the change of field direction can influence particle resuspension. For this purpose, the particle resuspension fractions are studied under negative field strength. Alumina and spore are two kinds of particles used in this study.

(1) Resuspension fraction for alumina particles

For the mineral particles of alumina, the resuspension fractions from chamber experiments are concluded in Table 30. There are two levels for the factor of field profile: one is the high profile and the other is the control profile. There are 12 experiments in total as shown in Table 30.

Table 30 Alumina resuspension fractions

Electrostatic field profile	Flooring type	replication number	Resuspension fraction	Mean resuspension fraction	Standard deviation
High	vinyl	1	4.86E-05	4.00E-05	7.50E-06
		2	3.63E-05		
		3	3.50E-05		
	Nylon carpet	1	3.36E-04	2.60E-04*	4.75E-05
		2	2.77E-04		
		3	2.42E-04		
Control	vinyl	1	3.74E-05	2.23E-05	1.42E-05
		2	2.03E-05		
		3	9.20E-06		
	Nylon carpet	1	1.87E-04	1.79E-04*	1.12E-04
		2	3.72E-04		
		3	1.71E-04		

* Unusual observations denoted by Minitab are not counted for mean.

ANOVA is carried out with Minitab on the experiment design shown in Table 30. The Minitab outputs are shown in Figure 56.

General Linear Model: Resuspension Fra versus E-field Profile, Floor

```
Factor           Type   Levels  Values
E-field Profile  fixed       2  Control, High
Floor            fixed       2  Nylon carpet, vinyl


Analysis of Variance for Resuspension Fraction, using Adjusted SS for Tests

Source                  DF     Seq SS     Adj SS     Adj MS       F      P
E-field Profile          1  0.0000000  0.0000000  0.0000000   27.60  0.002
Floor                    1  0.0000001  0.0000001  0.0000001  405.47  0.000
E-field Profile*Floor    1  0.0000000  0.0000000  0.0000000   11.31  0.015
Error                    6  0.0000000  0.0000000  0.0000000
Total                    9  0.0000001


S = 0.0000144728   R-Sq = 98.65%   R-Sq(adj) = 97.98%
```

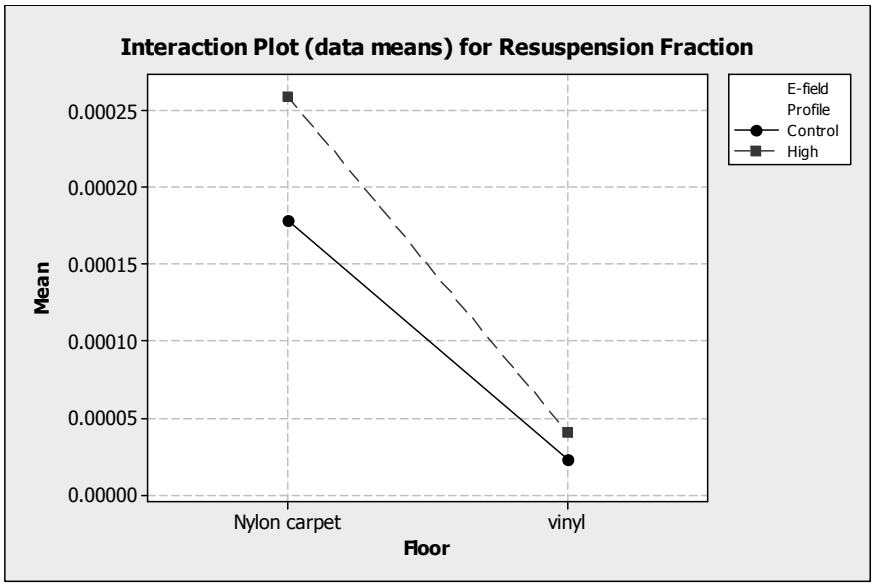

* Two resuspension fractions are reported as unusual observations and are treated as missing values in the analysis. These two observations are Control-Nylon carpet-2 and High-Nylon carpet-1.

Figure 56 Statistical analysis of alumina resuspension fractions

As denoted in Figure 56, two resuspension fractions are reported by Minitab as unusual observations. In Minitab, values are denoted as unusual value when the values are beyond the range of mean±(2×standard deviation). These unusual large or small

values (as compared to other values in the group) can be caused by unexpected or not well controlled parameters such as room humidity fluctuation. These observations tend to obscure the general trend and are not included in the analysis. All the p values are smaller than the significance level of 0.10. After this data processing, it can be concluded that field profile, floor type and their interaction all have significant influence on alumina particle resuspension.

Under high profile of electrostatic field, increases of resuspension fractions are observed on the surfaces of both vinyl and carpet. For vinyl, this agrees with the experimental results under positive high profile. The resuspension fractions are increased by about 79%, which is very close to the increase ratio of 87% under high profile of positive field. It can be observed that the resuspension fractions in control experiments are different from those in the control experiments in previous study (2.23×10^{-5} vs. 8.45×10^{-6} for vinyl; 1.79×10^{-4} vs. 4.06×10^{-5} for carpet). The difference is mainly caused by such uncontrollable parameters such as room relative humidity. However, as many particle resuspension experiments provide resuspension coefficient ranges over several orders of magnitude, this difference is not large and still shows good repeatability of the chamber experiments.

A significant difference, as compared to the experimental results under positive field strength, is that the significant increase of resuspension fractions of particles on carpet surface under negative high profile. In the experiments under positive high profile, the resuspension fractions over carpets are generally decreased by electrostatic attraction effect. However, it is important to notice that, for this control experiment, the calculation on the mean of alumina resuspension over carpet does not include a large observation since statistical analysis considers it as “unusual”. That is to say this data processing method may artificially magnify the difference between control experiments and high profile experiments on carpets.

(2) Resuspension fraction for spore particles

For the organic particles of spore, the resuspension fractions from chamber experiments are concluded in Table 31, with 12 experiments in total.

Table 31 Spore resuspension fractions

Electrostatic field profile	Flooring type	replication number	Resuspension fraction	Mean resuspension fraction	Standard deviation
High	vinyl	1	4.34E-05	3.80E-05	5.17E-06
		2	3.74E-05		
		3	3.31E-05		
	Nylon carpet	1	9.15E-05	8.77E-05	9.90E-06
		2	7.65E-05		
		3	9.52E-05		
Control	vinyl	1	4.74E-05	6.28E-05	1.38E-05
		2	6.69E-05		
		3	7.41E-05		
	Nylon carpet	1	1.21E-04	1.32E-04	9.85E-06
		2	1.40E-04		
		3	1.35E-04		

ANOVA is carried out with Minitab on the experiment design shown in Table 31. The Minitab outputs are shown in Figure 57.

General Linear Model: Resuspension Fra versus E-field Profile, Floor

```
Factor           Type   Levels  Values
E-field Profile  fixed       2  Control, High
Floor            fixed       2  Nylon carpet, vinyl


Analysis of Variance for Resuspension Fraction, using Adjusted SS for Tests

Source                  DF     Seq SS     Adj SS     Adj MS       F      P
E-field Profile          1  0.0000000  0.0000000  0.0000000   34.71  0.000
Floor                    1  0.0000000  0.0000000  0.0000000  102.89  0.000
E-field Profile*Floor    1  0.0000000  0.0000000  0.0000000    2.75  0.136
Error                    8  0.0000000  0.0000000  0.0000000
Total                   11  0.0000000


S = 0.0000101570   R-Sq = 94.61%   R-Sq(adj) = 92.59%
```

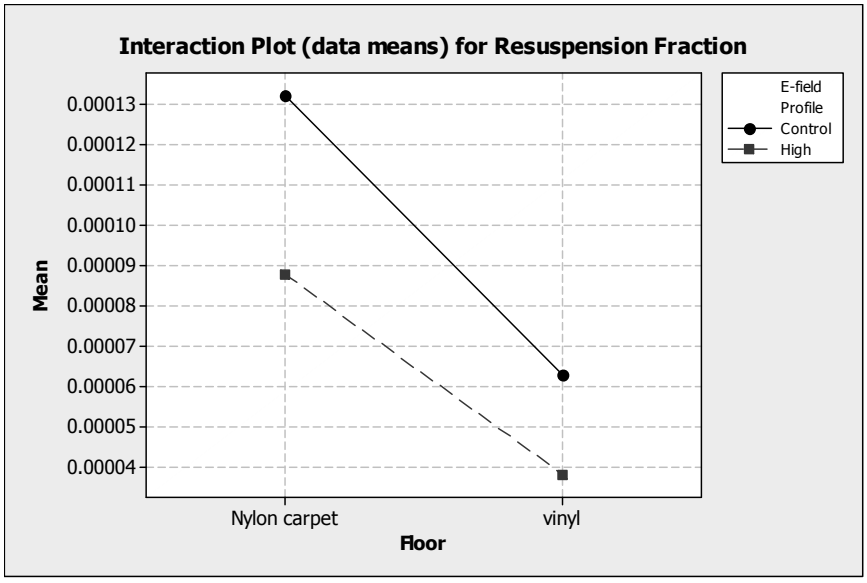

Figure 57 Statistical analysis of spore resuspension fractions

From the Minitab outputs, the p value of interaction between field profile and flooring type is 0.136, which is a little larger than the 0.10 critical value. The p values for each factor of field profile and floor type are much smaller than 0.10. Thus, it can be concluded that both field profile and flooring type have significant influence on spore particle resuspension.

A significant difference between this experiment and all the other experiments is that the particle resuspension fractions are reduced both on the vinyl and carpet surface after the negative electrostatic field is introduced, as compared to the zero field control experiments. The explanation for this is the inactivity of organic particles in negative field, as compared to mineral particles. When the electrostatic field is negative, the induction effect causes surface particles loose electrons to have positive charge. It is conjectured that the speed for such organic particles as spore to loose electrons is much slower than the speed to acquire external electrons under electrostatic induction effect. Thus the electrostatic force on particles is relatively weak for a short period of negative electrostatic field. However, the electrostatic attachment effect still has effect on floating particles around the charged plate (simulated shoe bottom). Thus, the electrostatic attraction effect takes lead over resuspension effect in this situation and the particle resuspension fractions are greatly reduced. Thus, it is observed in the experiments that the addition of negative electrostatic field decreases the spore particle resuspension fraction, as opposed to most of the other experiments.

For all the resuspension experiments under negative profiles, the particle resuspension fractions are concluded in Table 32.

Table 32 Particle resuspension fractions under negative electrostatic field

	Vinyl tile		Nylon carpet	
	High profile $\left(\times 10^{-5}\right)$	Control $\left(\times 10^{-5}\right)$	High profile $\left(\times 10^{-5}\right)$	Control $\left(\times 10^{-5}\right)$
Alumina	4.00	2.23	25.97	17.85
Spore	3.80	8.77	6.28	13.21

Table 32 shows that the particle resuspension fractions range between 2.23×10^{-5} and 2.60×10^{-4} for mineral particles, and between 3.80×10^{-5} and 1.32×10^{-4} for organic particles, which are close to the ranges under positive fields. Again the resuspension fractions of spores are very close to the resuspension fractions from literature reviewed by Chapter 1. Comparison shows that organic particles (spore) still

have larger resuspension fractions on vinyl tile than alumina particles (alumina), though this trend is not observed over the carpet surface.

It is important to notice that negative field has less effect in loosing the bond between spore particles and the surface, as compared to positive field. On the other hand, many particles resuspended into the air are attracted to the charged metal surface. As a result, the resuspension fractions of spores decrease when a negative field is added. However, the negative field still increased the resuspension fraction of alumina particles from vinyl surface by 79%. This shows that, depending on the particle type (mineral or organic), negative field strength does have different effects on particle resuspension.

CHAPTER 6. MODELING INDOOR PARTICLE RESUSPENSION AND DISPERSION

Simulation of indoor PM transport can be helpful for predicting the consequences of accidental and intentional contamination of a building. Deposition and resuspension of particles are important factors that can influence indoor particle dispersion process. Empirical models of particle deposition and resuspension (Sehmel 1984) have simple forms but the application is limited for complicated modeling. Computational fluid dynamics (CFD) can be a very sophisticated modeling tool in particle dispersion simulation (Lu et al 1999, Cicciarelli et al 2002, Zhang and Chen 2006). However, the large demand on computational power by CFD prohibits its application in simulation of such multi-zone spaces as buildings. Multi-zone modeling provides a means for studying the airflow and contaminant dispersion within complex building systems. However, the most widely used multizone models treat particulate contaminants as if they were gases. Simple generic models of sources and sinks that are used in such programs must be adapted to represent particle deposition and resuspension. In addition, existing multi-zone software does not track the cumulative amount of aerosol deposited on surfaces and update the reservoir concentration in the simulation of transient deposition and resuspension processes. An accurate reservoir concentration can be crucial for the prediction of particle resuspension by human activity.

The work in this chapter establishes a relationship between a particle deposition and resuspension empirical model and the source/sink model currently used in multi-zone software. The establishment of this relationship allows the evaluation of the ability of multi-zone software to model particulate contaminant transport in an indoor environment via a heating, ventilation and air-conditioning (HVAC) system. Particle resuspension rates measured from experiments are important boundary conditions for such multi-zone modeling of particle dispersion. An iterative procedure is also suggested to simulate the changing resuspension source term in a transient deposition and resuspension process, which can not currently be modeled directly by multi-zone software. The method is demonstrated and tested with a widely used public domain multi-zone modeling program,

CONTAM 2.1 (Dols and Walton 2002), in a three-zone office building with an HVAC system and with and without human activity.

6.1 Theoretical backgournd of particle dispersion modeling

6.1.1 The constant coefficient source/sink (CCSS) model in CONTAM

A constant coefficient source/sink (CCSS) model is one of several generic models used in CONTAM 2.1 to represent sources and sinks of airborne contaminants. While the other models in CONTAM such as pressure driven model and cutoff concentration model assume the contaminants in gas status, the CCSS model does not have such limitation and is considered applicable in particulate contaminant simulation. The CCSS model is described by Equation 59.

$$S = G - D \cdot C \tag{59}$$

Where: S = source rate of particulate contaminants, [particle #/time]; G = generation rate, [particle #/time]; D = effective removal rate, [volume of air/time]; C = current concentration of particulate contaminants, [particle # /volume of air].

6.1.2 Correlating the CCSS model with the empirical models

The particle deposition velocity and resuspension coefficients, as introduced in Chapter 1, can be related to the CCSS model in CONTAM. The source term G in Equation 59 can be related to the particle resuspension rate or resuspension fraction for monodisperse particles as shown in Equation 60.

$$G = C_S \cdot A \cdot RR = A_C \Lambda_C \cdot C_S \cdot r_f \tag{60}$$

Likewise, the sink term $D \cdot C$ in Equation 59 can be related to the particle deposition velocity as shown by Equation 61 and Equation 62 for monodisperse particles.

$$D = v_d \cdot A \qquad (61)$$

$$C = C_{Air} \qquad (62)$$

In multi-zone models, a particle deposition and resuspension process with multiple particle diameters can be treated as the superposition of multiple monodisperse particle deposition and resuspension processes. Each particle size can be treated as a unique contaminant in CONTAM. The terms G and D can be expressed by Equation 63 and 64 for polydisperse particles.

$$G_j = C_{S_j} \cdot A \cdot RR_{d_j} = A_C \Lambda_C \cdot C_{S_j} \cdot r_{f,d_j} \qquad (63)$$

$$D_j \cdot C_j = v_{d_j} \cdot A \cdot C_{Air,d_j} \qquad (64)$$

Where: j = 1, 2 … n.

In CONTAM, a particle deposition and resuspension process with continuously distributed particle sizes can also be approximated by a particle deposition and resuspension process with multiple particle diameters. The particle size range can be divided into multiple size bins. The number of size bins depends on the desired accuracy of the simulation. For each size bin, the particle deposition and resuspension process is approximated by the resuspension/deposition of a single diameter particle. The median diameter of the particle size bin can be used to represent particles within that bin. Thus, Equation 63 and Equation 64 also apply to the CONTAM simulation of particles with continuous diameter distribution.

Based on the preceding analysis, it can be concluded that particle resuspension coefficients and deposition velocity, which are widely used in current literature, can be related to such generic models as the CCSS model in CONTAM. In order to carry out

simulation of particulate contaminants using a multi-zone airflow and contaminant transport model, the definition of the source and sink term need to follow the relationships shown by Equations 60 through 64. Values for the resuspension rate (RR), resuspension fraction (r_f) and deposition velocity (v_d) are very important for calculating corresponding values of source (G) and sink (D) terms in the CCSS model of CONTAM. These values are acquired either from literature, field observations or controlled experiments. A reliable database of the above parameters needs to be established for particle deposition and resuspension simulation in multi-zone modeling.

6.1.3 Iterative method to simulate transient particle deposition and resuspension

For a transient particle deposition and resuspension process, the particle generation rate by resuspension varies because the surface concentration is changing with time. Multizone models, such as CONTAM 2.1, are not able to track the cumulative amount of particles deposited, which is needed to update the surface concentration and calculate particle source term G. Thus an iterative method is also suggested here to address such deficiency, allowing accommodation of time dependent reservoir source strengths.

The objective of the iterative process is to obtain the correct time-dependent surface reservoir concentration for the simulated conditions. In the following notation, the first argument t in the bracket represents time step while the second number represents the number of iteration. In the first iteration, the reservoir concentration $(N_s(t,1))$ is assumed to be constant throughout the simulated time period and equals the initial reservoir concentration $(N_s(t=0))$ before the particle deposition and resuspension process starts. That is to say, given a constant resuspension rate k_A, the particle source term $(G(t,1))$ is constant throughout the time in the first iteration. With this setting of surface source term and the initial airborne particle concentration, CONTAM can calculate the transient airborne particle concentrations $(N_{Air}(t,1))$ during the simulated period for the first iteration. As the reservoir concentration change is not tracked by CONTAM 2.1, the surface concentration needs to be calculated outside the multi-zone software and updated

after each iteration. At the end of the first iteration, a reservoir surface mass balance equation are used to adjust reservoir concentration $(N_S(t,2))$ and $(G(t,2))$ for the second iteration. In the second iteration, CONTAM calculates the airborne particle concentration $(N_A(t,2))$ using the updated source term $(G(t,2))$. This process continues until convergence is obtained. Convergence is defined by close agreement of variables of interest (airborne concentration, for instance) between each iteration at each time step for the whole transient process. The algorithm of the iteration method is shown in Figure 58.

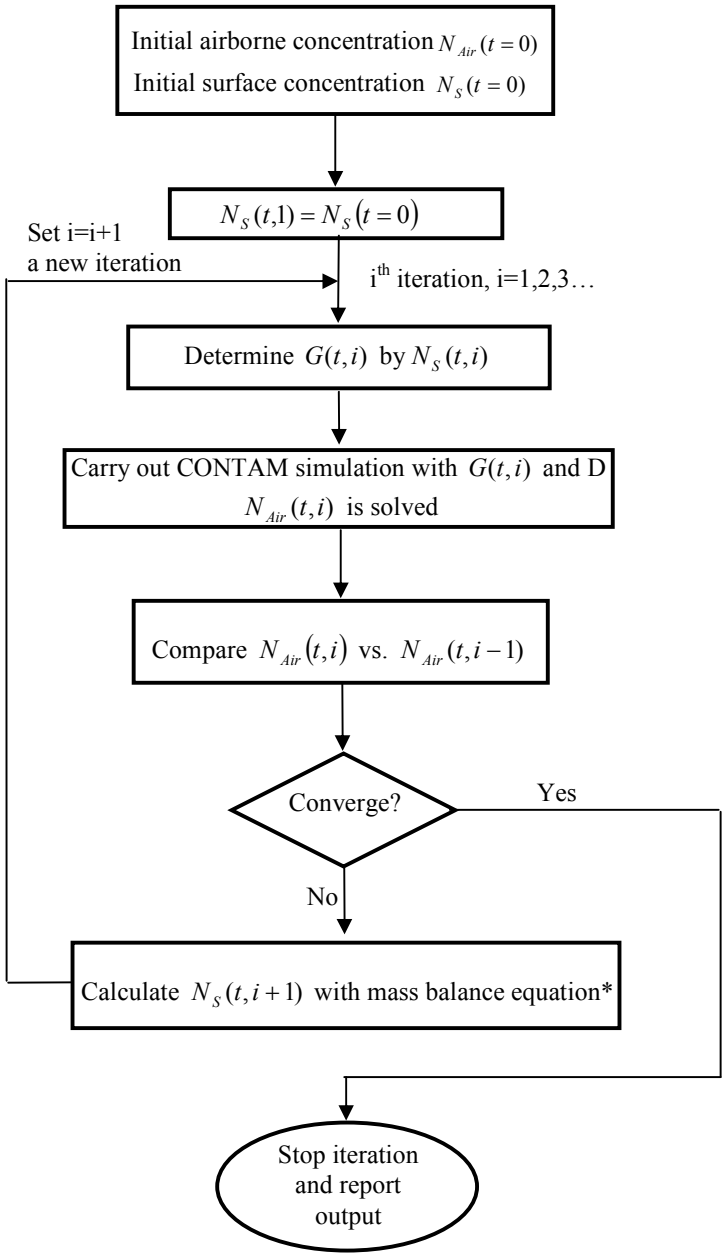

Figure 58 Algorithm of iteration method for transient simulation

* $N_S(t,i+1)=N_S(t,i)+\frac{D\cdot\Delta t}{A}\cdot\frac{N_A(t,i-1)+N_A(t-1,i-1)}{2}-k_r\cdot\Delta t\cdot\frac{N_S(t,i-1)+N_S(t-1,i-1)}{2}$

Where: i is the index of iteration; t is the index of time step; Δt is the time length of each time step.

In the iteration algorithm of Figure 58, except for the solution of transient airborne concentration, most of the data processing work including the updating of surface

concentration is handled outside CONTAM with software Excel (Microsoft 2003). This data process outside CONTAM causes extra effort in simulation so it is suggested that such function can be incorporated into CONTAM in later version.

6.1.4 Analytical models for indoor particle dispersion

Analytical models often provide accurate description of physical phenomena due to the accurate presentation of underlying physical principles by these models. However, one limitation of analytical models is that these models can only be used to solve relatively simple phenomena and often fail to describe a complicated real situation. The analytical model describing particle resuspension, deposition and dispersion is given by Equations 65 and Equation 66 (Karlsson, 1999). This analytical model assume that well-mixing between particles and air, and no coagulation between particles. For simplicity, these equations are used to describe the particles with a single diameter d and the symbol d does not appear in the subscript of each term in the equations. Equation 65 is the mass balance equation for floor surface particles and Equation 66 is the mass balance equation for airborne particles. These equations are coupled through particle exchanges due to resuspension, deposition and airflow transportation.

$$\frac{dC_{S,i}}{dt} = v_d \cdot C_{Air,i} - RR_i \cdot C_{S,i} \qquad (65)$$

$$\frac{dC_{Air,i}}{dt} = \left(\frac{\dot{V}_{SA,i}}{V_i}\right) \cdot C_{SA} - h_i \cdot C_{Air,i} - \left(\frac{A_i}{V_i}\right) \cdot v_d C_{Air,i} + \left(\frac{A_i}{V_i}\right) \cdot RR_i \cdot C_{S,i} + \sum_j \left(\frac{\dot{V}_{IA,ji}}{V_i}\right) \cdot \left(1 - f_{ji}\right) \cdot C_{Air,j} \qquad (66)$$

Where: i = room number; j = index for room adjacent to room i; $\dot{V}_{SA,i}$ = supply air rate from HVAC system to room i, m^3/s; V_i = volume of room i; A_i = floor area of room i; C_{SA} = particle concentration in the supply air, $\#/m^3$; h_i = air exchange in room i,

s^{-1}; $\dot{V}_{IA,ji}$= infiltration from room j to room i, m^3/s; f_{ji}= internal filter factor from room j to room i.

The resuspension and deposition term in Equations 65 and 66 can be related, as described in Section 6.1.2, with the source and sink terms (G and $D \cdot C$ in the CONTAM CCSS model).

6.2 MODELING SCENARIO

This study intends to investigate the applicability of the multizone model in simulation of particulate contamination in a multizone office building with a HVAC system. The iterative method described in Section 6.1.3 was applied in the simulation. Results obtained from CONTAM were compared with the analytical model introduced in Section 6.1.4, which were considered the benchmark. The analytical model was solved numerically with the Engineering Equation Solver (EES) (Klein 2004). The EES results are considered benchmark, accurate solutions. The CONTAM outputs based on the iteration method were compared with the EES outputs to check the accuracy and applicability of CONTAM CCSS model in the simulation of indoor particle deposition, resuspension and dispersion.

6.2.1 Building description

The three-zone building in Figure 59 represents the building used for the study and represents a simple single-story office-building.

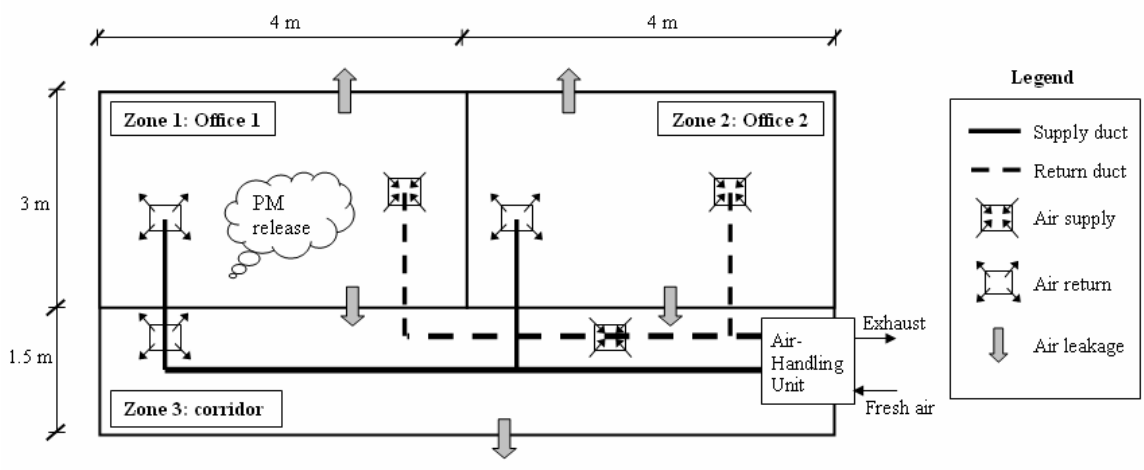

Figure 59 a three-zone office building equipped with HVAC system

Zone 1 and Zone 2 are offices, each with an area of 12 m^2. Each of the two zones is connected to a corridor through an internal door. The area of the corridor is also 12 m^2. The corridor has an external door connected to the outdoor environment. The height of each zone is 3.0 m. The air-conditioning system in this building is a simple constant air volume (CAV) system with duct return and without plenum. The supply air (SA) and return air (RA) of each zone are shown in Table 33. The total outdoor air (OA) is 15% of the total air supply (72 L/s). It is assumed that there is no PM brought into the indoor environment by the air conditioning system from the outdoor environment. The filter of the air conditioning system, located at the duct of mixed supplying air, is a MERV 6, which gives a 40% efficiency on PM 3.0 ~ 10.0 (ASHRAE 2004).

Table 33 Ventilation for the building

Zone information	Zone 1	Zone 2	Corridor	Total
Area (m^2)	12	12	12	36
Supply air (L/s)	24.0	24.0	24.0	72.0
Return air (L/s)	19.2	19.2	22.8	61.2
Outdoor air (L/s)	3.6	3.6	3.6	10.8

6.2.2 Simulation scenarios

There are three simulation scenarios as described in Table 34. Case I is similar to an accidental or intentional immediate release of a contaminant in to the air of the indoor environment. Case II resembles the situation that the particulate contaminant with the same amount as in Case I is initially dispersed evenly onto the floor surface. Case III is used as a control experiment of Case I. The only difference between Case I and Case III is that there is no human activity in the building. Each case was simulated for the business hours from 8:00 am to 5:00 pm, a period of 9 hours. The floor was considered the only location for particle deposition and resuspension.

Table 34 Description of the three modeling cases

Simulation case	Case description	
	PM release location	**Human activity**
Case I	In the air of Zone 1 and no PM on the floor initially	2 persons walking in Zone 1
Case II	On the floor of Zone 1 and no PM in the air initially	2 persons walking in Zone 1
Case III	In the air of Zone 1 and no PM on the floor initially	None

Constant human activity level was used for both Case I and Case II, i.e., two people walking around continuously within zone 1 at a rate of 75 steps per minute. The resuspension rate of this walking frequency was measured by controlled experiments (Karlsson et al. 1999). The particles used in Karlsson's experiments were clusters of *Bacillus subtilis* spores, with a Stokes diameter of 12 μm and a density of 1.3 g/cm^3. The measured resuspension rate (RR) of the particles was $8.75\times10^{-7}\,s^{-1}$, which corresponds to a resuspension fraction (r_f) of 5.0×10^{-4}. The measured mean deposition velocity (v_d) was $0.005 m\cdot s^{-1}$. These values were used in the simulation study of this work. For all three cases, the total amount of particles released into the building is the same: 1.6×10^9 particles of 12 μm and a total mass of 1.88 grams. No other particulate contaminants are considered in this simulation.

6.3 MODELING RESUTLS AND ANALYSIS

6.3.1 Simulation results convergence and accuracy check

The iterative method is used to solve transient airborne particulate concentration in each simulation case. The convergence of the iterations is checked by the maximum iteration error in each iteration. The iteration error is defined in Equation 67.

$$iteration\ \ error\ (t) = \frac{\left|C_{Air}(t,i) - C_{Air}(t,i-1)\right|}{C_{Air}(t,i)} \times 100\% \qquad (67)$$

The iteration stops when the maximum iteration error is smaller than 1.0%. The maximum iteration errors are reported in Table 35. It should be noticed that no iteration is needed for simulation Case III because there is no resuspension in this case and the surface source term is always zero.

Table 35 Convergence information for multizone modeling

Simulation case	# of iteration	% errors (maximum in each case)		
		1	2	3
Case I	**Zone 1**	100.00	1.48	0.08
Case II	**Zone 2**	100.00	1.41	0.00
	corridor	100.00	1.44	0.00
	Zone 1	1.41	0.03	-
	Zone 2	1.42	0.08	-
	corridor	1.43	0.06	-

From Table 35, it can be seen that the iteration algorithm converges very fast. To reach convergence, three iterations are needed for Case I and two iterations for Case II. However, difference can be observed between the iterations of Case I and Case II. In Case II, the iteration errors after the first iteration are smaller than 2%. This means the change of simulation results after the 1st iteration is very small. If the convergence standard is not too strict, the iterative method is not necessary for this simulation case.

The reason for this situation is that the reported particles resuspension rate is very small and the resuspension along does not change the surface concentration to a significant level in Case II. Thus, for surface particle release scenarios, the surface particle concentration can be treated as constant in the resuspension simulation when the requirement for simulation accuracy is not very strict. However, for the air release scenario in Case I, as the particles are initially released in the air and the airborne concentration changes rapidly overtime due to such effects as ventilation and deposition, the surface concentration of particles have a rapid changing profile after the air release takes place. Thus, in order to simulate such a rapid changing surface concentration profile, implementation of the iteration algorithm is very important.

The converged iterative solutions from the CCSS model in CONTAM are compared with EES solutions of the analytical models for the airborne particle concentration. The comparison is quantified by the maximum relative error for each zone, as shown in Table 36.

Table 36 Comparison between CONTAM outputs and analytical solutions

Relative error (%)	Zone 1	Zone 2	Corridor
Case I	1.60	1.43	1.45
Case II	0.26	0.29	0.28
Case III	1.68	0.91	0.92

In Table 36, the relative error for certain zone at each time step is calculated by Equation 68.

$$relative\ error(t) = \frac{\left| analyticalsolution(t) - CONTAMsolution(t) \right|}{analyticalsolution(t)} \times 100\% \tag{68}$$

Table 36 shows that the CONTAM simulation results are accurate when compared with the analytical solutions from EES. In each simulation case, the highest relative error of airborne particle concentration within the simulation period is about 1% for each zone.

6.3.2 Particle concentration analysis

Because of the importance of airborne concentration on human exposure, the multizone modeling results on airborne particle concentration versus time are plotted for the purpose of comparison and analysis. The comparison between Case I and Case III is shown in Figure 60.

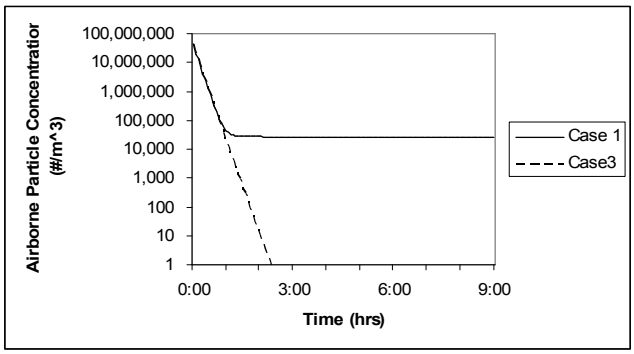

(a) Zone 1

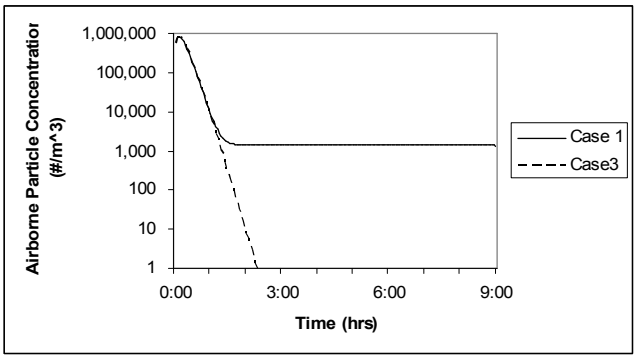

(b) Zone 2

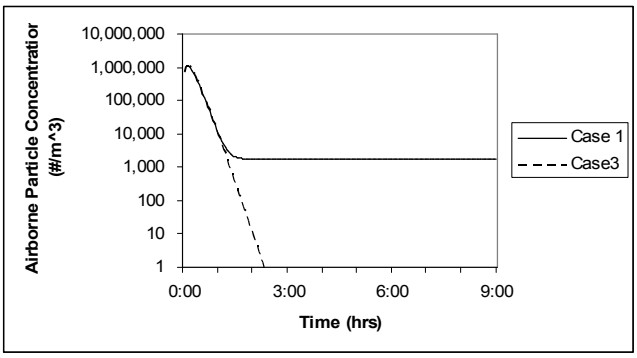

(c) Corridor

Figure 60 comparison between Case I and Case III

In Figure 60, it is shown that the presence of human activity in the particle releasing room can influence the time profile of airborne particle concentration. Given the well mixing assumption in CONTAM, the HVAC system transported the particles, initially released in the air of Office 1, to other zones very quickly. Without human activity to disturb the reservoir, the airborne particle concentrations in the building decreased to zero

(less than 1 particle per cubic meter) within 3 hours. With continuous human activity, the airborne particle concentration eventually reached quasi-equilibrium values for each zone.

The modeling results for Case II are shown in Figure 61. In Figure 61, the continuous human activity disturbance raises the airborne particle concentration to certain quasi-equilibrium values. Office 1 has the highest concentration because it is the location for the particle surface reservoir and human activity. The corridor has a slightly higher concentration than Zone 2 due to the infiltration from Zone 1 to the corridor.

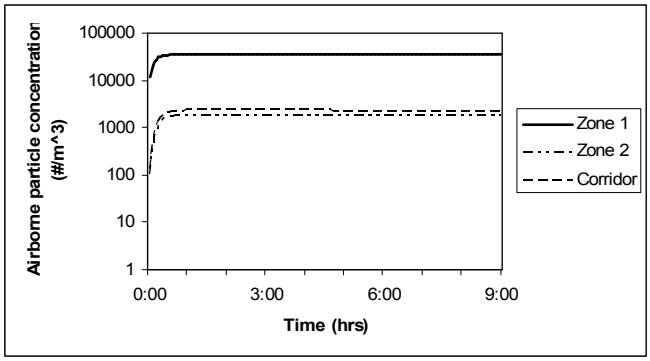

Figure 61 comparisons among each zone in Case II

6.3.3 Total inhaled dose analysis

The total particles that a person inhales into the respiratory system through breathing cycles can be calculated by Equation 69. To estimate actual deposition in the various parts of the respiratory system the capture and release efficiencies of the respiratory system for a given particle size and receptor would need to be included. Lung deposition is not considered here because the purpose of this study is to compare apparent exposure dosages from a direct particle release in to the air versus a gradual systematic resuspension from a surface reservoir.

$$N_{total} = \sum_{i=1}^{n} V_i \cdot C_{Air,i} \qquad (69)$$

Where: N_{total} = the total number of particles breathed in; n =total breathing cycles under consideration; V_i = the volume of air intake in the ith breathing cycle; $C_{Air,i}$ = the concentration of airborne particles in the ith breathing cycle.

Given an inhale volume of 0.5 L per breathing cycle and an inhalation rate of 0.72 m^3/hr for a healthy adult with slow activity level (EPA 1997), the total particle breathing-in dose for a person in Zone 1, which is most heavily contaminated, can be calculated and compared between each case in Table 37.

Table 37 Total calculated inhaled particle dose (#)

	Zone 1	Zone 2	Corridor
Case I	4.20E+06	2.16E+05	2.73E+05
Case II	2.23E+05	1.13E+04	1.44E+04
Case III	4.03E+06	2.07E+05	2.62E+05

From Table 37, it can be seen that release of particles into the air (Case I and Case III) can generate a much larger breathing dose than that from particles directly resuspended from the floor (Case II). When Case I and Case III are compared, it is shown that the existence of human walking can increase the breathing dose by 4.1%. For Zone 2 and the corridor, the particle breathing doses are caused by HVAC transportation and/or infiltration from contaminated space. The breathing doses in such areas are much smaller than that in the direct particle air- releasing room.

For Zone 1 in Case II, the human activity can cause a daily breathing dose of 5.5 percent of that in Case III with air release and no resuspension from human activity. For a surface reservoir of particulate contaminants under human activity disturbances, there could be a concern for long term particle exposure. As shown in Figure 60-a, the breathing dose of Case III is actually caused by the exposure of the first three hours after the contamination. After this short period, there is no further breathing dose since no human activity resuspend the particles fallen on the floor into the air again. However, as in Case II, if the human activity persists each following day for 9 hours, the resuspended

particles can cause a higher accumulated breathing dose to a person in a period of 20 days. This derivation assumes the surface concentration keeps approximately constant. As analyzed before, this assumption is reasonable because the daily remove rate of particles from surface by resuspension is very small as compared to the total surface load.

CHAPTER 7. CONCLUSIONS AND RECOMMENDATIONS

This study focuses on the particle resuspension effects of electrostatic fields introduced by human walking in indoor environment. A few conclusions and recommendations can be drawn from this thesis study.

1) There are four major particle resuspension force components introduced by human activity: aerodynamic drag, aerodynamic lift, mechanical vibration and electrostatic force. Particle gravitational force and adhesion force are the major forces preventing particles leaving the surface. Parametric study shows that, for micron-sized particles, all the resuspension force components are comparable to or larger than gravitational force. With electrostatic field strength of 1 kv/cm, the electrostatic force on micron-sized particles can be more than one order of magnitude larger than the gravitational force. The theoretical prediction of adhesion force of micron-sized particles is a few orders of magnitude larger than any of the three resuspension force components.

2) Field experiments are carried out to measure real particle to surface adhesion forces. For freshly deposited alumina particles ($d_e = 1.738 \mu m$), about 25% of all particles on the surface of vinyl and rubber tiles have adhesion forces below the value of 1.08×10^{-10} N. For freshly deposited spore particles ($d_e = 3.121 \mu m$), about 40% of all the particles have adhesion forces below the value of 2.93×10^{-11} N. These values are a few orders of magnitude lower than those predicted by the theoretical model, mainly due to imperfect contact.

3) Particle type, flooring type and particle-surface contact time are all important factors that can influence particle adhesion force and hence, particle resuspension coefficients. The experiments in this study shows, with similar size distribution, alumina generally have higher adhesion forces than spore particles on flat surfaces. The adhesion force of

newly deposited particles is lower than that of aged surface particles, which means a higher resuspension coefficient can be achieved for newly deposited particles.

4) In very dry indoor environment, electrostatic field occurs during foot landing and lifting in human walking process. The experiments on human subjects show that the gaits are very similar while the body voltage profiles vary from person to person, but obey the rule of electrostatic series. In each walking step cycle, the foot landing and re-lifting motion is considered to generate the most intensified electrostatic field over floor surface. A transient electrostatic field profile with peak value about 3660 v/cm is derived from field measurements of human body voltage and human gait. This profile is also used in following chamber experiments to simulate electrostatic disturbance to surface particles during walking.

5) Chamber experiments show that electrostatic fields introduced by walking have significant effects on particle resuspension. For positive field (shoes are charged positively while floor is charged negatively), particle resuspension fractions generally increased by 43% ~ 86% on vinyl surface. However, due to the increased air flow turbulence over carpet surface, the uniform increases of resuspension fractions are not observed over carpet surface. For negative field, the resuspension fractions of mineral particles still show an increasing trend while the values of organic particles show a decreasing trend. The later phenomena can be explained by that the electrostatic attraction effect overwhelms the electrostatic charging effect for organic particles. As particle type is considered, for similar particle size distribution, organic particles generally have larger resuspension fractions than mineral particles. In the chamber experiments, the measured resuspension fractions for organic particles range between 3.8×10^{-5} and 2.2×10^{-4}, while the values for mineral particles 8.5×10^{-6} and 2.6×10^{-4}. These resuspension fractions are very close to the values acquired from field experiments in literature. This validated the reliability to use particle resuspension chamber to simulate particle resuspension by human walking. The resuspension fractions' range in this study also overlaps that from similar chamber experiments of Gomes (2007), which focus on aerodynamic effects on particle resuspension. This shows the good repeatability

of chamber experiments on particle resuspension. Besides, this comparison also shows that the aerodynamic force has a higher influence on particle resuspension coefficients than the electrostatic force based on the narrower coefficient range from electrostatic disturbance experiments.

6) Multi-zone models such as CONTAM can be used to simulate indoor particle deposition, resuspension, and dispersion, if a few critical parameters, such as deposition velocity (v_d), resuspension rate (RR) and resuspension fraction (r_f) are known. The CCSS model within CONTAM is fit for this application. The iterative method suggested in this work can complement current multi-zone model by tracking surface reservoir concentration, which is important for particle resuspension prediction in a transient process.

7) Human activity in the contaminant release space can greatly infuence the airborne particle concentration profile, while particle release location (air vs. floor) can lead to quite different airborne particle concentration profiles. A breathing dose calculation shows that for a given amount of particles the direct air release gives a high short-term breathing dose, while the particle resuspension by human activity can cause a higher accumulated breathing dose over a longer period of time.

There are also a few recommendations from this work for the study of electrostatic effects on particle resuspension.

1) More systematic particle resuspension experiments are needed to establish a reliable database of particle resuspension coefficients by human activity.

2) To explain the decrease of organic particle resuspension under negative electrostatic field direction, it is conjectured that it is more difficult for organic particles to lose electrons than to acquire external electrons. More theoretical and experimental studies are needed for the validation of this conjecture.

3) A linear model is used to approximate the relationship between human gait and body voltage. An improvement in measurement and analysis methods is desired in order to capture more reliable transient floor surface electrostatic field profiles.

4) Multi-zone models need to incorporate the ability to track surface particle concentration variation during a transient deposition and resuspension process. This is important for modeling the influence of human activity on particle resuspension.

REFERENCES

Abu-Eid, R. M., R. B. Codell and N. A. Eisenberg. (2002). *Re-evaluation of the Indoor Resuspension Factor for the Screening Analysis of the Building Occupancy Scenario for NRC's License Termination Rule*. Draft report for comment, NUREG-1720. Washington, DC, Office of Nuclear Material Safety and Safeguards, US Nuclear Regulatory Commission.

ASHRAE. (2004). *ANSI/ASHRAE Standard 62.1-2004: Ventilation for Acceptable Indoor Air Quality*. American Society of Heating, Refrigerating, and Air Conditioning Engineers, Atlanta, GA.

Barrett, M. J. and D. K. Hollingsworth. (2003). Correlating friction velocity in turbulent boundary layers subjected to freestream turbulence. *AIAA Journal,* **41**(8): 1444-1451.

Beyeler, W. E., W. A. Hareland, F. A. Duran, T. J. Brown, E. Kalinina, D. P. Gallegos and P. A. Davis. (1999). *Residual Radioactive Contamination from Decommissioning, Parameter Analysis*. Draft report for comment, NUREG/CR-5512, Vol. 3. Washington D. C., U. S. Nuclear Regulatory Commission.

Brunskill, R. T. (1967). The relationship between surface and airborne contamination. *Surface Contamination*, Gatlinburg, Tennessee, USA, Pergamon Press, New York.

Buttner, M. P., P. Cruz-Perez, L. D. Stetzenbach, P. J. Garrett and A. E. Luedtke. (2002). Measurement of airborne fungal spore dispersal from three types of flooring materials. *Aerobiology*, 18: 1-11.

Carter, R. F. (1970). *The Measurement of Dust Levels in a Workshop Environment*. Aldermaston, Berks, England, United Kingdom Atomic Energy Authority.

Chamberlain, A. C. and R. C. Chadwick. (1953). Deposition of airborne radio-iodine vapor. *Nucleonics*, 8: 22-25.

Chapman, M. D. (2003). Indoor allergens. *Pediactric Allergy: Principles and Practice*, D. Y. M. Leung, H. A. Sampson, R. S. Geha and S. J. Szefler, Elsevier Science: 261-268.

Cicciarelli, B. A., D. L. Davidson, E. H. Hart and P. Robert Peoples. (2002). CFD analysis of the behavior of airborne allergens in carpeted and uncarpeted dwellings. American Society of Mechanical Engineers, Pressure Vessels and Piping Division (Publication) PVP, 448, 239-247.

Clancy, L., P. Goodman, H. Sinclair, D. W. Dockery. (2002). Effect of air-pollution control on death rates in Dublin, Ireland: an intervention study. *Lancet*, 360, 9341, 1210-1214.

Clayton, C. A., L. A. Wallace, H. Ozkaynak and J. D. Spengler. (1993). Particle total exposure assessment methodology (PTEAM) study: distributions of aerosol and elemental concentrations in personal, indoor, and outdoor air samples in a southern California community. *J. Expos. Anal. Envir. Epidemi.,* 6: 227-250.

Cleaver, J. W. and Yates, B. (1973). Mechanism of detachment of colloidal particles from a flat substrate in a turbulent flow. J. *Colloid Interface Sci.,* v44: 464-474.

Corn, M. and F. Stein. (1965). Re-entrainment of particles from a plane surface. *American Industrial Hygiene Associatin,* **26**: 325-336.

Custovic, A., H. Pahdi, R. Green, M. Chapman and A. Woodcock. (1998). Distribution, aerodynamic characteristics, and removal of the major cat allergenFel d 1 in Brithish homes. *Thorax*, 53: 33-38.

Dockery, D. W.. (2001). Epidemiologic Evidence of Cardiovascular Effects of Particulate Air Pollution. *Environ Health Perspect*, 109, Suppl 4, 483-486.

Dockery, D. W., H. Luttmann-Gibson, D. Q. Rich, M. S. Link, M. A. Mittleman, D. R. Gold, P. Koutrakis, J. D. Schwartz, R. L. Verrier. (2005). Association of air pollution with increased incidence of ventricular tachyarrhythmias recorded by implanted cardioverter defibrillators. *Environ Health Perspect*, 113, 6, 670-674.

Dols, W. S., and Walton, G. N. (2002). *CONTAMW 2.1 User Manual*. Building and Fire Research laboratory, National Institute of Standards and Technology.

EPA. (1997). *Exposure Factors Handbook*. Environmental Protection Agency, Washington, DC, USEPA: 5-5.

Ferro, A. R., Royal J. Kopperud and Lynn M. Hildemann (2004). Source strengths for indoor human activities that resuspend particulate matter. *Environmental Science & Technology*, 38(6): 1759-1764.

Fish, B. R., R. L. Walker, J. W. Royster and J. L. Thompson. (1967). Redispersion of settled particles. *Surface Contamination*, Gatlinburg, Tennessee, USA, Pergamon Press, New York.

Fukuchi, Y. and M. Takeuchi. (1998). A comparative study on toner adhesion force measurements by toner jumping and centrifugal methods. *1998 International Conference on Digital Printing Technologies*.

Glauberman, H., W. R. Bootmann and A. J. Breslin. (1967). Studies of the significance of surface contamination. *Surface Contamination*, Gatlinburg, Tennessee, USA, Pergamon Press, New York.

Gold, D. R., A. A. Litonjua, A. Zanobetti, B. A. Coull, J. Schwartz, G. MacCallum, R. L. Verrier, B. D. Nearing, M. J. Canner, H. Suh, P. H. Stone. (2005). Air pollution and ST-segment depression in elderly subjects. *Environ Health Perspect*, 113, 7, 883-887.

Gomes, C. A. S. (2005). *Resuspension of Allergen-containing Particles Subject to Mechanical and Aerodynamic Disturbance - Introduction to an Experimental Controlled Methodology*. Master Thesis, Department of Architectural Engineering, the Pennsylvania State Univ., USA.

Gomes, C. A. S. (2007). *Factors Impacting Allergen-Containing Particle Resuspension.* PhD Thesis, Department of Architectural Engineering, the Pennsylvania State Univ., USA.

Goren, S. L. (1970). Normal force exerted by creeping flow on a small sphere touching a plane. J. Fluid Mech., v41: 619-625.

Hambraeus, A., S. Bengtsson and G. Laurell. (1978). Bacterial contamination in a modern operating suite. 3. Importance of floor contamination as a source of airborne bacteria. *Journal of Hygiene*, 80: 169-174.

Hall D. (1988). Measurement of the mean force on a particle near a boundary in turbulent flow. *J. Fluid Mech.*, v187: 451-466.

Harriman L. G., G. W. Brundrett and R. Kittler. (2001). *Humidity Control Design Guide*. ASHRAE, Altanta, GA.

Healy, J. W. (1955). A prelimilary estimate of wind pickup and impaction of particles. Hanford, Atomic Products Operation, NTIS.

Heinsohn, R. J. and J. M. Cimbala (2003). *Indoor Air Quality Engineering: Environmental Health and Control of Indoor Pollutants*. New York, Marcel Dekker.

Hinds, W. C. (1999). *Aerosol Technology: Properties, Behavior, and Measurement of Airborne Particles*. New York, John Wiley & Sons, Inc.

Hu, B., J. Freihaut, C. Gomes and W. Bahnfleth. (2005). Literature review and parametric study: Indoor particle re-suspension by human activities. *Proceedings of the 10th International Conference on Indoor Air Quality and Climate*, Beijing, China.

Hu, B., J. Freihaut, W. Bahnfleth, P Aumpansub and Brandolyn Thran. (2007). Modeling the influence of human activity on particle resuspension and dispersion in a multizone indoor environment with HVAC system. Accepted by *ASCE Journal of Architectural Engineering*.

Hu, B., J. Freihaut and W. Bahnfleth. (2006). Simulating transient particle deposition/resuspension in indoor environments. *The 3rd International Building Physics/Science Conference*, Montreal, Canada.

Hughes, J. F. (1997). *Electrostatic Particle Charging: Industrial and Health Care Application*. New York, John Wiley & Sons Inc.

Jonassen, N. (1998). *Electrostatics*. New York, Chapman & Hall.

Jonassen, N. (2001). Mr Static: charging by walking. *Compliance Engineering,* **18**(2).

Jones, I. S. and S. F. Pond. (1967). Some experiments to determine the resuspension factor of plutonium from various surfaces. *Surface Contamination*, Gatlinburg, Tennessee, USA, Pergamon Press, New York.

Kamens, R., C. Lee, R. Wiener and D. Leith. (1991). A study to characterize indoor particle in three non-smoking homes. *Atmospheric Environment*, 25A: 939-948.

Karlsson, E., I. Fangmark and T. Berglund. (1996). Resuspension of an indoor aerosol. *J. Aerosol Sience*, 27(Suppl. 1): 441-442.

Karlsson, E., T. Berglund, M. Nordstrand and I. Fangmark. (1999). The effect of resuspension caused by human activities on the indoor concentration of biological aerosols. J. *Aerosol Science*, 30(Suppl.1): 737-738.

Klein, S. A. (2004). *Manual for EES: Engineering Equation Solver*. F-Chart Software.

Krishnan, S. and A. A. Busnaina. (1994). Adhesion-induced deformation and the removal of submicrometer particles. *Journal of Adhesion Science and Technology*, **8**(11): 1357-1370.

Lefcoe, N. M. and I. I. Inculet (1975). Particulates in domestic premises II. Ambient levels and indoor-outdoor relationships. *Arch. Envir. Health*, 30: 565-570.

Lioy, P. J., J. M. Waldman, T. Buckley, J. Butler and C. Pietarinen. (1990). The personal indoor, and outdoor concentrations of PM-10 measured in an industrial community during the winter. *Atmospheric Environment*, 24B: 57-66.

Long, D. 2005. Choosing the right ESD floor for laboratory and technical environments. *Conformity Magazine*.

Lu, W., Howarth, A. T., Adams, N. M., and Riffat, S. B. (1999). CFD modeling and measurement of aerosol particle distributions in ventilated multizone rooms. *ASHRAE Transactions*, 105, 116-127.

Matsumoto, G. (2003). Anthrax powder: state of the art? *Science,* **302** (11): 1492-1497.

Microsoft. (2003). *Microsoft® Excel 2003*. Microsoft Software.

Mitchell, R. N. and B. C. Eutsler. (1967). A study of Beryllium surface contamination and resuspension. *Surface Contamination*, Gatlinburg, Tennessee, USA, Pergamon Press, New York.

Murray, T. M., D. E. Allen and E. E. Ungar. (1997). *Steel Design Guide Series: Floor Vibrations due to Human Activity*. Chicago, IL, American Institute of Steel Construction.

Nagayama, M. and M. Takeuchi. (2000). Particle adhesion force measurements by electric field detachment method. *2000 International Conference on Digital Printing Technologies*.

National Center for Health Statistics (NCHS). (2001). *New Asthma Estimates: Tracking Prevalence, Health Care and Mortality*.

National Heart, Lung, and Blood Institute (NHLBI). (2002). *Morbidity and Mortality: 2002 Chart Book on Cardiovascular, Lung, and Blood Diseases*.

National Institute of Environmental Health Sciences (NIEHS). (1997). *Fact Sheet #9 "ASTHMA and its Environmental Triggers: Scientists Take A Practical New Look at a Familiar Illness"*.

National Instruments. (2005). *LabVIEW 7.0*.

Nicholoson, K. W. (1988). A review of particle resuspension. *Atmospheric Environment*, 22(12): 2639-2651.

Platts-Mills, T. A. E. (2000). Allergens derived from athropods and domestic animals. *Indoor Air Quality Handbook*, J. D. Spengler, J. M. Samet and J. F. McCarthy, New York, McGraw-Hill: 43.1-43.15.

O'Neill, M. E. (1968). Sphere in contact with plane wall in slow linear shear flow. *Chemical Engineering Science*, v23, n11: 1293-1298.

Punjrath, J. S. and D. R. Heldman. (1972). Mechanisms of small particle re-entrainment from flat surfaces. *Aerosol Science*, **3**: 429-440.

Raunemaa, T., M. Kulmala, J. Saari, M. Olin and M. H. Kulamala. (1989). Indoor air aerosol model: transport indoors and deposition of fine and coarse particles. *Aerosol Science and Technology*, 11: 11-25.

Reade. (1997). Electrostatic discharges (ESD): publicly available information. www.reade.com/Safety/esd.html.

Rich, D. Q., J. Schwartz, M. A. Mittleman, M. Link, H. Luttmann-Gibson, P. J. Catalano, F. E. Speizer, D. W. Dockery. (2005). Association of short-term ambient air pollution concentrations and ventricular arrhythmias. *Am J. Epidemiol*, 161, 12, 1123-1132.

Rich, D. Q., M. A. Mittleman, M. S. Link, J. Schwartz, H. Luttmann-Gibson, P. J. Catalano, F. E. Speizer, D. R. Gold, D. W. Dockery. (2006). Increased risk of paroxysmal arial fibrillation episodes associated with acute increases in ambient air pollution. *Environ Health Perspect*, 114, 1, 120-123.

Robinson, J. and W. C. Nelson (1995). National Human Activity Pattern Survey Dtat base. Reseach Triangle Park, NC, USEPA.

Robert, J. W., Ernest R. Crutcher, Earnest R. Crutcher, Gregory Glass, and Thomas M. Spittler. (1996). Quantitative analysis of road and carpet dust on shoes. *Measurement of Toxic and Related Pollutants*, Air & Waste Management Association, Pittsburg, 829-835.

Sarnat, S. E., H. H. Suh, B. A. Coull, J. Schwartz, P. H. Stone and D. R. Gold. (2006). Ambient Particluate Air Pollution and Cardiac Arrhythmia in a Panel of Older Adults in Steubenville Ohio. *Occup. Environ. Med.*, 6.

Schlichting, H. (1968). *Boundary Layer Theory*. New York, McGraw-Hill.

Schubauer, C. B. and H. K. Skramstad. (1947). Laminar boundary layer oscillation and stability of laminar flow. *J. Aeronaut. Sci.,* **14**: 69.

Sehmel, G. A. (1984). Deposition and resuspension. *Atmospheric Science and Power Production*, D. Randerson, eds., Technical Information Center, Office of Scientific and Technical Information, United States Department of Energy.

Thatcher, T. L. and D. W. Layton. (1995). Deposition, resuspension and penetration of particles within a residence. *Atmospheric Environment*, 29(13): 1487-1497.

Tsai, C.-J., D. Y. H. Pui and B. Y. H. Liu. (1991). Elastic flatterning and particle adhesion. *Aerosol Science and Technology*, **15**: 239-255.

Walker, R. L. and B. R. Fish. (1964). Adhesion of radioactive glass particles to solid surfaces. *Surface Contamination*, Gatlinburg Tennessee.

Wallace, L. (1996). Indoor particle: a review. *Journal of the Air & Waste Management Association*, 46(2): 98-125.

Walsh, C. (2002). *Calculation of Resuspension Doses for Emergency Response*. Chilton, National Radiological Protection Board, UK.

Wellenius, G. A., J. Schwartz and M. A. Mittleman. 2006. Particulate air pollution and hospital admissions for congestive heart failure in seven United States cities. *Am. J. Cardiol.*, 97(3): 404-408.

Wu, Y., G. S. Peter Castle and I. I. Inculet. (2003). Induction charge on freely levitating particles. *Powder Technology*, 135-136: 59-64.

Wu, Y., G. S. P. Castle, I. I. Inculet, S. Petigny and G. S. Swei. (2004). The effect of electric field strength on the induction charge of freely levitating particles. *IEEE Transaction on Industry Application*, v40, 6: 1498-1502.

Wu, Y., G. S. Peter Castle and I. I. Inculet. (2005). Induction charging of granular materials in an electric field. *IEEE Transaction on Industry Application*, v41, 5: 1350-1357.

Zhang, Z., Chen, Q. (2006). Experimental measurements and numerical simulations of particle transport and distribution in ventilated rooms. *Atmospheric Environment*, 40, 3396-3408.

Vita

Bin Hu

EDUCATION

- ***PhD*** in Architectural Engineering, The Pennsylvania State Univ., PA, USA 08/2002~05/2008
  Research interest: indoor air quality, building energy modeling
  Thesis topic: *An Investigation of Electrostatic Field Effects Introduced by Human Walking on Indoor Particle Resuspension*
  Thesis advisor: Dr. James D. Freihaut
- ***Master*** in Applied Statistics, The Pennsylvania State Univ., PA, USA 08/2005~06/2006
- ***B. S.*** & ***M. S.*** in HVAC Engineering, Chongqing Univ., Chongqing, China 09/1994~07/2001

PROFESSIONAL EXPERIENCE

- ***Sustainability Specialist***, Skidmore, Owings & Merrill LLP, Chicago, USA 07/2007~ current
- ***Engineering Intern***, Skidmore, Owings & Merrill LLP, Chicago, USA 07/2006~ 09/2006
- ***Engineer***, Chongqing Wanderful Ltd. Co., Chongqing, China 09/2001~06/2002

PROFESSIONAL ASSOCIATION PARTICIPATION

- American Society of Heating, Refrigerating and Air-Conditioning Engineers (ASHRAE) since 2002

REPRESENTATIVE HONORS/AWARDS

- Graduate School Fellowship, The Pennsylvania State University, USA 2003
- Department Scholarship, Chongqing Jianzhu University, China six consecutive years 1995~2000

PUBLICATIONS

- Hu, B., J. Freihaut, W. Bahnfleth, B. Thran. (2007). Measurements and factorial analysis of micron-sized particle adhesion forces to indoor flooring materials by electrostatic detachment method. Accepted by *J. of Aerosol Science and Technology*.
- Hu, B., J. Freihaut, W. Bahnfleth, P Aumpansub and Brandolyn Thran. (2007). Modeling the influence of human activity on particle resuspension and dispersion in a multi-zone indoor environment with HVAC system. Accepted by *ASCE Journal of Architectural Engineering*, v13, 4.
- Hu, B., J. Freihaut and W. Bahnfleth. (2006). Simulating transient particle deposition/resuspension in indoor environments. *The 3rd International Building Physics/Science Conference*, Montreal, Canada.
- Hu, B., Carlos Gomes and J. Freihault. (2005). Literature review: indoor particle re-suspension by human activities. *Indoor Air 2005*, Beijing, China.
- Hu, B., G. He, J. Srebric and X. (2005). Yang. The influence of contaminant source area on CFD simulations for indoor point sources. *Indoor Air 2005*, Beijing, China.